

ISSN 1916-9698 (Print)
ISSN 1916-9701 (Online)

INTERNATIONAL JOURNAL OF CHEMISTRY

Vol. 1, No. 2
August 2009



Canadian Center of Science and Education

Editorial Board

- Anne Brown Canadian Center of Science and Education, Canada
- Dilip Venkatrao Jarikote University College Dublin, Ireland
- Guy L. Plourde University of Northern British Columbia, Canada
- Ismail Ab Rahman Universiti Sains Malaysia, Malaysia
- Jiantao Guo The Scripps Research Institute, USA
- Jignasu P Mehta Bhavnagar University, India
- K. Girish Kumar Cochin University of Science and Technology, India
- Konstantinos Kasiotis Benaki Phytopathological Institute, Greece
- Mohamed Abass Ain Shams University, Egypt
- Monira Nessem Michael National institute of standards (NIS), Egypt
- Pankaj Das Dibrugarh University, India
- Patrick Marcel Schaeffer James Cook University, Australia
- Prathapan Sreedharan Cochin University of Science and Technology, India
- R. K. Dey Birla Institute of Technology, India
- Sagar Pal Birla Institute of Technology, India
- Shyamal Kumar Chattopadhyay Bengal Engineering and Science University, India
- Sirshendu De Indian Institute of Technology, India
- Sujatha. C.H Cochin University of Science and Technology, India
- Sushil Kumar Kansal Panjab University, India
- Waseem Hassan Universidade Federal de Santa Maria, Brazil



Contents

Organochlorine Pesticides Residues in Mussels of Greek Island Evia <i>Konstantinos M. Kasiotis</i>	2
Study on the Structure and Properties of a Hybrid Resins <i>Mingkang An, Daofang Shi & Guojun wang</i>	10
Synthesis of Oligomers of 12-Acryloyloxydodecanoic Acid via Reversible Addition Fragmentation Transfer (RAFT) Polymerisation <i>Lilian Tichagwa, Ron D. Sanderson & Harald Pasch</i>	20
Fiber Splitting of Bicomponent Meltblown Nonwovens by Ultrasonic Wave <i>Xiaobin Wang, Jinbo Yao & Xianmiao Pan</i>	26
Organotin(IV) Derivatives of N-Tolyl- <i>m</i> -methoxybenzohydroxamic Acid: Synthesis and Structural Elucidation <i>Abdualbasit Graisa, Yang Farina, Emad Yousif & Elhadi Elbay Saad</i>	34
Studies on Thermal, Mechanical and Morphological Behaviour of Caprolactam Blocked Methylenediphenyl Diisocyanate and Bismaleimide Modified Epoxy Matrices <i>Daofang Shi, Mingkang An & Guojun Wang</i>	48
Evaluate the Effectiveness of the Natural Cosmetic Product Compared to Chemical-Based Products <i>Qiushi Chen</i>	57
Preparation and Characterization of Nonwoven Polypropylene Fabric Irradiation-grafted with Acrylic Acid as Weakly Acidic Cation Exchange Fiber <i>Li Wei, Junfu Wei, Feng Yuan & Jing Dong</i>	60
A Study of Electrospinning of Degradable Polyesters <i>Binghui Wang, Gaojie Yun & Wenfan Li</i>	68
Study on Chemical Composition of <i>Nauclea Officinalis</i> Leaves <i>Kui Su, Min Gong, Jing Zhou & Shiming Deng</i>	77
Research on Antifouling and Easy Decontaminating by a New Method <i>Xiaojie Liang & Jinbo Yao</i>	83



Organochlorine Pesticides Residues in Mussels of Greek Island Evia

Konstantinos M. Kasiotis (Corresponding author)

Laboratory of Pesticides Toxicology, Benaki Phytopathological Institute

8 St. Delta Street, PO box 14561, Athens, Kifissia, Greece

Tel: 30-210-818-0384 E-mail: K.Kasiotis@bpi.gr

Abstract

A simple and effective analytical procedure was developed for the determination of some organochlorine residues in mussel samples of two sampling points in Evia Island, Greece. The sample extraction was performed on lyophilized samples using either the Microwave Assisted Solvent Extraction (MASE) or the Soxhlet extraction technique. Using both techniques aldrin, endrin and endosulfan sulfate were determined. The quantification of these pesticides was carried out by Gas Chromatography-Mass Spectrometry (GC-MS) working in the Selected Ion Monitoring (SIM) mode and the recoveries ranged from 75 to 102% at two spiking levels for 6 replicates.

Keywords: Organochlorine pesticides, GC-MS, Mussels, Microwave, Soxhlet, SIM mode

1. Introduction

The outburst of technological development and the continuously increasing population have resulted in enlarged production of basic agricultural products whose production and provision is associated with chemicals of organic origin applicable in cultivation. The latter, which is a result of human activities on land, are very persistent, and through the aquifer, end up into the aquatic environment. Persistent Organic Pollutants (POPs) are compounds that resist photochemical, biological and chemical degradation (Edujje, G. H., Kanan et. al 1994, Parimi et. al 2006). As hydrophobic compounds they display high affinity for lipids and a tendency to accumulate in marine organisms. Consequently, they bio-accumulate through the food chain causing damages to the human health and environment.

Organochlorine Pesticides (OCPs) are synthetic compounds which are common pollutants in coastal areas and estuaries (Perugini et. al 2004, Khaled et. al 2004). Their presence -including their metabolites- is of great importance since they are related to chronic adverse effects on both humans and wildlife. Despite the banning of PolyChlorinated Biphenyls (PCBs) and DichloroDiphenylTrichloroethanes (DDTs) since the early 1970s, in many countries (including Greece) these compounds are still found in analyses performed in various matrices, indicating either that they are still applied, or the fact that they are quite stable and persistent in many kinds of environmental media.

Organisms of aquatic environments can serve as typical media for the assessment of marine pollution. Previous studies have pointed to the usefulness of mussels as geographic bioindicators of chemical contamination. Therefore, they continue to be analyzed for the monitoring of marine environment pollution (Kurt, P.B., Ozkoc, H.B. 2004). In Greece, mussels are the only shellfish bred in large quantities. Mussels (*Mytilus Galloprovincialis*) have been used as biomarkers for the assessment of heavy metals' pollution in coastal areas (Vlahogianni et. al 2007, Richardson et. al 2008). Moreover, as it has been previously mentioned, several studies have shown that organic contaminants, such as OCPs, tend to accumulate in mussel tissues (Ozkoc et. al 2007). As a result, the estimation of the levels of OCPs can conceivably provide us either with valuable information regarding the pollution of the aquatic environment or possible human being exposure through dietary intake.

The marine environment in Evia is a characteristic example for the plethora of aquatic organisms. Although the 95% of mussels are bred in Northern Greece (Batzios et. al 2004), Evia still holds a significant position among Greece's top quality indigenous environments for bivalves, either in marine farm companies or by mere fishing. Nevertheless knowledge of the occurrence of OCPs compounds in the Evia's coastal area is extremely limited. Western and Central Evia are possibly affected by the sewage dumping of Chalkida, the capital of the island. Industrial waste spread throughout the island and shipping related pollution can possibly affect the coastal area. The latter, which is in

opposition to the continental Greece, can indirectly be influenced from the sewage and industrial waste that originate from the metropolitan region of adjacent Attica.

For the analysis purposes, an extraction with organic solvents takes place, and then a cleanup step, column fractionation and Gas Chromatography coupled with various detectors such as Mass Spectrometer or electron capture detector (GC-ECD). Liquid Chromatography Mass Spectrometry (LC-MS) has also been used as means for the determination and quantification of toxins in Greek Mussels (*Mytilus Galloprovincialis*) (Ciminiello et. al 2006).

2. Materials and Methods

2.1 Study Area and Sampling Points

This study focused on the analysis of indigenous mussels cultured on the island of Evia, Greece (Figure 1). This region is known for the bivalves' productions in which mussels (*Mytilus Galloprovincialis*) are included.

Mussels (*M. galloprovincialis*, 6-7cm shell length), never before being exposed to growth stimulants, were collected (1/2 kg) at Karystos in Southwest Evia island during September 2008. The second sample (1/2 kg) of *M. galloprovincialis* was collected in the territory of Orei at Northwest Evia during September 2008. Thus, neither of the samples was collected from territories near Chalkida city. This was decided on the basis of assessment of mussels' pollution away from a possibly highly affected area, since Chalkida and its surroundings have an active industrial zone and a plethora of agricultural activities.

Immediately after collection, mussels were transferred fresh into an ice cool box to the laboratory where they were dissected. After sucking the whole soft tissues of mussels from the two locations, they were pooled, homogenized, transferred to beakers and lyophilized. The resultant reddish-brown powder was further analyzed.

2.2 Reagents and Materials

Organochlorine pesticides standard solutions for aldrin, endrin, dieldrin, α -endosulfan, β -endosulfan and endosulfan sulfate were prepared from the respective standards purchased from Supelco (Bellefonte, PA, USA). All solvents used were pesticide residue analysis grade from Merck (Darmstadt, Germany).

2.3 Soxhlet Extraction

The approach of extracting organic compounds from various matrices with Soxhlet apparatus is popular within toxicologists who are involved in the identification of toxic substances in biological organisms or plants. In this context, 7 g of lyophilized mussels were placed with equal amount of sodium sulfate at the bottom of the Soxhlet apparatus covered above with glass wool. The solvent of choice was *n*-hexane (200 mL) and the extraction time was 6 hours. After the extraction the solvent was removed in vacuum and the mixture was reconstituted with hexane, SPE filtered and eluted directly to the gas chromatograph mass spectrometer (GC-MS).

2.4 Microwave-Assisted Solvent Extraction (MASE)

Microwave assisted extraction is a time and cost effective way of extracting valuable compounds from lyophilized or non lyophilized biological samples (García et. al 2008). In this case the mussels were homogenized, lyophilized and then placed in a specific Teflon vessel used in the microwave extractor apparatus (CEM Corporation, MARS microwave extractor). The solvent of choice was *n*-hexane (60 mL) and it was applied to 2.1 g of lyophilized mussels in order to be comparable with the amounts used in the Soxhlet extraction. Equal volume of *n*-hexane was placed in an anti-parallel vessel into the extractor. The program used in the latter extraction is the following: Functioning of MARS extractor at 800Watt, with gradual increase of temperature reaching 100°C in 10 min, and staying at that temperature for 15 min. A subsequent cool down period of 5 min was applied. By prolongation of the time of MASE extraction it was not obtained higher concentration of the compounds analyzed.

2.5 Solid Phase Extraction (SPE) - Purification

SPE was applied prior to the injection to the GC-MS system. For this purpose an IST VacMaster apparatus was used with the appropriate vacuum pump and the respective Florisil SPE cartridges (Waters, SEP-PAK[®] Cartridges). Three fractions were collected after elution with hexane, hexane/dichloromethane 5:5 and pure dichloromethane in equal volumes (5 mL) in order to extract compounds of variable polarity. Aldrin was identified in the hexane fraction, endrin and dieldrin in the hexane/dichloromethane fraction. As far as the endosulfan group is concerned, endosulfan-a was collected from the second fraction while endosulfan-b and endosulfan sulfate from the dichloromethane fraction. The extracts were evaporated by a gentle stream of nitrogen until the volume of 2 ml.

2.6 Gas Chromatographic Conditions

Analysis was carried out on an Agilent 6890N chromatograph equipped with a split-splitless injector and a 5975B inert XL EI/CI MSD (Agilent Technologies) connected to MSDChemStation G1701 DA MSD software, version D.03.00.611. The capillary column was a DB-5MS (30m × 0.25mm × 1.0 μm) with 5% diphenyl-95% dimethylsiloxane. The injector and detector were operated at 300°C and 280°C, respectively. The sample (1 μL) was injected into the pulsed splitless

mode and the oven temperature was programmed as follows: 100 °C for 2 min, raised to 180°C (15°C /min), raised to 240°C (3°C /min), raised to 285°C (10°C /min) for 10 min. Helium was the carrier gas (1.8 mL/min) and nitrogen (30 mL/min) the make-up gas.

3. Results and Discussion

3.1 Validation of the Analytical Method

The linear dynamic range, recovery, precision, limits of detection (LOD) and quantification (LOQ) were established for the validation of the developed analytical method. For the linear dynamic range, the calibration samples were prepared using appropriate dilution of the stock aldrin, endrin, dieldrin, α -endosulfan, β -endosulfan and endosulfan sulphate (stock solutions of 100 ppm for each pesticide) solutions in *n*-hexane. Five concentration levels were studied with 3 replicates at each level. Good linearity of the response was found at specific concentration range indicated in Table 1, with the respective correlation coefficient (r^2) for each pesticide.

3.2 Limit of Detection – Limit of Quantification, Precision

The LOD and LOQ were determined via statistical calculations using calibration plots established at concentration levels close to the expected LOD. The LOD was defined as $3.3(Sy/x)/a$ and the LOQ as $10(Sy/x)/a$, where Sy/x represents the residual standard deviation and a is the slope of the calibration plot. Thus, retention time, LOD, LOQ and the respective m/z monitored in the SIM mode are depicted in Table 2.

Recovery was assessed using spiked mussel samples at two concentration levels. The recovery of each active substance from the matrix was the main criteria for quantitative quality control of the analytical results of the present work. The recovery was studied in the laboratory as part of the method validation. The applied analytical method for the determination of aldrin, endrin and endosulfan sulfate covered the needs of the present study. Satisfactory results were obtained for all levels with recoveries for low and high concentrations, well above the cut off value of 70%. RSD's for both low and high concentrations were < 5%. The precision of the method was studied by measuring the repeatability (intra-day) and reproducibility (inter-day) of the results obtained. For repeatability studies, five analyses of standard - spiked mussels samples were successively analyzed in 1 day (Table 3). The inter-day precision was tested by analysis of standard-spiked mussels samples (Table 3) for five consecutive days.

The obtained RSD values are depicted in Table 3 and ranged from 4.8% to 9.2% (intra-day precision) and from 5.3% to 11.1% for inter-day precision (as expected since the RSD values for inter-day precision are usually higher than the ones of intra-day) - for all analytes – confirming the satisfactory performance of the methodology developed in this work.

3.3 Analysis

In Table 4 the concentrations of the pesticides found are depicted. Aldrin and endrin were detected by both MASE and Soxhlet technique with concentrations above the corresponding LOD. Endosulfan sulphate was also detected when both techniques were employed. Furthermore traces of dieldrin were detected by MASE extraction in the sample of Orei region however they were below the corresponding LOD and thus not quantified. Figure 2 shows the magnified GC-chromatogram of the area where aldrin is eluted and in Figure 3 the respective m/z ratios for aldrin. The chemical structure of the fragment ions of the selected pesticides are an outcome of ionization, successive chlorine loss and sometimes ring saturation. A characteristic fragment of aldrin is the one which corresponds to the loss of two chlorine atoms and one hydrogen atom to form the $[M-2Cl-H]$ fragment at 293 (m/z value). Moreover the typical fragment at 263 (m/z value) corresponds in the case of endrin to $C_7H_3Cl_5$. This fragment also appears in the case of aldrin and dieldrin. For endosulfan sulphate the base peak is m/z 387 and represents the loss of HCl group from the molecular ion.

The confirmation of the aldrin existence was achieved by spiking with aldrin the vial with the real mussel sample. The increase in the abundance of aldrin peak at the same retention time indicated the aldrin presence in the Karystos sample (Figure 4 and 5). By following the same procedures endrin and endosulfan sulphate were detected and quantified.

3.4 Levels of Organochlorine Pesticides-Comparison with Similar Matrices at Different Sampling Points

In the whole Mediterranean Sea, the bivalve *Mytilus galloprovincialis* and the red mullet (*Mullus* sp.) have been immensely studied reflecting the contamination which can be attributed to the land based origin (sediment). The findings of this research can be compared with the mussel watch survey which was conducted in 1973/1974 and 1988-1989 along the Mediterranean Coast of France and Italy by Villeneuve et. al (1999), between Sete and Genoa. In this research it was found that concentrations of DDTs were the highest ranging from 20 to 630 ng g^{-1} (dry wt.).

Traces of dieldrin which were found in our case are less than the concentration findings of Villeneuve et. al (1.8-36 ng g^{-1} dry wt.) indicating the gradual decrease of this pesticide in mussels and seawater although the sampling stations (points) were not the same. Aldrin and endrin levels in Karystos samples are surprisingly higher than the levels in Villeneuve's report (which were less than 1 ng g^{-1} dry wt for aldrin and less than 2.3 ng g^{-1} dry wt for endrin), indicating the persistent character of these two pesticides in the specific seawater sampling point.

A variety of scientific efforts have also been extensively carried out in Mediterranean coastal waters near Alexandria, Egypt (Barakat, A.O. 2004). In seawater aldrin was determined in the range of (10-70 ng/L), dieldrin (<0.1-5 ng/L) and endrin between <0.1-53 ng/L. Cyclodiene pesticides (aldrin, endrin, dieldrin) concentrations were also detected in bivalves (*Donax* sp) in the same study below 2 ng g⁻¹ ww. Similar conclusions in this report were derived for fish and aquatic birds. Another scientific research which was conducted by Kucuksezigin (Kucuksezigin et. al 2001) in Eastern Mediterranean (Aegean Sea) revealed the levels of aldrin in red mullet. The levels of aldrin varied between 0.10 and 0.61 ng g⁻¹ dry wt. It must also be reported the large survey conducted in United States (US) concerning the chemicals concentrations in mussels and oysters which were collected along US and updates until 2003 (O'Connor, T.P., Lauenstein, G.G. 2006).

The findings of this research indicate the need for an expanded survey regarding Evia Island which is one of the largest islands of the Mediterranean basin in order to assess in depth the presence or absence of a variety of pesticides which were used in the past or are administered nowadays near to Evias' coastal areas. The high levels of cyclodienes detected constitutes an intriguing target for scientists implemented in toxicology or aquatic environmental studies in order to control the pollution and inform the population involved in fishing or live to adjacent coastal areas (Carreño et. al 2007).

4. Conclusions

In this report it was developed a new analytical method for the detection of six organochlorine pesticides in mussels whose origin is Evia Island, Greece. The results of this research showed the presence of residues of aldrin, endrin and endosulfan sulfate although these pesticides are banned. By MASE technique higher concentrations of the identified pesticides were obtained than with the typical Soxhlet. The persistence of organochlorines in the aquatic environment raises problems of chronic toxicity to humans who are frequently exposed to these contaminants, either by bivalves or fish-related dietary intake or by work-related exposure. Thus, repetitive and continuous examination and analysis of these bivalves and other marine organisms is required in order to assess their contamination levels and control with safety the subsequent provision to humans.

References

- Barakat, A.O. (2004). Assessment of persistent toxic substances in the environment of Egypt. *Environment International*, 30, 309-322.
- Batzios, C., Angelidis, P., Papapanagiotou, E. P., Moutopoulos, D. K., Anastasiadou, C., Chrisopolitou, V. (2004). Greek consumers image of the cultured mussel market. *Aquaculture International*, 12, 239-257.
- Carreño, J., Rivas, A., Granada, A., Lopez-Espinosa, M.J., Mariscal, M., Olea, N., Olea-Serrano, F. (2007). Exposure of young men to organochlorine pesticides in Southern Spain. *Environmental Research*, 103, 55-61.
- Ciminiello, P., Dell' Aversano, C., Fattorusso, E., Forino, M., Magno, S., Santelia, F., Tsoukatou, M. (2006). Investigation of the toxin profile of Greek mussels *Mytilus galloprovincialis* by liquid chromatography-mass spectrometry. *Toxicon*, 47, 174-181.
- Eduljee, G.H. *Budget and source inventories: issues and challenges*. In: Harrad, S. (Ed.) *Persistent Organic Pollution: Environmental Behaviour and Pathways for Human Exposure*. Kluwer Academic Publishers, London, pp. 1-28.
- García, I., Ignacio, M., Mouteira, A., Cobas, J., Carro, M. (2008). Assisted solvent extraction and ion-trap tandem mass spectrometry for the determination of polychlorinated biphenyls in mussels. Comparison with other extraction techniques. *Analytical Bioanalytical Chemistry*, 390, 729-737.
- Kannan, K., Tanabe, S., Williams, R.J., & Tatsukawa, R. (1994). Persistent organochlorine residues in foodstuffs from Australia, Papua New Guinea and the Solomon Islands: contamination levels and human dietary exposure. *Science of the Total Environment*, 153, 29-49.
- Khaled, A., El Nemr, A., Said, T.O., El-Sikaily, A., Abd-Alla, A.M.A. (2004). Polychlorinated Biphenyls and chlorinated pesticides in mussels from the Egyptian Red Sea Coast. *Chemosphere*, 54, 1407-1412.
- Kucuksezigin, F., Altay, O., Uluturhan, E., Kontas, A. (2001). Trace metal and organochlorine residue levels in red mullet (*Mullus Barbatous*) from the Eastern Aegean, Turkey. *Water Research*, 35, 2327-2332.
- Kurt, P.B., Ozkoc, H.B. (2004). A survey to determine levels of chlorinated pesticides and PCBs in mussels and seawater from the mid Black Sea coast of Turkey *Marine Pollution Bulletin*, 48, 1076-1083.
- O'Connor, T.P.; Lauenstein, G.G. (2006). Trends in chemical concentrations in mussels and oysters collected along the US coast: Update to 2003. *Marine Environmental Research* 62, 261-285.
- Ozkoc, H.B., Bakan, G., Ariman, S. (2007). Distribution and bioaccumulation of organochlorine pesticides along the Black Sea coast. *Environmental Geochemistry and Health*, 29, 59-68.

Parimi, S., Meinke, L.J., French, B.W., Chandler, L.D., Siegfried, B.D. (2006). Stability and persistence of aldrin and methyl-parathion resistance in western corn rootworm populations (coleoptera: chrysomelidae). *Crop Protection*, 25, 269-274.

Perugini, M., Cavaliere, M., Giammarino, A., Mazzone, P., Olivieri, V., Amorena, M. (2004). Levels of polychlorinated biphenyls and organochlorine pesticides in some edible marine organisms from the Central Adriatic Sea. *Chemosphere*, 57, 391-400.

Richardson B.J., Mak, E., De Luca-Abbott, S.B., Martin, M., McCellan, K., Lam, P.K.S. (2008). Antioxidant responses to polycyclic aromatic hydrocarbons and organochlorine pesticides in green-lipped mussels (*Perna Viridis*): Do mussels “integrate” biomarker responses? *Marine Pollution Bulletin*, 57, 503-514.

Villeneuve, J.P., Carvalho, F.P., Fowler, S.W., Cattini, C. (1999). Levels of PCBs, chlorinated pesticides and petroleum hydrocarbons in mussels from the NW Mediterranean Coast: comparison of concentrations in 1973/1974 and 1988/1989. *Science of the Total Environment*, 237/238, 57-65.

Vlahogianni, T., Dassenakis, M., Scoullou, M. J., Valavanidis, A. (2007). Integrated use of biomarkers (superoxide bismutase, catalase and lipid peroxidation) in mussels for assessing heavy metals' pollution in coastal areas from the Saronikos Gulf of Greece. *Marine Pollution Bulletin*, 54, 1361-1371.

Table 1. Calibration data, concentration range and linearity of the studied OCs

OCPs	Equation	Range (µg/mL)	Linearity (r ²)
aldrin	y = 1354925x + 8719	0.02-0.10	>0.993
endrin	y = 319268x + 30752	0.02-0.20	>0.999
dieldrin	y = 92467x - 2555	0.20-1.10	>0.997
α-endosulfan	y = 63023x + 3192	0.27-1.20	>0.999
β-endosulfan	y = 43495x + 1344	0.10-1.00	>0.999
endosulfan sulfate	y = 73969x - 22094	0.50-2.00	>0.995

Table 2. Retention times for the OCs, limits of detection and quantification (LOD, LOQ) and selected ions of the studied OCs

OCs	t _R (min)	LOD ^a	LOQ ^a	m/z
aldrin	24.28	0.014	0.044	66, 79, 91, 263, 265, 293
endrin	30.58	0.068	0.205	67, 79, 81, 82, 263, 281, 317, 345
Dieldrin	29.74	0.069	0.212	79, 263, 265, 277
α-endosulfan	28.55	0.042	0.126	207, 237, 241, 339
β-endosulfan	30.99	0.018	0.054	195, 237, 339
endosulfan sulfate	32.25	0.164	0.497	272, 274, 387

^a(µg/mL)

Table 3. Results of the precision for the proposed method of organochlorine pesticides in mussels samples

Pesticides	Spiking level ^a	Intra-day precision	Inter-day precision
		(R.S.D.%)	(R.S.D.%)
aldrin	0.05	8.1	8.8
endrin	0.10	5.6	6.2
dieldrin	0.60	6.5	6.9
α -endosulfan	0.70	9.2	9.6
β -endosulfan	0.55	4.8	5.3
Endosulfan sulfate	1.10	9.1	11.1

^a ($\mu\text{g/mL}$)

Table 4. Pesticides detected and the respective concentrations

OCs	<i>Orei</i>	<i>Orei</i>	<i>Karystos</i>	<i>Karystos</i>
aldrin	n.d. ^a	n.d. ^a	0.043	0.057
endrin	n.d. ^a	n.d. ^a	0.117	0.178
Dieldrin	n.d. ^a	n.d. ^c	n.d. ^a	n.d. ^a
α -endosulfan	n.d. ^a	n.d. ^a	n.d. ^a	n.d. ^a
β -endosulfan	n.d. ^a	n.d. ^a	n.d. ^a	n.d. ^a
endosulfan	0.519	0.615	n.d. ^a	n.d. ^a

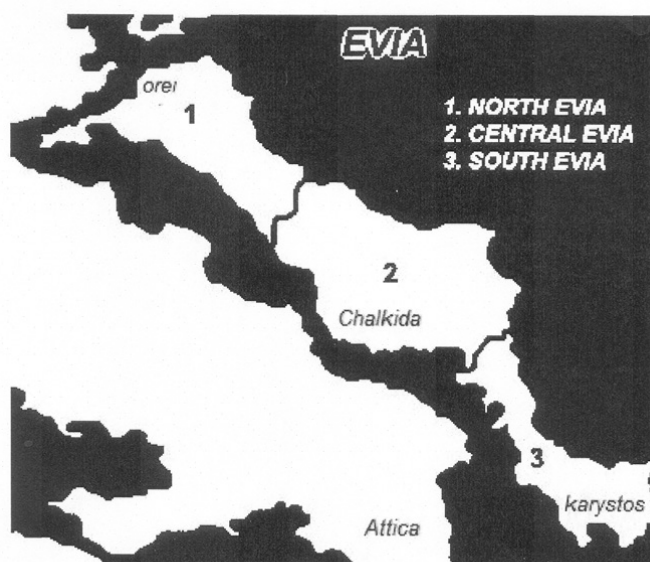
^a not detected; ^b concentrations in ($\mu\text{g/mL}$); ^c traces of the compound were detected

Figure 1. Map with sampling areas

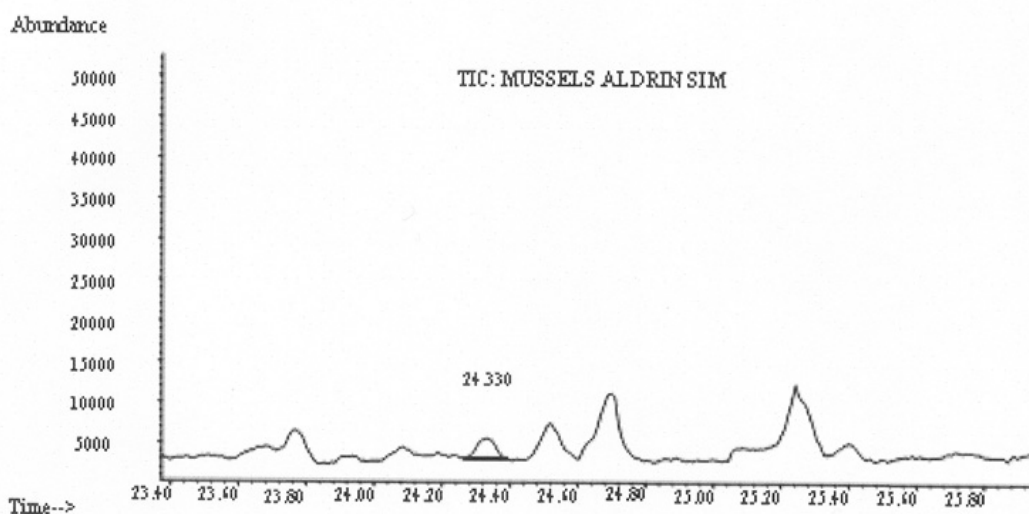


Figure 2. Magnified GC chromatogram of aldrin in real mussel sample of Karystos

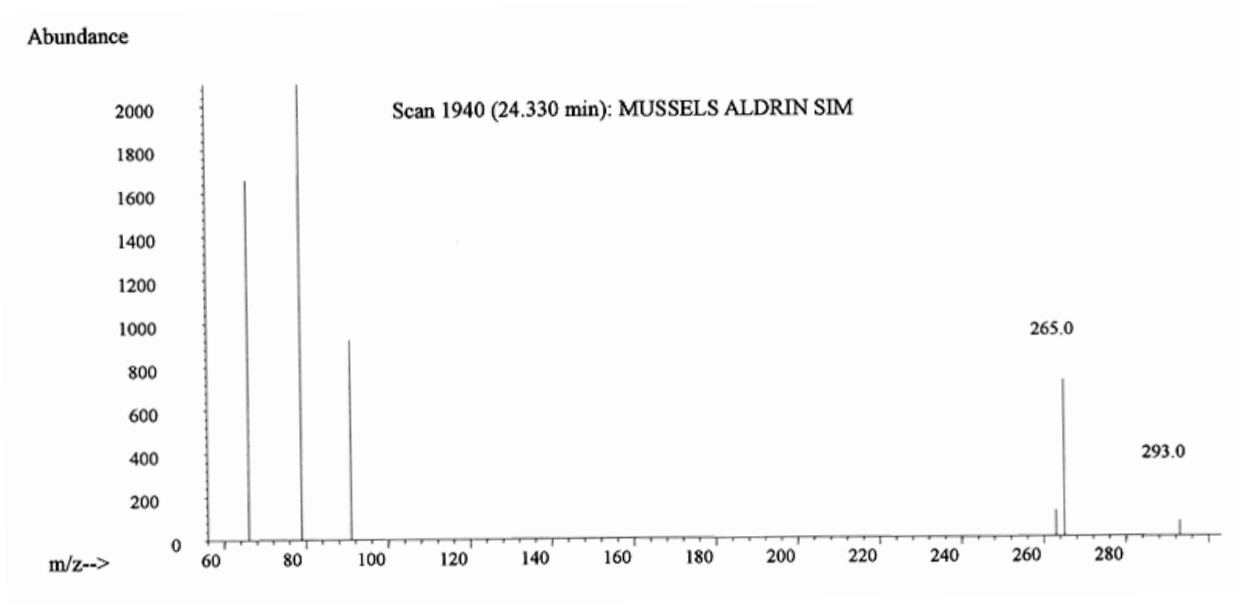


Figure 3. Respective m/z ratios for aldrin

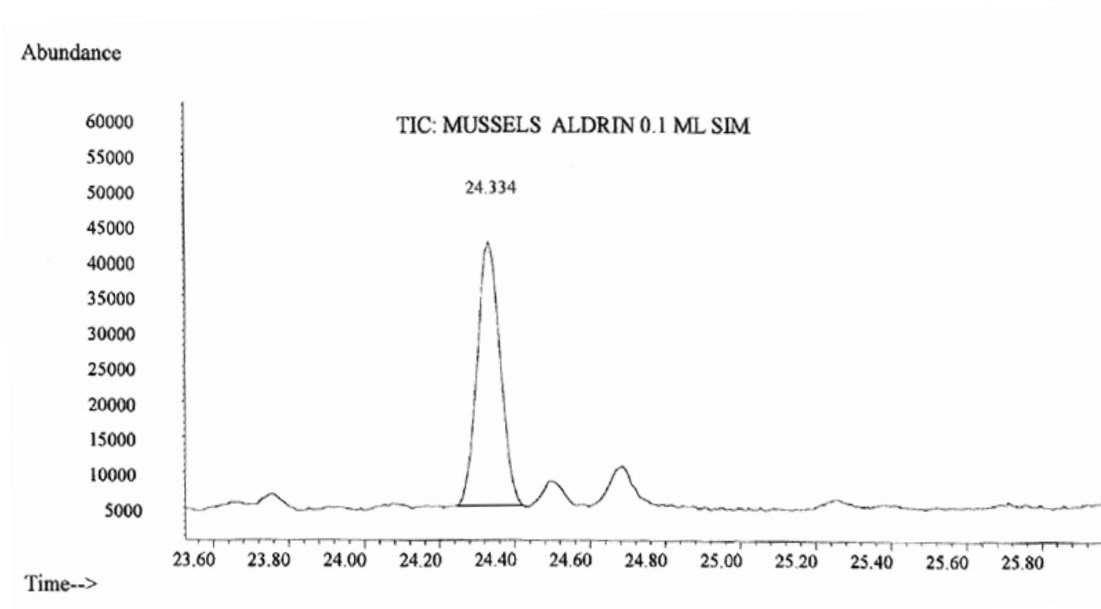


Figure 4. GC chromatogram of spiked with aldrin mussel sample

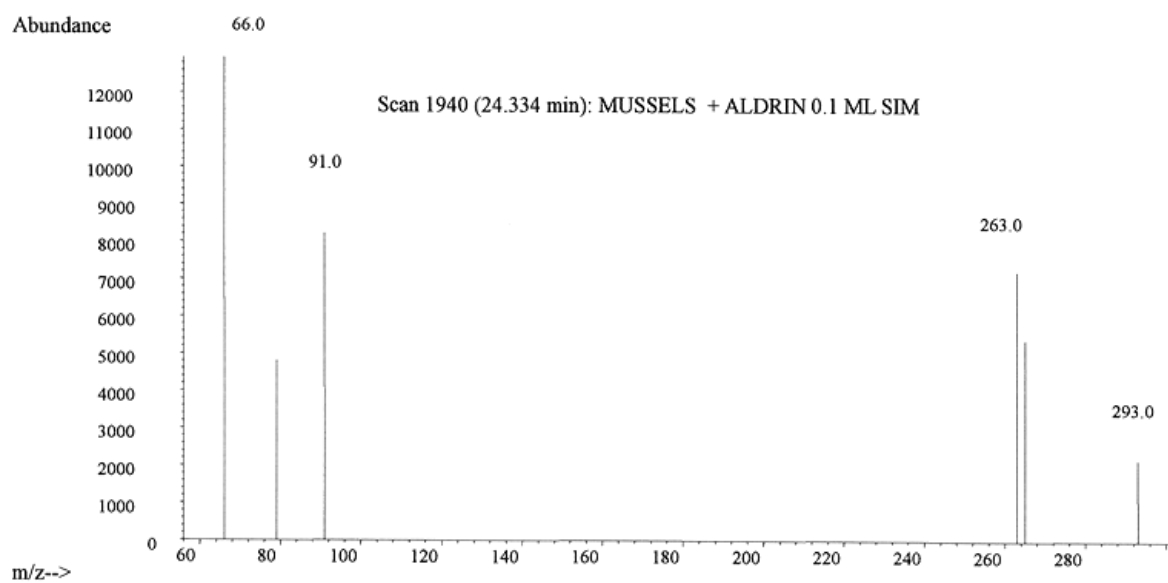


Figure 5. Respective m/z ratios for aldrin in the spiked sample



Study on the Structure and Properties of a Hybrid Resins

Mingkang An

Tianjin Polytechnic University

NO.63 Cheng Lin Zhuang Road, Tianjin 300160, China

E-mail: amk_8496@126.com

Daofang Shi

Tianjin Polytechnic University

NO.63 Cheng Lin Zhuang Road, Tianjin 300160, China

E-mail: sdf_1103@126.com

Guojun wang

Tianjin Polytechnic University

NO.63 Cheng Lin Zhuang Road, Tianjin 300160, China

E-mail: wangguojun1001@163.com

Abstract

Polysilicate modified polyurea/vinyl ester hybrid resins were produced by dispersing water glass (WG) in a mixture of vinyl ester (VE) and polyisocyanate in presence of a liquid phosphate as emulsifier. As styrene-crosslinkable VE resins bisphenol A (BA) and novolac types (N), whereas as polyisocyanate a polymeric methylene diphenyl isocyanate (PMDI) were used. The structure and selected properties of the hybrid resins were determined and compared to those of the neat VEs and polysilicate filled polyurea (denoted as 3P resin). Using VE for resin hybridization, which worked as an additional emulsifier for the WG/PMDI/phosphate system, resulted in a fine particle dispersion of the polysilicate. It was found that the type of VE affected not only the dispersion of WG (and thus of the polysilicate) but also the network formation of the polyurea/VE hybrids and their properties. Information about the structure of the polysilicate filled hybrid resins was gained from dynamic-mechanical thermal analysis (DMTA), scanning electron and atomic force microscopic measurements. It was argued that the resin hybridization yielded a conetwork instead of an interpenetrating one. The properties of the hybrid systems were determined by DMTA, fracture mechanical tests, thermogravimetric analysis and flammability measurements. It was established that the stiffness and resistance to thermal degradation of the initial 3P resin was strongly improved by hybridization with VEs. The fracture toughness (K_{Ic}) proved to be less sensitive to the formulation of the hybrid resins. On the other hand, the fracture energy (G_c) and limiting oxygen index experienced a positive deviation from the additivity as a function of the 3P/VE composition, at least in a given range.

Keywords: Fracture mechanics, Morphology, Network formation, Polyisocyanate, Polyurea, Vinyl esterresin, Water glass, Polysilicate

1. Introduction

Inorganic-organic hybrid materials became under spot of interest due to the beneficial combination of properties of polymers and ceramics. Nowadays considerable efforts are dedicated to produce composites in which the fillers of different aspect ratios are nano-scaled dispersed in the polymer matrix. This problem has been studied previously (Nalwa, 2003, and Utracki, 2004). For the in situ production of the inorganic phase usually different routes of the sol-gel chemistry are followed. This problem has been studied previously (Nalwa, 2003, and Kickelbick, 2003, pp.83-114). The related precursor compounds are mostly alkoxysilanes-titanates and the like, which all are rather expensive. Water glass (WG) can be considered as a cheap alternative precursor. Note that the sol-gel transition of WG (termed also to hardening, silicification) is known from ancient times. This problem has been studied

previously(Stoye,1993, p.94-96). The basic reaction of the silicification when induced by atmospheric CO₂ is given by:



Silica gel (Hydro- or xerogel)

The above reaction can be reproduced when dispersing WG in polymeric isocyanates. In the corresponding water (WG)-in-oil (polyisocyanate) type emulsion (W/O) the isocyanate groups react first with water via releasing CO₂:



The primary amine group reacts with the isocyanate whereby a polyurea chain forms:



The CO₂ formed (cf. Eq. (2)) induces the silicification of WG (cf. Eq. (1)) resulting in polysilicate particles in the polyurea matrix. In order to control the course of reactions 1-3 an emulsifier is needed for which liquid phosphates proved to be the most suitable? This problem has been studied previously(US Patent 5 622 999,1997). The emulsifier is responsible for controlling the W/O-emulsion and slowing down the reaction of the polyurea formation (cf. Eq. (3)). In the final crosslinked product it works as plasticizer. Using polymeric isocyanates with a functionality of >2 crosslinked polyurea based composites can be produced. Recall that they contain polysilicate particles derived from the WG. This proprietary system marketed by Polinvent Ltd. (Budapest, Hungary) is denoted 3P resin (from polyisocyanate, phosphate, polysilicate). These resins possess some remarkable properties, such as curing under water which allows us the repair of leaking or corroded buried pipes without their digging. On the other hand, the mechanical properties and the resistance to thermal degradation of the 3P resins are modest. This is due to the complex chemistry of the related systems. Note that Eqs. (2) and (3) represent the major reactions apart from which several by-side reactions, such as di- and trimerisation of the isocyanates, biuret formation between the urea and isocyanates, etc. take place. It has to be mentioned here that the crosslinking chemistry of the 3P resin and its hybrids was not addressed in this work. This work was aimed at improving the mechanical and thermal properties of 3P a resin by hybridization with styrene-crosslinkable vinyl ester resins (VE). This patented hybridization strategy considers three major aspects. This problem has been studied previously(Hungarian Patent Application P04 01799,2004). First, VE resins can be additionally crosslinked by adding polyisocyanates. In the corresponding vinyl ester-urethane hybrids, marketed by DSM Composite Resins (Zwolle, The Netherlands), additional crosslinks form between the secondary -OH groups of VE and -NCO groups of the polyisocyanate. The crosslinking, properties and property modifications of such vinyl ester-urethane hybrids are well reported in the literature. This problem has been studied previously(Jost, 2002, p.1383-9; Gryshchuk, 2002, p.4763-8; Gryshchuk, 2002, p.672-80 and Gawdzik, 2001, p.2062-7). Second, VEs are known as chemically resistant and thus able to withstand strong alkali media such as WG. Third, the VE itself may act as an additional emulsifier for the dispersion of WG (W/O emulsion) and thus may also influence the WG-induced reactions. So, VE is expected to reduce the mean particle size of the in situ formed polysilicate phase and to form a conetwork with the polyisocyanate/polyurea through urethane formation. This occurs between the -NCO of the polyisocyanate and the -OH groups of the VE. Both above mentioned changes should be associated with an improvement of the properties according to our working hypothesis. The novel hybrid resins are foreseen as matrix materials for traditional composites which are produced by resin transfer molding and wet filament winding techniques.

2. Experimental

2.1 Formulations

Polymeric methylene diphenyl isocyanate (PMDI), Ongronat CR-30-60 was purchased from Borsodchem Rt (Kazincbarcika, Hungary) and exhibited the following characteristics: NCO content 30-31.5 wt%, viscosity: 520–680 mPa s. WG (Sodium silicate type, Betol 3P) was purchased from Woellner Silikat GmbH (Ludwigshafen, Deutschland). This WG had a modulus SiO₂/Na₂O=2.0±0.05, and viscosity: 600 ± 100 mPa. As primary emulsifier for the PMDI/WG system tris(1-chloro-2-propyl)phosphate (Fyrol PCF, Akzo Nobel, Duren, Germany) was used. The base 3P resin contained 42 wt% PMDI, 18 wt% phosphate and 40 wt% WG. For the hybridization of the above 3P resin a styrene diluted (30 wt%) bisphenol-A type VE (Daron-XP-45-A2) and novolac type VE (Atlac590 HV) of DSM Composite Resins (Zwolle, The Netherlands) were chosen. Their chemical build-up is given in Ref. For their crosslinking 1.5 phr (parts per 100 g of resin) dibenzoyl peroxide (peroxide content 50 wt%; Lucidol CH-50 L of Akzo Nobel, Duren, Germany) and 1.5 phr N,N-diethylaniline (active component content: 10 wt%; NL-64-10 of Akzo Nobel) served. The above VE resins are referred further on as VE (BA) and VE (N), respectively. In order to study the effect of resin hybridization, the formulations listed in Table 1 were prepared.

2.2 Preparation of the hybrid resins

The reference 3P resin was produced by homogenizing the phosphate with the PMDI with a propeller mixer (1 min,

2000 rpm). Then WG was introduced and dispersed to receive a stable W/O emulsion (1 min, 800 rpm). In case of the VE/3P hybrids first the peroxide was introduced in the VE and homogenized. Afterwards WG was added to this composition (denoted as A component) and mixed (1 min, 2000 rpm). In another beaker the component B was prepared. This contained the necessary amount of PMDI, phosphate and activator (the latter was used only for the neat VE resins) which were homogenized accordingly. The A and B components were then unified and homogenized again (1 min, 800 rpm).

All resulting mixtures were degassed in vacuo prior to pouring them into the moulds. Plates (170×10×4 mm) and compact tension (CT) specimens were produced by pouring the homogenized and degassed resins in PTFE moulds. Crosslinking of the resins occurred according to the following regime: room temperature for 20 h and 100 °C for 4 h.

2.3 Tests

The phase structure of the samples was characterized by dynamic-mechanical thermal analysis (DMTA). DMTA spectra were taken on rectangular specimens (50×10×4length×width×thickness) in flexural mode at 10 Hz using an Eplexor 150 N device of Gabo Qualimeter (Ahlden, Germany). The static and cyclic (sinusoidal) loading components were set for 10 N and 5 N, respectively. DMTA spectra, viz. complex modulus (E^*) and its constituents (storage and loss moduli, E' and E'' , respectively), mechanical loss factor ($\tan \delta$) as a function of temperature (T), were measured in the interval $T = -100 \dots + 200$ °C at a heating rate of 1 °C/min.

To determine the mean particle size and particle size distribution of the silicate phase the fracture surfaces of the CT specimens were inspected in a scanning electron microscope (SEM; JSM 5400 device of Jeol, Tokyo, Japan). The surfaces were coated with an Au/Pd alloy prior to SEM investigations. SEM pictures of minimum 3 showing more than 100 particles were taken into consideration when determining the particle size distribution. It is noteworthy that the related SEM pictures served also to deduce the major failure mechanisms.

For the thermogravimetric analysis (TGA) of the hybrids a TG50 device of Mettler Toledo (Giessen, Germany) was used. The TGA experiments were conducted in air in the temperature range $T = 25 \dots + 630$ °C with heating rate 10 °C/min.

To determine the flammability of the resins the limiting oxygen index (LOI) test according to ISO 4589-2 was performed. LOI means the minimum concentration of oxygen in a nitrogen/oxygen mixture which is required just to support the combustion of a test sample under specified test conditions. A material has fire retardant performance if its LOI value is higher than 21 vol% which is the concentration of oxygen in the air. The higher this value is, the better the flame resistance of the material is.

The fracture toughness (K_{Ic}) and fracture energy (G_c) were according to ISO 13586-1 standard. The tests were done with a Zwick universal testing machine type 1445 (Ulm, Germany) at room temperature (RT) with a crosshead speed of $v = 1$ mm/min. The CT-specimens (dimension: 35×35×4/thickness/mm³) were notched before loading by sawing. The sawn notch of the CT specimens was sharpened by producing a sharp crack with a razor blade that was placed on the notch root before hitting it in a fixing rig with a hammer.

3. Results and discussion

3.1 Phase structure

Fig. 1a displays the E_0 vs. T and $\tan \delta$ vs. T traces for the 3P, VE (BA) and their hybrid resins. One can recognize that combining 3P with VE (BA) the stiffness (E') is increased considerably at least below a given threshold temperature. The latter depends on the actual 3P/VE (BA) composition and lies between ca. 100 and 150 °C. One can also see that the E_0 values of the hybrids do not follow the trend with the compositional ratio in the whole temperature range (cf. Fig. 1a). The glass transition temperature (T_g), when assigned to the peak temperature of the $\tan \delta$ (cf. Fig. 1b), is increasing above a 3P/VE (BA) ratio of 75/25. It is noteworthy that the T_g of the neat 3P resin could not be determined due to premature failure of the tested specimen. Nevertheless, the related $\tan \delta$ vs. T trace suggests that it is at $T > 200$ °C. Note that the intensity of the $\tan \delta$ peak of VE (BA) is reduced owing to the hybridization with 3P and also broadened at the same time (cf. Fig. 1b).

The DMTA behavior of the hybrids 3P/VE (N) is similar to that of the 3P/VE (BA) variants. However, when comparing the E_0 vs. T traces in Figs. 1a and 2a, one can see that the stiffness is dominated by the VE (N) below $T \approx 50$ °C irrespective to its actual amount in the hybrids. Again the intensity of the T_g -relaxation of VE (N) is reduced through hybridization with the 3P resin. Moreover, the T_g -relaxation became broader and the T_g was shifted to higher values for composition 3P/VE (N) $\geq 75/25$ (cf. Fig. 2b).

The DMTA behavior of the hybrids suggests the formation of a heterogeneously crosslinked network. This may be a conetwork or a grafted interpenetrating one (g/IPN). As a g/IPN should be phase-segregated while a conetwork not, attempt was made to shed light on this issue by AFM.

Completely different, but still nanostructured morphology can be concluded for the 3P resin. The related heterogeneity

is likely the outcome of the various chemical reactions involved in the crosslinking of this 3P resin. Note that the related crosslinking pathway is not yet known.

The morphology of the hybrids 3P/VE (BA) = 75/25 and = 50/50 resembles to that of the neat 3P. One can claim that in these hybrids a conetwork has been formed. So, the styrene crosslinkable VE has been built in the polyurea-based network mostly through the reactions between the -NCO groups of PMDI and -OH groups of the VE. Effects of the compositional ratio in the hybrids should appear-among others- in their mechanical behavior at higher temperatures. This expectation is based on the DMTA behavior of the hybrids as shown before (cf. corresponding E' vs. T traces in Fig. 1a).

The structure of the 3P/VE (BA) = 25/75 differed markedly from that of the neat 3P and its hybrids at high 3P contents. In this system, a phase-segregated nanogel structure is present showing clear similarities with that of the crosslinked VE (BA)

It is worth of noting that the phase structure of the 3P/VE (N) hybrids was similar to the 3P/VE (BA) formulations (and thus not shown here). The only exception was noticed for the 3P/VE (N) = 25/75 hybrid for which the g/IPN structure (if any) was poorly resolved. This finding is, however, in concert with the DMTA behavior – cf. corresponding E' vs. T trace in Fig. 2a.

3.2 Polysilicate dispersion

Characteristic SEM pictures taken from the fracture surfaces of the 3P/VE hybrids are depicted in Fig.3.

One can observe that the VE worked as additional emulsifier for the initial W/O-type emulsion (i.e. WG dispersed in PMDI and phosphate) as expected. This corroborates our earlier results achieved however on a different VE (BA)/3P system. The hybrid system reported in Ref. differed from the present one not only in the base 3P resin composition but also in the WG and phosphate used. The main particle size of the polysilicate was reduced owing to the emulsifying action of the VE. Parallel to that the distribution of the polysilicate particles became narrower. The latter was characterized by the ratio of the weight (dw) to number-average mean particle size (dn) – cf. Table2.

SEM pictures in Fig.3 and the data in Table 2 indicate that VE (N) is a slightly better emulsifier than VE (BA). It is noteworthy that a finer and more uniformly dispersed silicate phase should be associated with improvements in the mechanical performance. This expectation is based on the fact that in such systems the stress concentration field induced by the particles is leveled off which depresses premature failure of the specimens.

3.3 Thermal and flame resistance behavior

The first indication that the hybridization followed might have affected the thermal resistance was delivered. Recall that the ablation induced by Ar^+ ion bombardment is basically a thermal degradation process. The TGA curves (mass loss vs. T) for the 3P and its hybrids with VE (BA) and VE (N) are shown in Figs. 4 and 5. Note that the 3P resins starts to degrade at rather low temperature ($T \approx 150^\circ C$), however, becomes markedly stable to thermal degradation at higher temperatures ($T > 400^\circ C$) – cf. Figs.4 and 5. On the other hand, both VEs are quite stable initially (up to ca. $350^\circ C$), but degrade very fast and almost without residue afterwards. It has to be mentioned that no attempt was made to determine the degradation kinetics and trace the related products in this work. The TGA traces in Figs.4 and 5 suggest that the change in the thermal resistance as a function of the VE/3P composition follows in the first approximation the additivity rule (rule of mixture), at least for selected temperature intervals. A similar statement holds for the LOI results, However, The results indicate for the presence of some synergistic effect in the VE/3P range 50/50. . 75/25. It has to be mentioned that outstanding flame resistance of the 3P resin is owing to the chlorine-containing phosphate which was used as primary emulsifier in our case. The positive effect of this chlorine-containing phosphate is well resolved for the VE/3P hybrids, as well. The observed synergism in LOI can likely be assigned to the morphology development discussed before.

3.4 Fracture mechanical response

Effects of the compositional changes for the fracture toughness (K_{Ic}) and fracture energy (G_c) are depicted. It is interesting to note that the fracture toughness (K_{Ic}) does not change markedly as a function of the composition and VE type. Clear improvement in K_{Ic} can be noticed only for the VE (N)/3P systems. The fracture energy (G_c) is far more sensitive to the formulation of modified resins including hybrid ones. It was shown that the fracture energy of VE (BA) and VE (N) can be strongly enhanced by incorporating functional star-shaped polymers. These compounds influenced the crosslinking process and created a nanoheterogeneous morphology, which favored the targeted shear deformation. Note that G_c experiences a positive deviation from the additivity (synergism) for the hybrids with both VEs. The only difference is related with the compositional range where synergism occurs (this is the whole composition range for VE(N), whereas for VE(BA) synergism in G_c can be concluded for the VE(BA) rich hybrids). The high K_{Ic} and G_c values of the neat 3P resins are due to its complex crosslinking which affects the morphology development. The resulting heterogeneous morphology is linked with low stiffness as already shown in the DMTA traces. Note that the

stiffness (E or Young's modulus) can be estimated by considering the above fracture mechanical data via $E \approx K^2/G_c$ (which strictly holds for plane strain conditions). The so calculated E -moduli lay somewhat below those derived at ambient temperature from the DMTA test (cf. Figs. 1a and 2a). Recall that the latter was measured in flexure mode. On the other hand, tensile E -moduli can be estimated from the CT tests which were used to determine the K_c and G_c values. The flexural and tensile moduli may differ from one to another, especially for such complex systems as these hybrid resins.

3.5 Failure behavior

The SEM pictures in Fig. 3 demonstrate that the silicate particles are involved in crack pinning and crack bifurcation events. Crack pinning is obvious by the merging sections of the running crack front behind the particles in form of "tails".

Crack bifurcation means deviation from the planar crack surface, the characteristic features of which are ridges, steps on the fracture surface. Crack bifurcation and pinning are dominant in the 3P and VE/3P hybrids albeit the polysilicate particles are not covalently bonded to the matrix. This problem has been studied previously (Karger-Kocsis, 2007, p.853-9 and Erdelyi, 2007, p.21-31). The particles are partly or fully debonded from the matrix as the hydrogel/xerogel transition of WG is accompanied with pronounced volume shrinkage. Anyhow, the related "partly filled holes" still act as stress concentrators and trigger the stress release mostly via bifurcation. The shear deformation of the matrix is hindered in the hybrids, especially at high 3P contents. On the other hand, shear deformation (being a very efficient energy absorbing mechanism) is well resolved for the system VE/3P = 75/25. This is the reason why for these systems higher G_c values were found than the expected ones according to the additivity.

It is the right place to mention that for these systems a g/IPN structure was proposed. IPN structured systems are, on the other hand, predestined for shear deformation as discussed in the literature. This problem has been studied previously (Sperling LH, 1981).

Finally, a basic question has to be posed: was the property improvement achieved by changes the silicate dispersion or matrix morphology? The results, presented above, suggest that the network hybridization is a more efficient tool for property upgrade than the creation of a fine and uniform dispersion of the silicate particles.

4. Conclusions

This work was devoted to study the effects of resin hybridization on the structure, thermal and fracture mechanical properties of thermosets produced from polyisocyanate, water glass (WG) and vinyl ester resins (VE), whereby the type and amount of the VE were varied. It was established that VE acts as an additional emulsifier for the 3P resin being initially a water-in-oil type emulsion (i.e. WG dispersed in a phosphate containing polymeric isocyanate). The size of the in situ formed polysilicate particles was reduced by VE hybridization. Based on DMTA and AFM investigations the formation of a conetwork was concluded, at least for the hybrid systems with high 3P resin contents (P50%). Hybridization with VE resins improved the stiffness and resistance to thermal degradation of the 3P resin. With respect to the flame resistance (LOI) and fracture energy (G_c) synergistic effects were found for the hybrid resins at least in a given composition range. The latter depended on the type of the VE. The novel hybrid resins proved to be suited to produce composite parts using wet filament winding.

References

- Erdelyi S, Karger-Kocsis J, Nagy G. (2007). Polyurea resins with in situ produced silicate filler from water glass: static and dynamic mechanical properties. *J Marcomol Sci Part B: Phys*, 46, 21–31.
- Gawdzik B, Matynia T. (2001). Synthesis and modification of epoxy-based divinyl ester resin. *J Appl Polym Sci*, 81: 2062–7.
- Gryshchuk O, Jost N, Karger-Kocsis J. (2002). Toughening of vinyl ester-urethane hybrid resins by functional liquid nitrile rubbers and hyperbranched polymers. *Polymer* 43, 4763–8.
- Gryshchuk O, Jost N, Karger-Kocsis J. (2002). Toughening of vinyl ester-urethane hybrid resins through functionalized polymers. *J Appl Polym Sci*, 84, 672–80
- Hungarian Patent Application P04 01799 (to Polinvent Ltd.); (2004).
- Jost N, Karger-Kocsis J. (2002). On the curing of a vinyl ester-urethane hybrid resin *Polymer*, 43: 1383–9.
- Karger-Kocsis J, Erde'lyi S, Nagy G. (2007). Polyurea/vinyl ester hybrid thermoset resins with in situ produced silicate filler: preparation and static mechanical properties. *J Appl Polym Sci*, 103, 853–9.
- Kickelbick G. (2003). Concepts for the incorporation of inorganic building blocks into organic polymers on a nanoscale. *Prog Polym Sci*, 8, 83–114.
- Nalwa HS, editor. (2003). Handbook of organic–inorganic hybrid materials and nanocomposites. Los Angeles (CA,

USA): American Scientific Publishers.

Sperling LH. (1981). Interpenetrating polymer network and related materials. New York: Plenum.

Stoye D, editor. (1993). Paints, coatings and solvents. Weinheim (GER): VCH. p. 94–96.

US Patent 5 622 999 (to Polinvent Ltd.); (1997).

Utracki LA. (2004). Clay-containing polymeric nanocomposites. Shawbury (UK): Rapra Technology.

Table 1. Composition and designation of the VE/3P hybrids studied

<i>Material code</i>	<i>VE content(%)</i>	<i>3P content(%)</i>	<i>PMDI content(%)</i>	<i>WG content(%)</i>	Phosphate content(%)
3P	0	100	42	40	18
VE(BA)	100	0	0	0	0
VE(BA)/3P 75/25	75	25	10.5	10	4.5
VE(BA)/3P 50/50	50	50	21	20	9
VE(BA)/3P 25/75	25	75	31.5	30	13.5
VE(N)	100	0	0	0	0
VE(N)/3P 75/25	75	25	10.5	10	4.5
VE(N)/3P 50/50	50	50	21	20	9
VE(N)/3P 25/75	25	75	31.5	30	13.5

Table 2. Number (dn) and weight-average diameter (dw) of the polysilicate particles in the VE/3P hybrids

<i>Composition</i>	<i>dn(μm)</i>	<i>dw(μm)</i>	dw/dn
VE(BA)/3P=75/25	2.57	7.01	2.72
VE(N)/3P=75/25	1.21	2.30	1.88
VE(BA)/3P=50/50	4.13	8.12	1.97
VE(N)/3P=50/50	3.11	4.48	1.44
VE(BA)/3P=25/75	8.58	21.45	2.50
VE(N)/3P=25/75	4.00	5.96	1.49
VE/3P=0/100	7.81	22.05	2.82

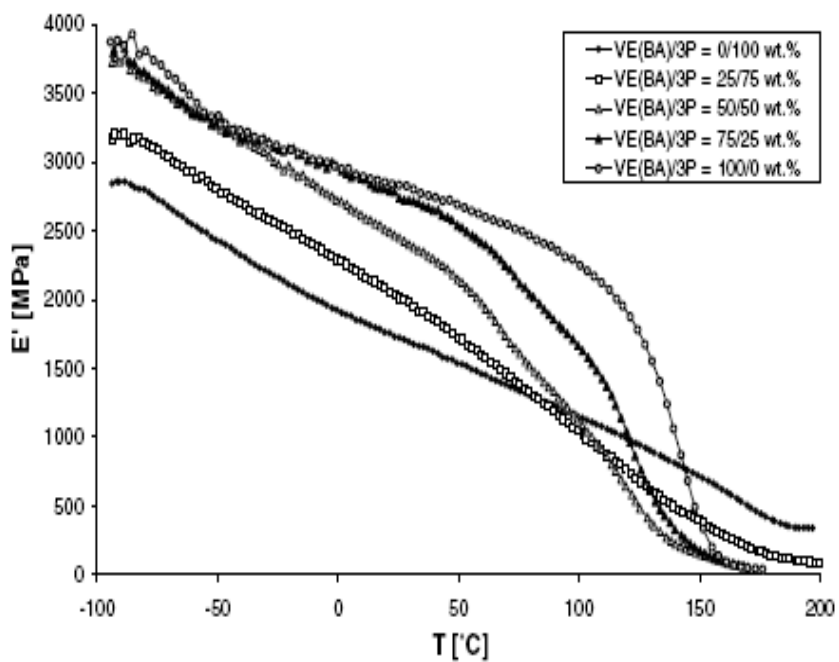


Figure 1a. E_0 vs T traces for the 3P, VE(BA) and their hybrid systems

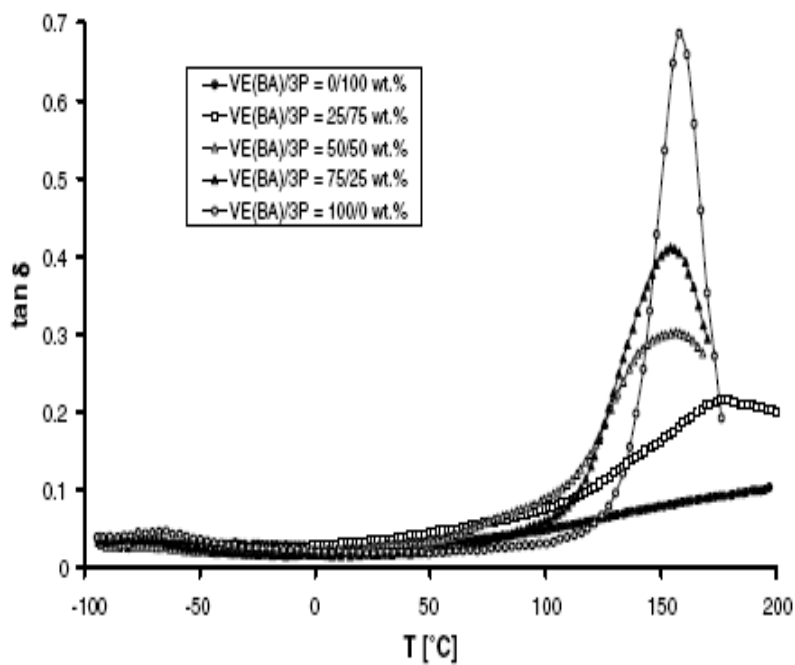


Figure 1b. $\tan\delta$ vs T traces for 3P, VE(BA) and their hybrid systems

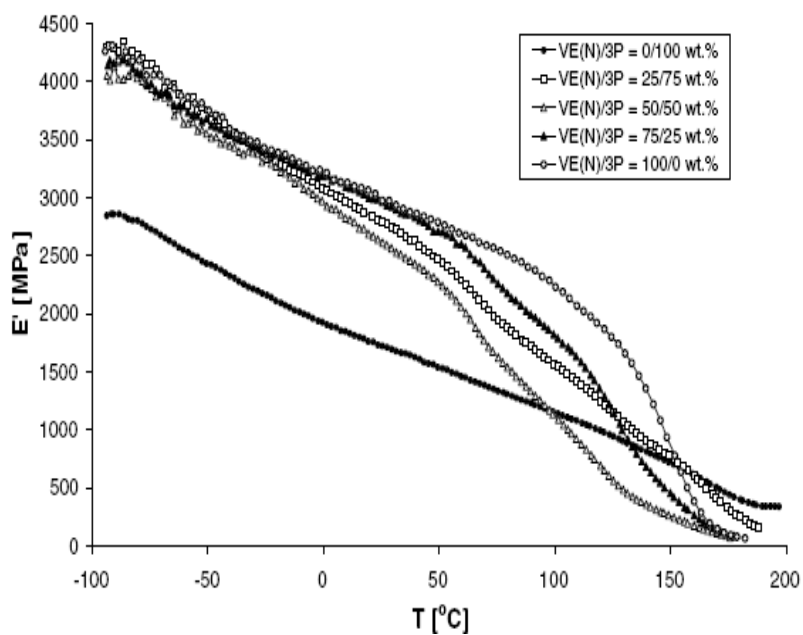


Figure 2a. E' vs T traces for the 3P, VE(N) and their hybrid systems

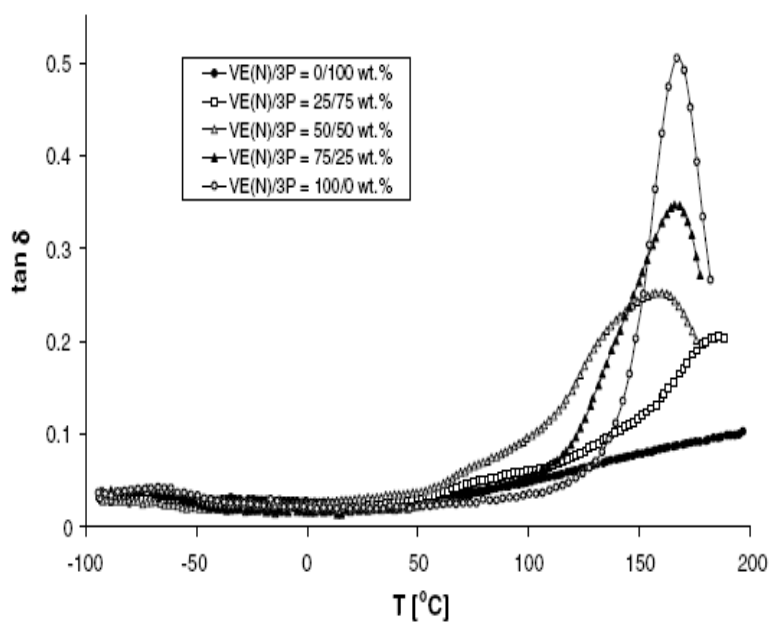


Figure 2b. $\tan \delta$ vs. T traces for 3P, VE(N) and their hybrid systems

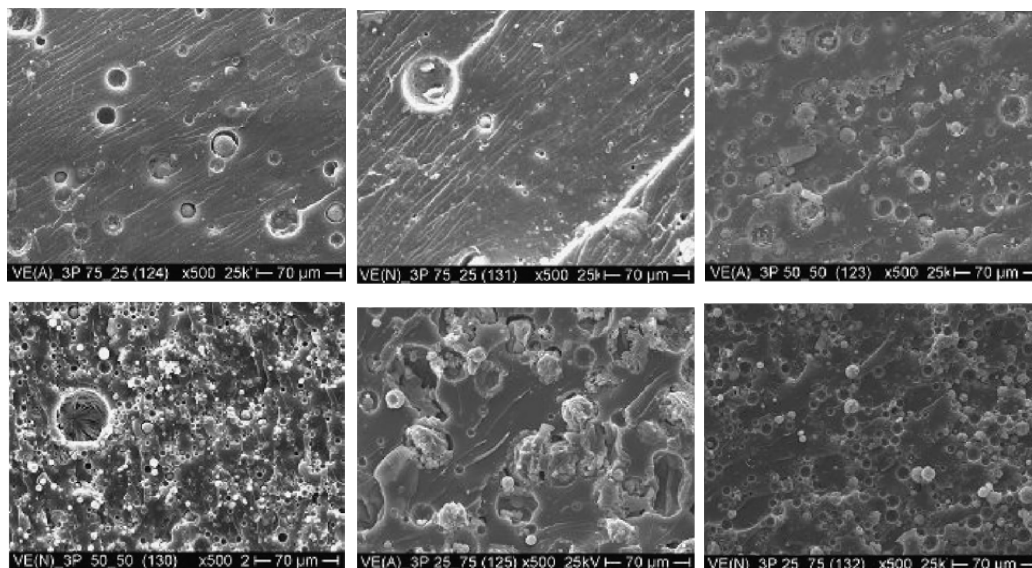


Figure 3. SEM pictures showing the difference in the silicate dispersion as functions of VE resin type and VE/3P composition. Designations: hybridized with VE (BA) – left; hybridized with VE (N) – right. From top to bottom: VE/3P = 75/25, =50/50, 25/75

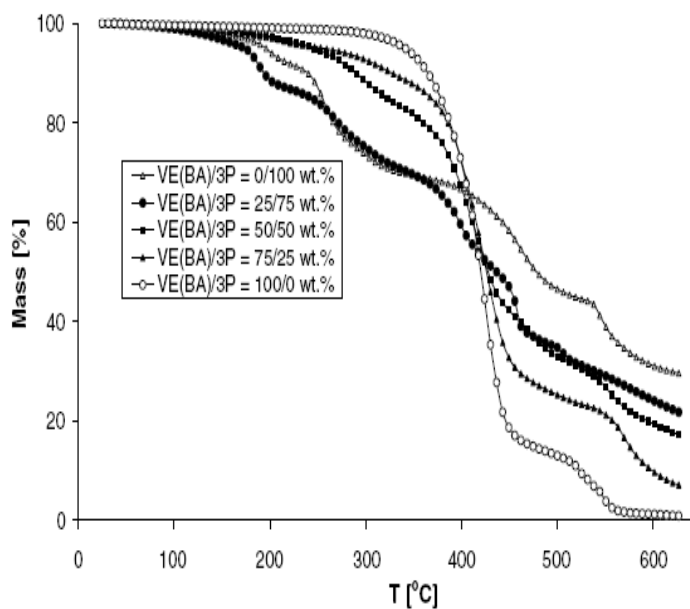


Figure 4. TGA traces of the 3P resin and its hybrids of VE (BA)

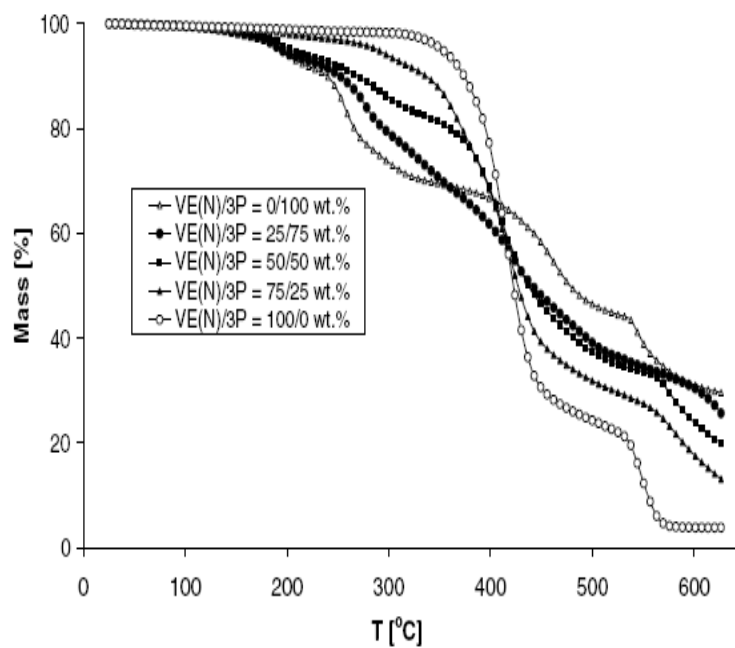


Figure 5. TGA traces of the 3P resin and its hybrids of VE (N)



Synthesis of Oligomers of 12-Acryloyloxydodecanoic Acid via Reversible Addition Fragmentation Transfer (RAFT) Polymerisation

Lilian Tichagwa (Corresponding author)

Department of Chemistry, University of Fort Hare

Private Bag X1314, Alice 5700. South Africa

Tel: 27-406-022-266 E-mail: ltichagwa@ufh.ac.za

Ron D. Sanderson

Department of Chemistry and Polymer Science, University of Stellenbosch

Private Bag X1, Matieland 7602. South Africa

Tel: 27-218-083-172 E-mail: rds@sun.ac.za

Harald Pasch

Department of Chemistry and Polymer Science, University of Stellenbosch

Private Bag X1, Matieland 7602. South Africa

Tel: 27-218-083-367 E-mail: hpasch@sun.ac.za

This research was financed by the National Research Foundation and the University of Stellenbosch.

Abstract

A long chain fatty acid carrying an acryloyl functionality, 12-acryloyloxydodecanoic acid (12-ADA), was prepared from 11-hydroxydodecanoic acid and acryloyl chloride and used as monomer in the synthesis of oligomers of 12-ADA via the RAFT controlled polymerisation process. Reversible Addition Fragmentation Transfer (RAFT) reagents were prepared and used to control the polymerisation process and produced an oligomeric product with few monomeric units instead of a high molecular weight polymer of 12-ADA. The transfer reagents were prepared from Grignard intermediates from a reaction of dithioacids with free radical initiators 2,2-azobisisobutyronitrile (AIBN) and 4,4-azobis(4-cyanopropanoic acid) (ACP). It was found that short-chain oligomers in the form of dimers and trimers characterized by Electrospray Mass Spectrometry, ESMS and Gel Permeation chromatography, GPC were the major products obtained when RAFT reagents had been used in the controlled polymerisation. As a control, polymerisation was carried out in the absence of RAFT reagents and high molecular-weight polymers were obtained. This confirmed the effectiveness of the prepared RAFT reagents as polymerisation controllers and provided a way for the synthesis of oligomers. Here, the preparation of oligomers of 12-ADA using AIBN-RAFT reagents is reported. The method is expected to provide one way of preparing oligomers of controlled chain length/molecular mass which also carry a carboxylic acid functional group at one end.

Keywords: Chain transfer, Controlled polymerisation, Oligomers, RAFT, Polydispersity index

1. Introduction

Controlled radical polymerisations lead to the synthesis of polymers with controlled molecular masses. Reversible addition fragmentation transfer polymerisation, RAFT, is one of the methods for controlling radical polymerisation which offers versatility in providing a route to the synthesis of oligomers (Chieffari et al, 2003, p. 2273). This can be achieved by performing the polymerisation in the presence of chain transfer agents such as dithio compounds which act as RAFT chain transfer agents and provide the polymerisation with "living" characteristics. The amount of transfer agent added determines the extent of control of the polymerisation process and the subsequent molecular mass of the

products. The RAFT technique relies on a sequence of addition-fragmentation chain transfer reactions (Moad et al, 2003, p 520).

RAFT chain transfer agents with the general structure Z-C(S)S-R have been used in controlled polymerisation reactions (Lowe A.B., & McCormick C.L. 2002, p. 4177). The Z group activates the C=S bond towards radical addition while R needs to be a good free radical leaving group capable of reinitiating free radical polymerization (de Brouwer, 2000, p. 9239). The RAFT reagents have Z and R moieties that provide high transfer constants which lead to oligomers with narrow polydispersities. In this study two types of RAFT chain transfer agents based on dithiobenzoates were used, one from the free radical initiator 2,2-azobisisobutyronitrile (AIBN) and the other from 4,4-azobis(4-cyanovaleric acid) (ACP) and used as reagents in polymerisation reactions (Thang et al, 1999, p. 2435) even though AIBN-RAFT polymerisation was the focus of this report. The RAFT reagents were prepared by first preparing Grignard reagents, which were converted to dithioacids and subsequently to bis-thiobenzoyl disulphide compounds as illustrated in Scheme 1. The reagents were then used in the controlled polymerisation of 12-ADA to give corresponding oligomers of 12-ADA. RAFT chain transfer reagents produced from dithioacids were successfully used to produce methacrylate-derivative oligomers with a target degree of polymerization of 10 (Hosseini et al, 2008, p. 2277).

2. Synthesis of RAFT reagents

Free radical initiators and dithioacids were used as the main reagents for the synthesis of RAFT reagents.

2.1 Materials

Recrystallised AIBN initiator (Sigma); ACP initiator (Sigma); bromobenzene (Acros); carbon disulphide (Sigma); Mg turnings, dry diethyl ether, dry THF

2.2 Method

A Grignard reagent was prepared and cooled before carbon disulphide was slowly added followed by water resulting in a precipitate which was filtered off. The resulting red dithioacid product was acidified to pH 1 with fuming HCl and the resulting compound extracted with diethyl ether. The ethereal phase was worked up and dried with anhydrous magnesium sulphate.

To 172 mmol of dithioacid produced above, 353 mmol DMSO and 100 ml dry ethanol solvent were added and the mixture stirred for an hour. The pink product formed was washed with ethanol and dried under vacuum to give crystalline bis(thiocarbonyl) disulphide. To 136 mmol bis(thiocarbonyl) disulphide; (dissolved in 100 ml ethyl acetate) and corresponding initiator, AIBN also dissolved in 100ml ethyl acetate, were added and the resulting mixture stirred and purged with nitrogen and allowed to reflux for about 24 hours. The resulting deep red product was purified by running through a 60-cm silica gel chromatographic column using a 5:1 heptane/ethyl acetate mixture as elution solvent for AIBN-RAFT. The solvent was removed and the resulting RAFT reagent collected as red oil (28% yield). The RAFT reagent was analysed using ¹H-NMR and ESMS.

3. Synthesis of 12-ADA

3.1 Materials

Analytical grades of 11-hydroxy dodecanoic acid (Sigma), acryloyl chloride (Sigma), triethylamine (Acros), dichloromethane (Merk) were all used as purchased.

3.2 Method

The monomer 12-ADA was prepared using a procedure described by Finkelmann H., & Schafheutle M.A. 1986, p. 786) and was prepared according to Scheme 2. The monomer was prepared from 11-hydroxy dodecanoic acid and acryloyl chloride in the presence of triethylamine. Once prepared, the 12-ADA was dried and purified by first dissolving it in a mixture of 4:1 acetone/methanol and filtered before running it down a 60cm long silica gel chromatographic column. Different fractions were collected and verified by TLC. Solvent was removed under vacuum in the dark to avoid spurious polymerisation. The total yield was 76 % and the product was analysed by ¹H-NMR and ESMS.

4. Synthesis of RAFT polymers of styrene

Materials: Styrene monomer from Sigma was vacuum distilled; AIBN initiator from Sigma was recrystallised.

4.1 Method

The effectiveness of the AIBN-RAFT transfer agent was tested by carrying out bulk polymerisation of styrene in a 3-neck flask using 1.43 mol styrene, 2.80 mmol AIBN initiator and 0.83 mmol AIBN-RAFT reagent. The polymerisation was carried out at 75°C and the variation of molar mass of the oligomers with time studied using Gel Permeation Chromatography (GPC) and the results summarized in Table 1.

5. Polymerisation of 12-ADA

The monomer 12-ADA had poor solubility in most of the common solvents and so the polymerisation was carried out in DMSO at 75°C.

In a 3-neck flask, 3,7 mmol of 12-ADA and 0,99 mmol RAFT reagent were dissolved in 10 ml DMSO and 0,33 mmol AIBN initiator dissolved in 1 ml DMSO were added, degassed and polymerised at 70°C for 60 hours. After removing most of the solvent under vacuum, the mixture was diluted with CH₂Cl₂ before being run down a silica gel chromatographic column (70-230 mesh-*Macherey-Nagel*). Seven fractions were obtained and these were analysed by thin layer chromatography (TLC). The polymeric fraction could not be run down the column. The collective yields obtained were about 60 % oligomeric, 32 % monomeric and about 8 % polymeric fractions. The polymerisation reaction was followed by drawing 3 fractions (F1, F2 and F3) at different stages between the early and last stages of the polymerisation. The fractions were analysed using ¹H-NMR. After the controlled polymerisation, the final oligomer was also analysed by ¹H-NMR in CHCl₃ and ESMS.

6. Results and Discussion

6.1 Results

ESMS spectrum of AIBN-RAFT:

ESMS (acetonitrile/methanol):

The following were observed: m/z = 120.72 due to - C(CH₃)₂CNS; 154.5 due to C(CH₃)₂CN; and 221.47=(M⁺ of C₆H₅CS₂C(CH₃)₂CN

ESMS spectrum of 12-ADA:

ESMS (methanol): m/z = 268.59 (M⁺)

ESMS spectrum of the oligomer:

ESMS (acetonitrile-methanol) m/z = 215.09; 1030.06(M⁺)

The ¹H-NMR spectra of the AIBN RAFT agent, monomeric 12-ADA, products from a RAFT polymerization and oligomeric product are given in Figures 1,2,3 and 4 respectively.

6.2 Discussion

From the proton NMR and ESMS results of 12-ADA, it can be confirmed that the monomer had been successfully prepared because the analysis results were as expected for the compound with an estimated purity of > 90%. The RAFT reagent was also successfully prepared as seen by the results of the NMR and ESMS analysis and this also showed an estimated purity of > 90%. The 12-ADA and AIBN-RAFT were then used for the oligomerisation/polymerisation. The test for polymerisation control was illustrated with the use of styrene polymerisation. This showed the difference between RAFT controlled and uncontrolled styrene polymerisations with the controlled polymerisation giving narrow molecular weight distributions and the uncontrolled polymerisations giving polymers with large molecular masses with wide polydispersities.

The NMR and ESMS analyses of the products from the polymerisation confirm the presence of oligomers when transfer reagents are used in the polymerisation. The NMR of Fraction 1 shows a product which is very similar to monomer 12-ADA suggesting that there was ample monomer in the reaction flask. Fraction 2 shows that some reaction had occurred as the NMR spectrum exhibited evidence of monomer depletion as well as the appearance of product carrying an aromatic group which must have been due to the RAFT moiety. The third fraction clearly suggests formation of oligomeric product which was confirmed by the absence of double bonds from monomeric 12-ADA. This was confirmed by giving an NMR spectrum similar to that given by the final oligomer.

On examining the ESMS spectrum of the oligomeric product, it was apparent that mainly trimers and some tetramers had been produced. The base peak at about m/z = 1030, relates to the molar mass of the trimer of 12-ADA (the molar mass of 12-ADA is 270 g/mol) carrying a RAFT moiety which is M⁺ = 221.47 was illustrated by the ESMS spectrum of the AIBN-RAFT reagent which is the fragment of C₆H₅CS₂C(CH₃)₂CN. Furthermore, the ESMS of the oligomer showed a peak around m/z = 215 suggesting the loss of the fragment CH₂=CH-C=O, which signifies possible cleavage of the weak ester linkage at C-O accounting for the mass of the fragment which is 55 g/mol and agrees well with the value of 215+ 55 = 270 g/mol for the remaining monomer fragment. The ESMS spectrum also shows that further fragmentation occurred as illustrated by a number of very small and insignificant peaks of lower molecular masses. The spectrum confirmed the presence of oligomers of 12-ADA which had not been prepared before. The experimental run without RAFT reagent did not result in oligomers but instead produced a high molecular mass product which appeared crosslinked as it could not be dissolved in any of the available solvents and was therefore difficult to analyse. The NMR of the oligomer when compared with that of 12-ADA confirmed that 12-ADA did oligomerise to give the trimeric

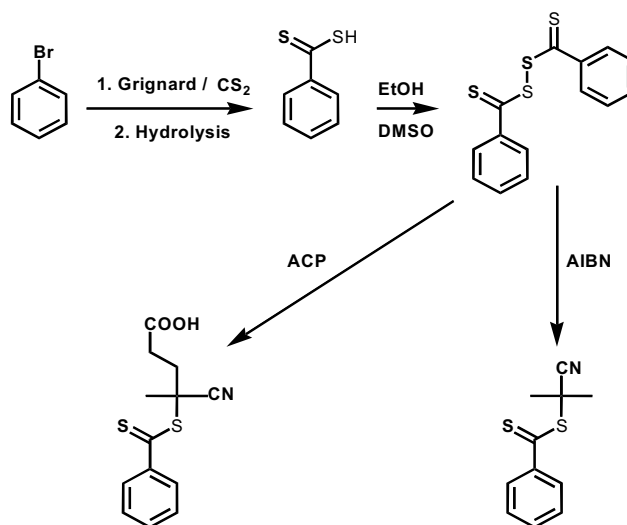
oligomer. This confirmed that the RAFT reagents prepared were effective in controlling molecular mass through a control of the polymerisation process leading to oligomers rather than polymers of 12-ADA.

7. Conclusion

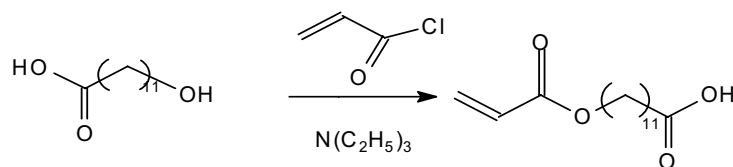
Oligomers of 12-ADA were prepared using RAFT reagents which controlled the polymerisation reaction and stopped the polymerisation from continuing to produce high molar mass products. The control was also demonstrated on the polymerisation of styrene. It would be interesting to extend the methods described to the synthesis of other short-chain compounds which would otherwise give long-chain compounds. In addition to the controlled polymerization, the methods described in this report may be applied in the synthesis of a carboxylic acid-functionalised oligomer.

References

- Chiefari J., Mayadunne R.T.A., Moad C., Moad G., Rizzardo E., Postma A., Skidmore M.A., & Thang S.H. (2003). *Macromolecules*, 36, 2273-2283.
- De Brouwer H., Monteiro M.J., Tsavalas J.G., & Schork F.J. (2000). *Macromolecules*, 33, 9239- 9246.
- Finkelmann H., & Schafheutle M.A. (1986). *Colloid Polym. Sci.* 264, 786- 790.
- Hosseini N.E., Castgnolles P., Gilbert R.G., & Guillaeneuf Y. (2008). *Polym Sc. Part A: Polym Chem.* 46, 2277-2289.
- Lowe A.B., & McCormick C.L. (2002). *Chem Rev* 102, 4177- 4189.
- Moad G., Mayadunne R.T.A., Rizzardo E., & Skidmore M. (2003). *Advances in controlled/Living Radical polymerization.* (1st ed.). Washington DC: Oxford University Press, p. 520- 535.
- Thang S.H., Chong Y.K., Mayadunne T.A., Moad G., & Rizzardo, E. (1999). *Tetrahedron Letters*, 40, 2435-2438.



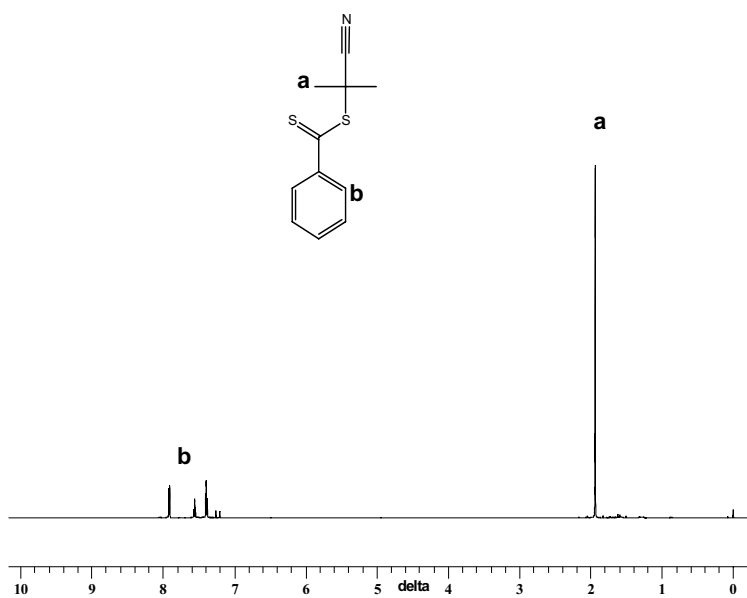
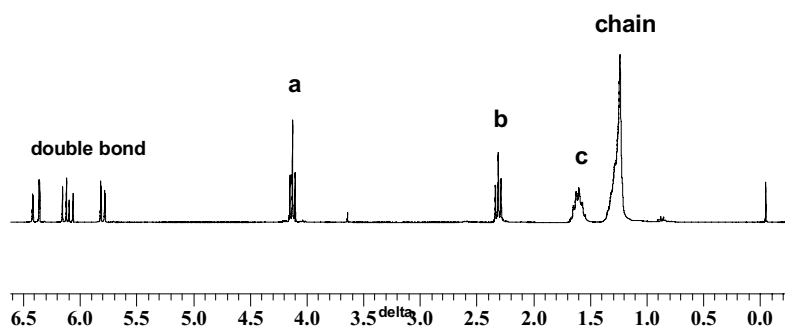
Scheme 1. Reactions showing the synthetic routes to RAFT transfer agents



Scheme 2. Synthetic route to 12-ADA

Table 1. Molar masses of products from polymerisation runs of styrene with & without RAFT reagents

	PS (RAFT)	PS
RAFT reagent added	AIBN	None
Temperature °C	75	75
Polymerisation time in min / M_n / PDI	40 / 1900 / 1.17	40 / 128 000 / 12.1
Polymerisation time in min / M_n / PDI	60 / 2600 / 1.21	60 / 124 000 / 14.1
Polymerisation time in min / M_n / PDI	80 / 3200 / 1.25	80 / 132 000 / 12.6

Figure 1. Proton NMR of AIBN-RAFT reagent in $CDCl_3$ Figure 2. Proton NMR spectrum of 12-ADA in $CDCl_3$

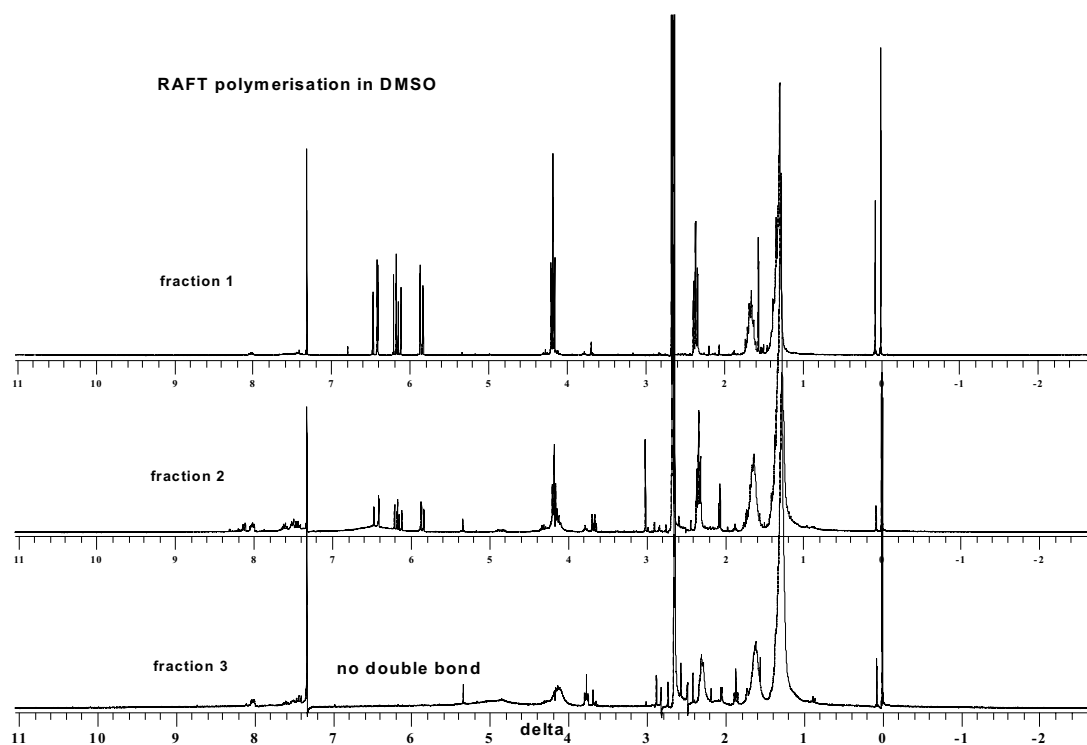


Figure 3. Proton NMR in CDCl₃ of products from a RAFT polymerisation in DMSO as solvent

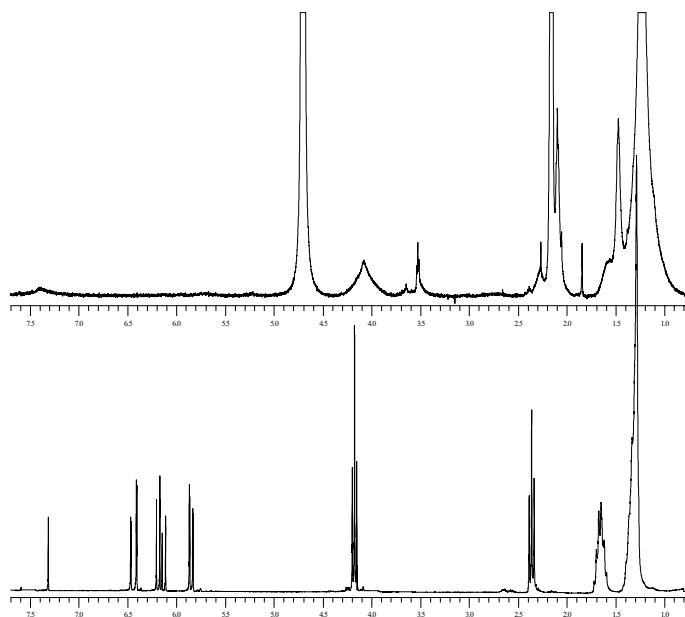


Figure 4. Proton NMR of oligomeric 12-ADA (top) and 12-ADA monomer (bottom)



Fiber Splitting of Bicomponent Meltblown Nonwovens by Ultrasonic Wave

Xiaobin Wang, Jinbo Yao & Xianmiao Pan
Textile College, Tianjin Polytechnic University
Tianjin 300160, China
E-mail: wxbin2010@yahoo.cn

Abstract

Many technologies have been used to produce finer fibers due to their super advantages such as higher specific surface area, filtration/barrier property and absorption, as well as moderate porosity. Finer fibers are thus the great interest of many researchers in the nonwoven world, and many technologies have been used to make finer fibers. In this study, the authors addressed a novel avenue to produce finer fibers by splitting side-by-side bicomponent meltblown nonwovens composed of polyethylene terephthalate (PET) and polyamide 6 (PA6) by means of ultrasonic wave, in caustic soda and benzyl alcohol solutions respectively. The efficiency of fiber splitting was characterized in terms of dyeing ratio/percentage of the tested webs. Other properties were also examined, including fiber diameter, web weight loss, air permeability and thickness. In addition, SEM was used to observe fiber damage and fiber structure in the relevant webs.

Keywords: Bicomponent fibers, Meltblown nonwovens, Fiber splitting, PET/PA6, Benzyl alcohol, Sodium Hydroxide, Ultrasonic wave

1. Introduction

Meltblowing (MB) is a one-step process for making microfiber nonwovens directly from thermoplastic polymers with the aid of high velocity hot air to attenuate the melt filaments extruded from the orifices, originated in US Navy Laboratory in the Early 1950s. Exxon Company began to study on the MB technology in the Mid-1960s, and developed superfine fibers after five years. Subsequently, other companies produced the MB nonwovens with their own technologies, such as 3M (US), Freudenberg (Germany), NKK (Japan), etc. (Can Hong, 2004).

The nonwovens produced with MB technology are obviously featured with fine fibers compared to fibers from other technologies. The latest bicomponent MB equipment has consistently produced MB nonwoven webs containing fibers with average fiber distribution being 0.6 μm ; among which, more than 70% of the fibers have diameters less than 1 μm , indicating that bicomponent MB technology might produce fine fibers at micro-nano scale (Xiao Jin, 2006), and thus the absorption and filtration efficiency would be improved due to the increase in specific surface area. However, it is necessary to further slenderize fine MB fibers to further improve the adsorption and filtration performance of the MB webs.

Many technologies have been employed to develop finer fibers in nonwoven field, such as direct drawing, island-in-the-sea, alkali treatment etc. For the island-in-the-sea method, bicomponent polymers are spun into island-in-the-sea bicomponent MB fibers and then dissolve the sea parts of the bicomponent fibers with appropriate solvent, resulting in finer MB fibers even at nanometer scale. Caustic soda may reduce MB fiber size to a certain degree, but the fibers are seriously damaged both in morphology and mechanical property. Drawing fibers may directly produce fine fibers, but more challenging spinning technologies will get involved, making this technology more complicated and energy-consuming, compared to the simpler post treatment technologies.

In this study, the authors would investigate the possibility of making fine MB fibers through bicomponent fiber splitting post treatments. Some researchers (Ron, 2003; Myung-Ja, 2001; Baopu Yin, 2003) applied post treatment technologies to split bicomponent MB fibers, e.g., alkali weight-reduction, hydroentanglement, heat treatment and solvent swelling methods for finer fibers with increased fiber surface area and hence the improved adsorption and filtration properties. However, such post treatments returned no significant efficiency in fiber splitting.

Based on the theory of "similarity and intermiscibility", a solute can only be dissolved or swollen in the solvent which

is of the similar solubility to the solute. According to the Second Law of Thermodynamics, the mixing free energy ΔG_M must be negative to ensure a spontaneous mixing progress, i.e.,

$$\Delta G = \Delta H_M - T\Delta S_M \quad (1)$$

Where ΔG_M — free energy of mixing, ΔH_M — heat of mixing, and ΔS_M — mixing entropy. The mixing entropy tends to be positive due to disordered alignment of the molecules during the process of mixing, and ΔH_M is also positive if the non-polar solute and solvent containing no H-bonds mix together. Therefore, the above conditions can only be satisfied when the heat of mixing is less than the product of temperature and the mixing entropy. The heat of mixing could be expressed with the following formula, if the total volume remains unchanged during mixing:

$$\Delta H_M = \varphi_1\varphi_2(\delta_1 - \delta_2)^2V \quad (2)$$

Where φ_1 and φ_2 stand for the volume fractions of solvent and polymer, respectively; δ_1 and δ_2 represent the solubility parameters of solvent and polymer, respectively; and V is the total volume of the solution.

Combining Equations (1) and (2) we can find that spontaneous dissolving readily occur when a smaller ΔH_M value is available, i.e., when the values of δ_1 and δ_2 are close to each other. Generally, dissolving or swelling of the solute will occur when the difference between δ_1 and δ_2 is less than 1.7~2.0, which is shown in Equation 3 as below:

$$|\delta_1 - \delta_2| < 1.7 \sim 2.0 \quad (3)$$

In this study, PET/PA6 melt blown nonwoven web samples were treated with alkali and benzyl alcohol solutions respectively, with the aid of ultrasonic wave, to produce finer fibers through fiber splitting technology. The solubility parameters of PET and PA6 are $10.7\text{cal}^{1/2}/\text{cm}^{3/2}$ and $13.0\text{cal}^{1/2}/\text{cm}^{3/2}$ respectively, and that of the splitting reagent, i.e., benzyl alcohol, is $11.6\text{cal}^{1/2}/\text{cm}^{3/2}$.

2. Experimental

2.1 Web sample description

The side-by-side (S/S) MB nonwoven sample composed of 50PET/50PA6 was produced from Textile and Nonwoven Development Center (TANDEC), The University of Tennessee, Knoxville, USA.

2.2 Post-treatment

The specimens were treated in benzyl alcohol and in NaOH solutions respectively, at the concentration of 5g/L, liquor ratio of 1/100, temperature of 60°C, for 45 minutes, with the aid of ultrasonic wave at the powers of 0, 100, 120, 150, 180, 210 and 240W, respectively. Five specimens (20cm by 20cm for each) were used in each experiment.

2.3 Characterization

Along with the controls, the treated web samples were tested for air permeability (ISO9237-1995), thickness (ISO9073-2-1989), dyeing rate, weight loss, and fiber diameter.

2.3.1 Fiber diameter and web morphology

The optical microscope system and image analyzing software were utilized to capture the images of fibers and measure fiber diameter. The averages of 200 readings of fiber diameters for each specimen were recorded. The coefficients of variance in fiber diameter were in the range of 20% to 32%. The web morphologies were examined with a KYKY-2800 scanning electron microscope (SEM).

2.3.2 Degree of fiber splitting

The degree of fibers splitting was characterized in terms of dyeing rate. Firstly, specimens were treated with the penetrating agent of JFC at 1g/L, 40°C for 5 minutes, and then, the weakly acidic red dye, GRS was added to the treatment solution at 0.5% owf and 100/1 liquor ratio. The dye absorption remained for 45 minutes at 40°C. After dye absorption, the treated web samples were thoroughly rinsed with 50°C water and then let dry at room temperature. The maximum absorption wavelength of GRS was detected on the visible spectrophotometer VIS-723, and the absorbencies of the dyeing bath before and after dyeing, A_0 and A_i , were measured respectively at the maximum absorption wavelength. The dyeing rate can be calculated as:

$$S = (1 - A_i/A_0) \times 100 (\%)$$

Where A_0 and A_i stand for the absorbencies of the dyeing bath before and after dyeing, and S represents dyeing rate. Specimens were conditioned for 24 hrs at standard temperature and humidity, before being measured on JA5003 electronic balance (accuracy: 0.001g). Weight loss was characterized based on the equation below:

$$W = (W_0 - W_i)/W_0 \times 100 (\%)$$

Where W_0 and W_i are the weight values of the samples before and after dyeing, and W is weight loss.

3. Result and Discussion

3.1 Change in web morphology

The SEM photos of the web samples before and after post treatments were shown in Figure 1.

It was observed after comparing the photos in Figure 1, that the web structure showed no obvious change when specimens were treated in NaOH solution at low concentration of 5g/L, while fiber diameter decreased mainly due to the effect of fiber splitting and hydrolysis of ester group in PET and amide group in PA6. This effect became extremely significant, especially when ultrasonic wave was incorporated.

Benzyl alcohol is one of the swelling agents of PA6, whose molecules may pass amorphous region, occupying the space among chain segments of PA6.

It has been reported based on SAXS observations that the swelling agent only swelled amorphous region inside the fiber along fiber axis (Zeyong Zheng, 1989), whereas the molecules in crystalline region across the fiber axis still exhibited a dense arrangement, indicating no swelling effect from the swelling agent along this direction, which resulted in significantly anisotropic swelling effect from benzyl alcohol on PA6 fiber swelling (J. Baldrian, 1991). The bicomponent would become separated when the stress at the interface of PET and PA6 was generated and became large enough; the addition of ultrasonic wave would enhance the bicomponent splitting, and hence shorten the time for this process.

3.2 Change in fiber diameter

Figure 2 showed a consistent tendency that the fiber diameter decreased with the power of applied ultrasonic wave during the three post treatments, suggesting that ultrasonic wave, as an auxiliary means, could indeed assist fiber splitting in PET/PA6 side-by-side bicomponent MB fibers. However, it was found that ultrasonic treatment alone only resulted in fiber splitting to a limited extent; it only could help the splitting agent enter into the interface between PA6 and PET. In bicomponent fiber splitting, swelling/splitting agent played a key role, while ultrasonic wave only assisted the diffusion of swelling agent in the bico fibers. When the bico fibers were treated with NaOH solution, with the aid of ultrasonic vibration, NaOH solution might enter into the interface of the bicomponent in PET/PA6 fiber, resulting in the different shrinkage ratios of PET and PA6 components in the bico fibers (less shrinkage from PET; more from PA6), and thus expanding the crack at the interface (Bin Yang, 2002); meanwhile, ultrasonic application further enhanced the crack, and eventually leading to the fiber splitting; therefore, fiber size decreased significantly. On the other hand, at 60°C, the ultrasonic vibration enhanced the hydrolysis effect from NaOH on the ester bonds in PET, and the whole fiber became thinner, as a result. Therefore, finer fibers were the result from both the foregoing action processes. As for benzyl alcohol, it served as a swelling agent of PA6, favoring the splitting of PA6 and PET with no caustic effect on the fiber; ultrasonic treatment would play the same role in fiber splitting, as addressed before.

3.3 Change in web adsorption

The separation of the two components in bico fibers would definitely cause the increase in specific surface area of the fibers and hence the adsorption property of the webs, which could be characterized with the degree of adsorption to certain dye, in terms of Dyeing ratio (percentage). Therefore, the values of dyeing ratio would be an index indicating the degree of fiber splitting in bico MB webs in this study. The weak acidic red dye GRS, which only could be absorbed by PA6, was selected to dye PET/PA6 bico MB webs, and 40 °C was chosen as the initial dyeing temperature, to lower the possibility of the dye to penetrate inside the bulk fibers and thus minimize the experimental error. The results from the dyeing experiments were shown in Figure 3. It was observed from the dyeing results that the dyeing percentage (%) of all the web samples treated with ultrasonic wave, NaOH/ultrasonic wave and benzyl alcohol/ultrasonic wave increased with the increasing ultrasonic power, which indicated the increase of specific surface area of the split fibers. This suggested that the dyeing experimental results were consistent with those from fiber diameter measurement tests and hence it could be concluded that fiber splitting in bico MB webs resulted in finer fibers and thus increased surface adsorption ability.

3.4 Change in web weight loss

The results from weight loss measurement tests were summarized in Figure 4. As can be seen in Figure 4, the webs after three different treatments (i.e., ultrasonic, NaOH/ultrasonic and benzyl alcohol/ultrasonic) lost their weights and the weight loss increased with increasing ultrasonic power. This phenomenon could be explained by the characteristics of MB nonwoven webs. As we know, MB webs were produced in one-step process, during which the fibers were formed by the attenuation from the hot air, and the semi-molten state fibers were deposited on the web screen to form MB webs immediately by self-adhesion. Therefore, the bonding/adhesion between MB fibers was not strong enough to survive the ultrasonic vibration treatment, and thus the MB fibers might be pulled out of the MB web, leading to the weight loss of the treated MB webs. Increasing ultrasonic power would provide more vibration energy to detach the weakly bonded fibers from the MB webs, and even split the poorly adhered bicomponent in the MB fibers, resulting in increasing

weight loss of the treated web samples.

The web samples treated with alkali solution/ultrasonic wave showed much higher weight loss compared with the web samples treated with ultrasonic wave alone or benzyl alcohol/ultrasonic wave, indicating the possibility that alkali solution hydrolyzed and thus damaged the fibers in the nonwoven webs.

Small fibers were found to be left in the residue of benzyl alcohol solution. However, no short fibers were found in the residue of NaOH solution, possibly because these fibers were hydrolyzed in the alkali solution with the help of ultrasonic wave at 60°C.

Furthermore, the weight loss curve of the web samples treated with ultrasonic wave showed similar tendency to that with benzyl alcohol/ultrasonic wave treatment; and thus, it was suggested, on the other hand, that benzyl alcohol treatment brought no damage to the fibers.

3.5 Change in web thickness

Figure 5 shows an increasing web thickness with increasing ultrasonic power, which was because that ultrasonic vibration energy could impart fibers in the webs with sufficient dynamic energy for fibers to detach from the webs and then further entangled one another, which finally caused the web shrinkage to occur. Also, post treatment of the nonwoven webs in 60°C aqueous solution would cause the relaxation of the processing stress created during bico MB web production, and finally result in web shrinkage and thickness increase. More powerful ultrasonic wave would provide the fibers with more mobility to move around and get entangled together.

Furthermore, benzyl alcohol molecules might enter into the interface between PET and PA6 and then split the two components, leading to increased specific volume per unit mass of the treated webs, and the increased porosity in the webs, which actually increased the bulkiness of the treated webs, in terms of thickness, as shown in Figure 5. In the case of caustic soda, although the alkali solution also could cause bico fiber to split and thus lead to the increase in the web thickness, it would additionally hydrolyze the fibers in the treated webs and thus attenuate the web thickness eventually. With the aid from the auxiliary ultrasonic wave, the attenuating effect from the alkali hydrolysis of the fibers became dominant and thus the NaOH/ultrasonic wave treated bico MB webs showed less thickness than the ones treated with ultrasonic wave alone, which could be easily seen in Figure 5.

3.6 Changes in air permeability

Figure 6 shows relations between air permeability and the ultrasonic power used. Air permeability decreased, as a whole, with the increasing ultrasonic wave power used, which was consistent with the results from the change in thickness (Figure 5); usually air permeability of nonwoven webs exhibit decreasing trend with increasing web thickness.

For the ultrasonic wave treatment alone, 100 Watt ultrasonic wave power was possibly not sufficient to split large amount of bico MB fibers, only caused fibers to entangle one another, and the relaxation of the processing stress existed in the fibers, the ultrasonic wave treated webs only shrank, as a result, generating no additional pores in the treated web samples, which led to the web samples with the least air permeability, compared to other samples treated with the other methods.

But in the existence of ultrasonic wave, both the webs treated with benzyl alcohol and alkali solutions showed higher air permeability than that treated with ultrasonic wave alone, indicating that benzyl alcohol treatment and alkali treatment could both split bico MB fibers in the webs and thus increased the porosity of the webs, with NaOH treated web samples showing higher air permeability due to the extra fiber hydrolysis effect from the alkali solution.

The air permeability of the web treated with ultrasonic wave alone increased initially and then decreased with the increasing power of ultrasonic wave; this was possibly because at lower ultrasonic wave energies, fibers were split and interstice of fibers was increased, that resulted in the air permeability increased. When the power of ultrasonic wave was increased continuously, the decrease of the air permeability was caused by fibers entangling severely.

When the power of ultrasonic wave was increased all the way up to 250 Watt, the web samples treated with ultrasonic wave alone showed significantly higher air permeability than those treated with the other two methods. This was possibly because that swelling agents brought about fibers entangling and nonwoven shrinkage, especially samples treated at high power, and that the phenomenon became more serious.

4. Conclusion

The ultrasonic technology was successfully applied to fiber splitting for side-by-side PET/PA6 bicomponent MB webs, and had a remarkable effect. The fiber diameter was reduced from 3.62µm to 2.11µm, when NaOH, the concentration of 5g/L, and ultrasonic wave, whose power was only 240w, were utilized. The weight loss was only 8.34% by the way, while 50% in tradition (J. Baldrian, 1991). SEM photograph shows damage of fibers was less, and main loss was attributable to fibers which were reinforced in webs. The porosity of treated specimens was reduced 7.59% than control,

which was 449.5m/s.

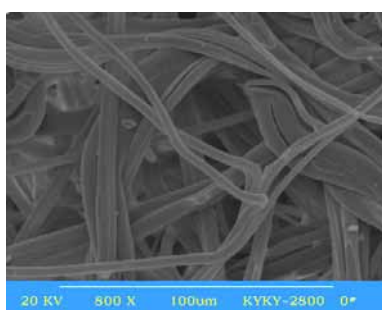
Benzyl alcohol was selected as separation reagent to swell PET and PA6 on the basis of similarity and intermiscibility, because solubility parameters are close. Dyeing rate of webs treated reached 50.47%, while control 19.00%. It was proved that benzyl alcohol was useful to fiber splitting of PET/PA6. At the same time, damage of webs was less by benzyl alcohol. Finer fibers whose specific surface area was greater, could absorb more particles. And benzyl alcohol is recycled and utilized repeatedly, and it is consistent with Green environmental protection and Energy Saving.

Acknowledgements

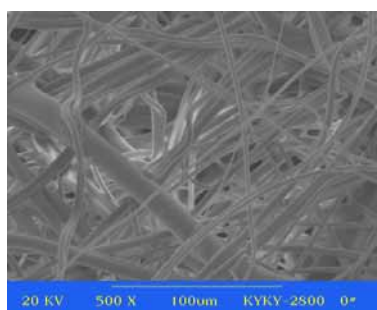
The authors thank Kun Wang and Weidan Shi for their assistance in the experiment. They are grateful to Qiang Zhou, for his helpful advice on SEM analysis, and to Wei Li, Yi Zhang from Textile College, for their encouragement and support. Finally, authors thank TANDEC for materials.

References

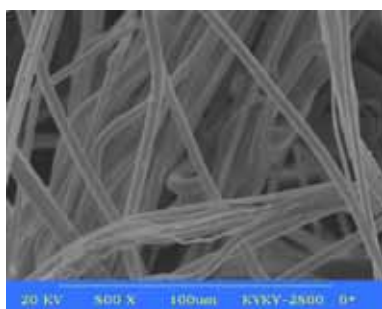
- Yin, Baopu, Jin, Xiangyu. (2003). Principle of fiber being split and performance of microfiber spunlaced nonwoven. *Journal of Donghua University*, (3):55-58.
- Yang, Bin, Yu, Zhicheng. (2000). Study on detaching mechanism and wearability of PET/PA microfiber, *Journal of Textile Research*, 21(3):137-147.
- Hong, Can. (2004). Manufacture and application about the melt-blown non-woven fabric and the preparation of the special material. *Chemical Industry and Engineering Progress*, 23(7): 778-781.
- J. Baldrian. (1991). Effect of swelling on the structure of oriented polyamide 6. *Polymer*, 32(4):740-744.
- Myung-Ja Park, Seong Hunkim. (2001). Effect of splitting and finishing on absorption/adsorption properties of split polyester microfiber fabrics. *Textile Research Journal*, 71(9): 831-841.
- Zhao, Ron (Rongguo), Larry C Wadsworth,* Sun, Christine & Zhang, Dong. (2003). "Properties of PP/PET bicomponent melt blown microfiber nonwovens after heat-treatment". *Polymer International*, 52: 133-137.
- Jin, Xiao, Wu, Haibo. (2006). The Influence of Parameters in PP/PE Blends Meltblowing Process on Web Properties. *Nonwovens*, 14(5):23-26.
- Zheng, Zeyong et al. (1989). Swelling equilibrium and the superstructures of uniaxially oriented α Nylon 6 in solvent mixtures. *Polymer Journal*, 21(1): 65-76.



(a)



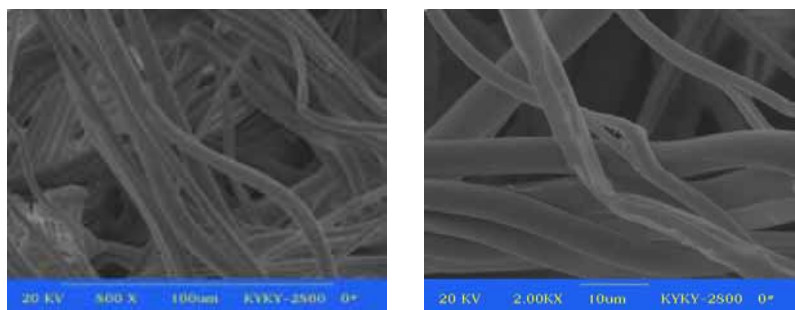
(b)



(c)



(d)



(e) (f)

Figure 1. SEM photographs (a) control (b) ultrasonic treatment(c) NaOH treatment (d) NaOH and ultrasonic treatment (power 240W)(e) benzyl alcohol treatment (f) benzyl alcohol and ultrasonic treatment(power 240W)

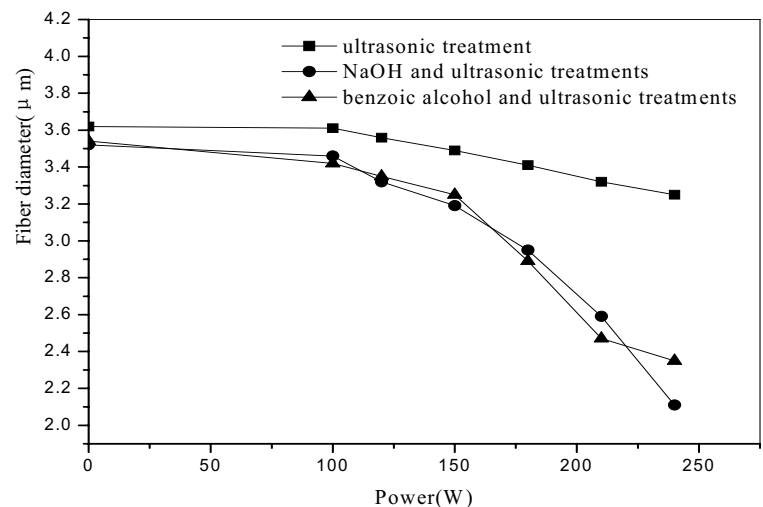


Figure 2. The effect from ultrasonic power on fiber diameter during ultrasonic treatment, NaOH/ultrasonic treatment and benzyl alcohol/ultrasonic treatment

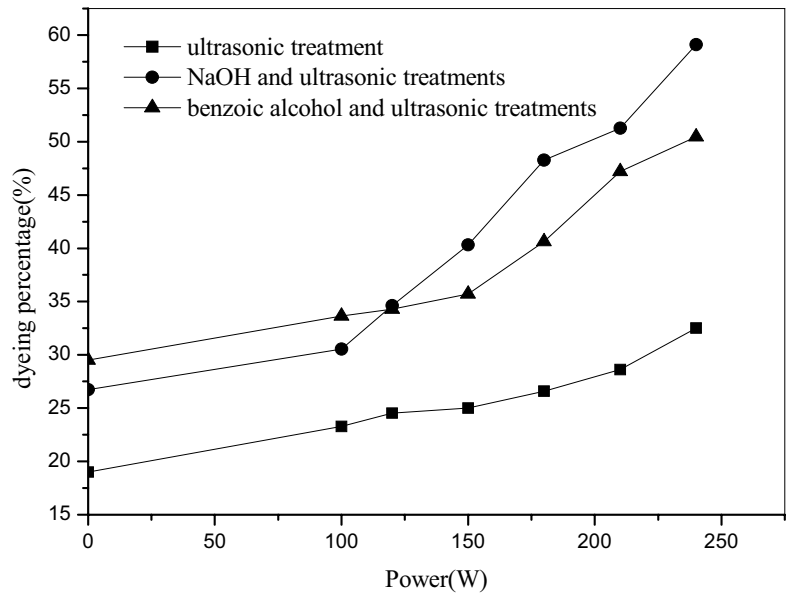


Figure 3. Dyeing rate of webs at various powers

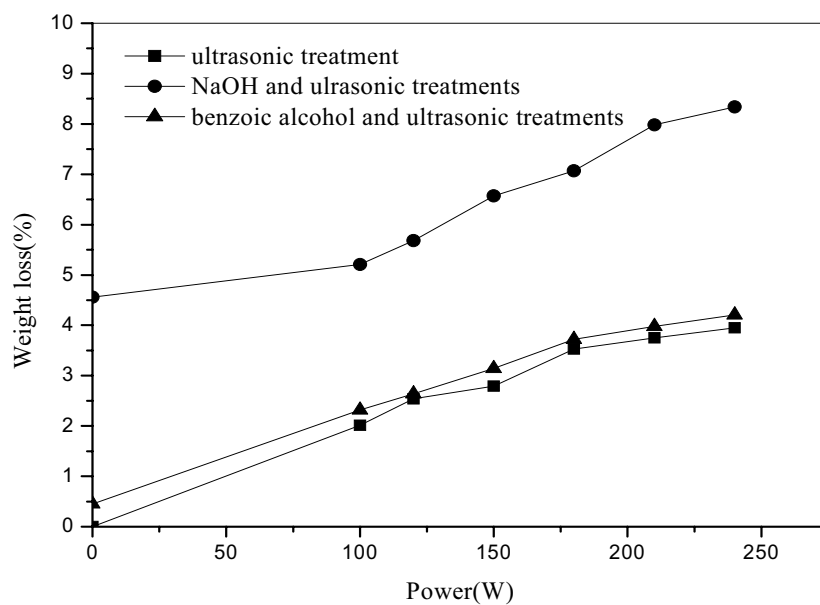


Figure 4. Weight loss of webs at various powers

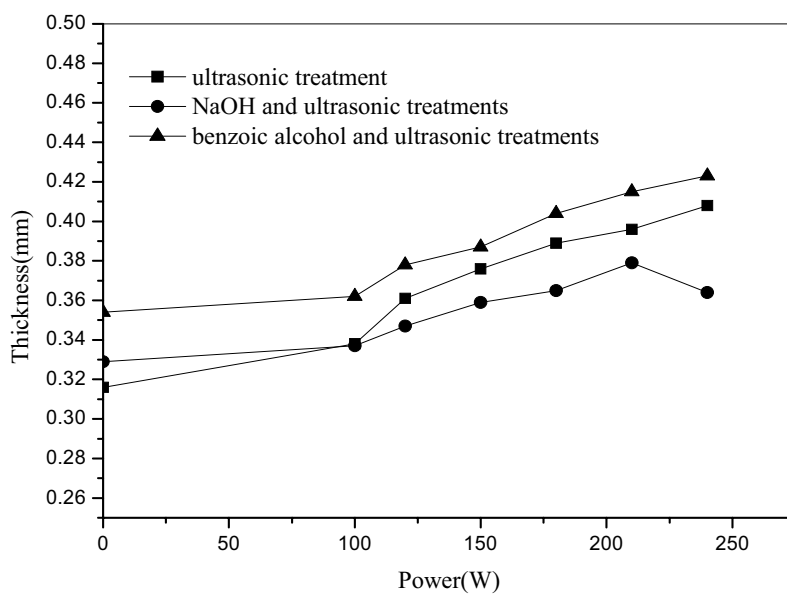


Figure 5. Thickness of treated webs at various powers

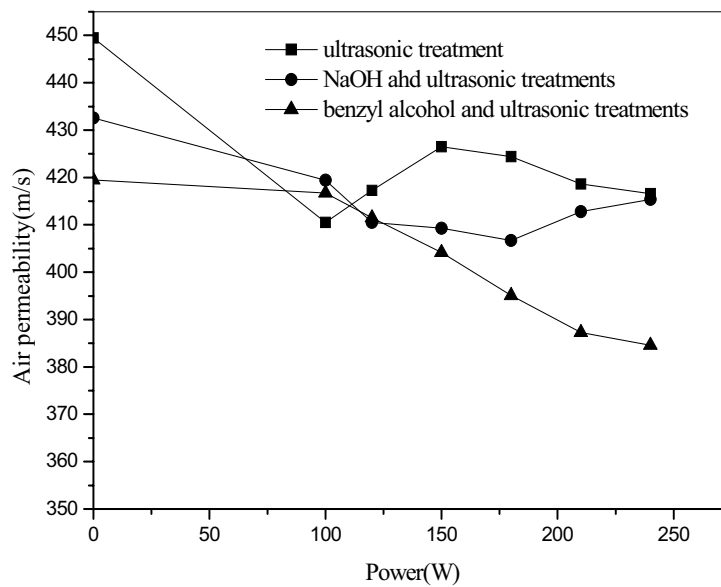


Figure 6. Air permeability of webs at various powers



Organotin(IV) Derivatives of *N*-Tolyl-*m*-methoxybenzohydroxamic Acid: Synthesis and Structural Elucidation

Abdualbasit Graisa, Yang Farina
School of Chemical Science & Food Technology
University Kebangsaan Malaysia, Malaysia

Emad Yousif (Corresponding author)
Department of Chemistry, College of Science
Al-Nahrain University, Baghdad, Iraq
E-mail: emad_yousif@hotmail.com

Elhadi Elbay Saad
Department of Chemistry, Faculty of Science
Sebha University, Sebha-Libya

Abstract

A series of organotin (IV) complexes of the type R_2SnL_2 , where R = phenyl, butyl and methyl and HL = *N*-Tolyl-*m*-methoxybenzohydroxamic acid were synthesized and characterized by physico-chemical (elemental analysis, and electrolytic conductance) and spectral Infrared and (1H , ^{13}C and ^{119}Sn NMR) techniques. Monomer structures for the complexes, bidentate and octahedral geometry was proposed for the complexes prepared.

Keywords: *N*-Tolyl-*m*-methoxybenzohydroxamic acid, Diorganotin(IV) Complexes, Spectral studies

1. Introduction

In the past decades the chemistry of tin compounds has gained considerable importance, both in basic research and in industrial applications. There are many interesting aspects of inorganic and organic tin chemistry discussed in various reviews. Tin (IV) and organotin (IV) compounds, a deceptively simple area of inorganic and metal-organic chemistry, have been receiving more attention due to the important industrial (Tammy and Georges, 2005) and environmental applications. Nitrogen, oxygen, and sulfur donor ligands have been used to enhance the biological activity of organotin derivatives (Mohammad et al., 2004; Jason et al., 2000). Also organotin compounds with such ligands have widely been tested for their possible use in cancer chemotherapy (Shang et al. 2008; Zhou et al. 2005). The coordination chemistry of tin is extensive with various geometries and coordination numbers known for both inorganic and organometallic complexes (Katsoulakou et al. 2008; Baul et al. 2007; Farina et al. 2008). Hydroxamic acids constitute a very important class of chelating agents with versatile biological activity (Farkas et al. 2002; Wang et al. 2003)

In view of the diverse fields of applications of organotin complexes, we have synthesized new ligand *N*-methyl-*m*-nitrobenzohydroxamate(HL) and its organotin(IV) compounds Diphenyltin(IV) Bis(*N*-Tolyl-*m*-methoxybenzohydroxamate) (Ph_2SnL_2), Dibutyltin (IV) Bis (*N*-Tolyl-*m*-methoxybenzohydroxamate)(Bu_2SnL_2) and Dimethyltin(IV) Bis (*N*-Tolyl-*m*-methoxybenzohydroxamate)(Me_2SnL_2)

2. Materials and Methods

2.1 Synthesis of *N*-Tolyl-*m*-methoxybenzohydroxamic acid

An ether solution of *m*-methoxybenzoyl chloride (0.01 mole) was added dropwise to a stirred cold ethereal solution of *N*-Tolylhydroxylamine (0.01 mole) containing sodium hydrogen carbonate (0.01 mole). The precipitate was filtered and washed with cold ethanol. Good quality crystals suitable for X-ray analysis were obtained by recrystallization from ethyl acetate.

<Scheme 1>

2.2 Preparation of Complexes

Complexes were synthesized by dissolving the free ligand *N*-Tolyl-*m*-methoxybenzohydroxamic acid (5 mmol) in hot toluene and adding the organotin (2.5 mmol) to the solution. The solution was refluxed for 6 hours with magnetic stirrer and then cooled and filtered. The filtrate was reduced under vacuum to a small volume and solid was precipitated by the added of petroleum ether (60-80 °C).

3. Instrumentation

The percentage compositions of the elements (CHN) for the compounds were determined using an elemental analyzer CHNS Model Fison EA 1108. Molar conductance measurements were made in anhydrous DMF at 25 °C using Inolop-Cond Level 1 WTW, The infrared spectra were recorded as potassium bromide discs using a Perkin-Elmer spectrophotometer GX. The ¹H and ¹³C nuclear magnetic resonance spectra were recorded using the JEOL JNM-ECP 400 spectrometer. Electronic UV-Vis spectra were recorded with 1650 PC SHIMADZU Spectrophotometer in the range 200-400 nm. And for ultraviolet using Shimadzu-UV-Vis spectrophotometer UV -2450, DMSO used as solvent. Crystals structures determination were carried out on a Bruker Smart APEX CCD area detector diffractometer equipped with graphite monochromatised Mo-K_α (λ=0.71073 Å) radiation in each case. All data collection was carried out at room temperature. The program *SMART* (Siemens 1996) was used for collecting frames of data, indexing reflections and determination of lattice parameters, *SAINT* (Siemens 1996) for absorption correction, and *SHELXTL* (Sheldrick 1997)

4. Results and Discussion

The ligand was prepared by the reaction of *m*-methoxybenzoyl chloride with one mole *N*-Tolyl-*m*-hydroxylamine in presence of sodium hydrogen carbonate as a catalyst. The purity of the ligand and its complexes were checked by TLC using silica gel-G as adsorbent. The conductance of these complexes has been recorded in DMF at room temperature in the range 10-19 ohm⁻¹ cm² mol⁻¹, suggesting their non-electrolytic nature. Their physical properties and analytical data are recorded in Table (1). The calculated values were in a good agreement with the experimental values.

4.1 Infra-Red Spectroscopy

Solid state infrared spectra of the *N*-Tolyl-*m*-methoxybenzohydroxamic acid are recorded in the range 4000-370 cm⁻¹ and the most important bands are presented in the below table studied here. In agreement for diagnostic purpose, the principal infrared absorption bands are those due to -OH, C=O, C-N and N-O stretching vibrations of the hydroxamate group free hydroxamic acids have been shown to exist principally in the keto form. In compound (C=O) group is positioned at 1617cm⁻¹ significantly, below the typical ketonic (C=O) of 1600 cm⁻¹. The (O-H) band is located at 3251 cm⁻¹ as broad band. The presence of the carbonyl band at lower frequency where together with the broad OH band. In general, the (C-N) and (N-O) bands occur as a sharp peak in the ranges 1429, 953 cm⁻¹ respectively (Shahid et al.2002).

On complexation, there are clear differences between the infrared spectra of the free ligand and the diorganotin(IV) complexes. In all cases, the most important features of the infrared spectra are the absence of the (OH) bands due to the complexation of the metal to the ligand through oxygen of the carbonyl group. This suggests the deprotonation of the hydroxamate group on complex formation, and (C=O) group are shifted to lower frequencies in the range 1624-1691 cm⁻¹ in there respective diorganotin (IV) complexes. The bands for ν(Sn-C) and ν(Sn-O) are assigned in the range of (573-445) and (454-443) cm⁻¹ respectively (Saad et al. 2003). The IR data of the complexes are shown in Table (2). The Table lists the stretching frequency (ν) for some of the characteristics groups exhibited by the ligand and complexes. Major bands in the electronic spectra of the ligand and their tin(IV) complexes also are given in Table (2), Figure (1 to 4).

4.2 Nuclear Magnetic Spectroscopy

The ¹H NMR spectra for all compounds were recorded in [₂H⁶] DMSO using tetramethylsilane as the internal standard. The data are compiled in Table (3). The conclusion drawn from ¹H NMR studies of a few compounds lend further support to suggested formation of *N*-Tolyl-*m*-methoxybenzohydroxamic acid. Ligand (HL) give a singlet -OH resonance near δ 10.64 ppm due to hydroxy group. The hydroxy resonances is absent in the spectra of the complexes indicting deprotonation and coordination of Tin to the oxygen. There is a small upfield shift of the aromatic protons resonances of the ligand upon chelation with the diorganotin(IV) moiety. The complexes Ph₂SnL₂, Bu₂SnL₂ and Me₂SnL₂ Show additional signals. The methyltin (Sn-CH₃) accure at 1.36, 1.34 and 1.32 ppm as on the sharp singlet at integrates for the protons accompanied by satellites due to the ¹H-¹¹⁹Sn coupling that corresponds to the hydrogen atom of the methyl protons of the Me-Sn for the Me₂SnL₂ (Najeeb et al. 2009). In dibutyltin(IV) complex the butyl protons appears as a multiple and a triplet in the range 1.53-0.70 ppm due -CH₂CH₂CH₂CH₃ group. The aromatic protons in Ph-Sn appears in the 7.16-8.18 ppm (Shahid et al.2002), Figure (5 to 8).

The ¹³C NMR of the ligand and its complexes are presented in Table (4). The C=O resonance group of the complexes at (159.44-159.18) ppm where shifted downfield compared with the position in the free ligand which appeared at 158.64

ppm. It is most likely that shift is due to the decrease of electron density at carbon atoms when oxygen is bonded to metal ion (Saad et al. 2003), (Figure 9 to 12).

On the basis of the observed spectral evidence, the following structure suggested for the prepared complexes

<Scheme 2>

4.3 X-ray structural studies of *N*-tolyl *m*-methoxybenzohydroxamic acid

The structure contain an $C_{15}H_{15}NO_3$ ligand, which is a molecule of 3-methoxybenzoyl chloride bonded with *N*-Tolyl hydroxylamine. The bond angles which will connect Sn atom with the ligand are: C(7)-N(1)-O2 = 117.43(16) , O(1)-C(7)-N(1)=120.14(15), respectively, giving the conformation of an octahedral with the oxygen atoms later at the bottom and the tin atom at the top. This coordination sphere is completed by the both oxygen atoms of the ligands and will be *cis* positions covering the oxygen atoms. The methoxybenzoyl chloride and tolyl hydroxylamine are chelated by carboxyl groups as shown bellow. And other data in table below.

<Scheme 3>

5. Conclusion

The ligand *N*-Tolyl-*m*-methoxybenzohydroxamic acid was successfully synthesized. The ligand was treated to different diorganotin(IV) oxide metal to afford the corresponding complexes. It may conclude that the ligand coordinated through oxygen to the Tin atom leading to the formation of five member ring chelate. Octahedral geometry was proposed for the prepared complexes.

Acknowledgment

The authors are grateful of School of Chemical Sciences and Food Technology, Universiti Kebangsaan Malaysia, for provision of laboratory facilities. We would like to thank Prof Dr Buhari Ben Yamin for Analysis X Ray Data. We would like to thank the Libyan government by General Committee of High Education for their financial support.

References

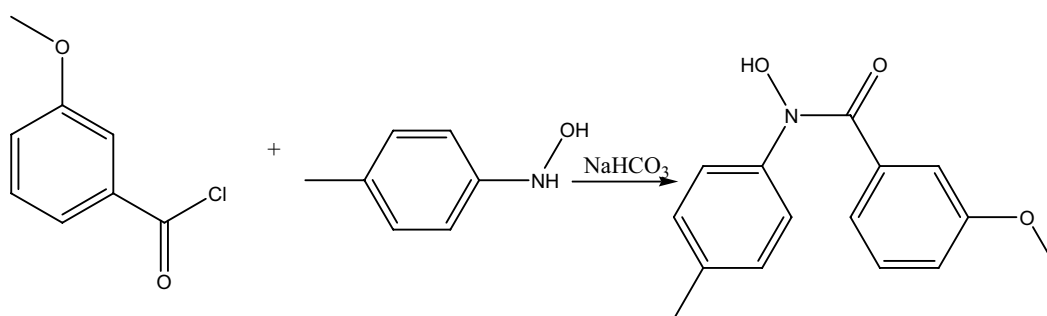
- Baul, T., C. Masharing, G. Ruisi, R. Jira'sko, M. Holcapek, D. De-Vos, D. Wolstenholme and A. Linden, (2007). Self-assembly of extended Schiff base amino acetate skeletons, 2- $\{[(2Z)-(3\text{-hydroxy-1-methyl-2-butenylidene})\text{amino}\}\text{phenylpropionate}$ and 2- $\{[(E)-1-(2\text{-hydroxyaryl})\text{alkylidene}]\text{amino}\}$ phenylpropionate skeletons incorporating organotin(IV) moieties: Synthesis, spectroscopic characterization, crystal structures, and in vitro cytotoxic activity, *Journal of Organometallic Chemistry*, 692: 4849–4862.
- Farina Y., Graisa A., Kassim M. & Yousif E. (2008). Preparation and Spectroscopic Studies of Diorganotin(IV) Complexes of *N*-Phenyl-*m*-Nitrobenzohydroxamic Acid. *European Journal of Scientific Research* 22(4): 602-607.
- Farina Y., Graisa A., Kassim M. & Yousif E. (2008). Synthesis and Characterization of Some Diorganotin (IV) Complexes of *N*-Tolyl- *m*-Nitrobenzohydroxamic Acid. *ARPJ Journal of Engineering and Applied Sciences* 3(6): 47-50.
- Farkas, E., Csoka H., Gama S. and Santos M., (2002). Dihydroxamate based siderophore model, piperazine-1,4-bis-(*N*-methyl-acetohydroxamic acid (PIPDMAHA), as a chelating agent of molybdenum(VI), *Talanta*, 57: 935–943.
- Jason, H., C. Kieran and R. Pratt. (2000). Inhibition of Serine Amidohydrolases by Complexes of Vanadate with Hydroxamic Acids. *Biochemical and Biophysical Res. Communications*, 274: 732–735.
- Katsoulakou, E., Tiliakos M., Papaefstathiou G. , Terzis A., Raptopoulou C., Geromichalos G., Papazisis K., Papi R., Pantazaki A., Kyriakidis D., Cordopatis P. and Zoupa E. (2008). Diorganotin(IV) complexes of dipeptides containing the α -aminoisobutyryl residue (Aib): Preparation, structural characterization, antibacterial and antiproliferative activities of $n\text{-Bu}_2\text{Sn}(\text{H}_2\text{L})$ (LH = H-Aib-L-Leu-OH, H-Aib-L-Ala-OH). *Journal of Inorganic Biochemistry*, 102: 1397–1405.
- Mohammad, M., S. Khadija, M. Sohail, A. Saqib and B. Moazzam. (2004). Synthesis, Spectral Characterization and Biological Applications of Tri- and Diorganotin(IV) Derivatives of 2-[*N*-(2,6-Dichloro-3-methylphenyl)amino]benzoic acid. *Turkish Journal of Chemistry*, 28: 17- 26.
- Najeeb D., Shalan N., Ibraheem H., Farina Y. and Yousif E., (2009). Synthesis and fungicidal activity of some diorganotin(IV) with benzamidocysteine, *Journal of Al-Nahrain University (Science)*, 12(1): 24-28.
- Saad, E., Y. Farina, I. Baba and H. Othman. (2003). Synthesis and Characterization of Some Diorganotin bis(*N*-methyl *O*-nitrobenzohydroxamate), *Sains Malaysiana*, 32: 79-86.
- Shahid, S., S. Ali, M. Hussain, M. Mazhar, Mahmood S. and S., Rehman. (2002). Synthesis, Characterization and Thermal Analysis of Organotin(IV) Derivatives of 4-(*N*-Maleoyl)Butanoate. *Turkish Journal of Chemistry*, 26: 589 – 597.

Shang, X., J. Cui, J. Wub, A. Pombeiro and Q. Li. (2008). Polynuclear diorganotin(IV) complexes with arylhydroxamates: Syntheses, structures and in vitro cytotoxic activities, *Journal of Inorganic Biochemistry*, 102: 901–909.

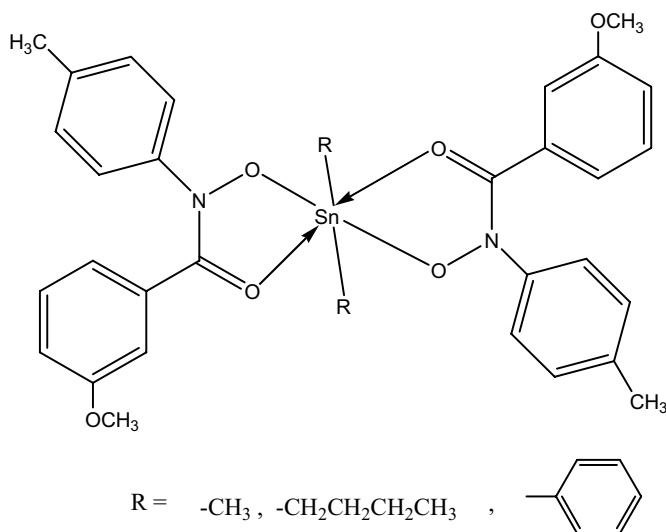
Tammy L. and M.Georges. (2005). New applications of LC–MS and LC–MS2 toward understanding the environmental fat of organometallics, *Trends in Analytical Chemistry*, 24: 7-12.

Wang, W., N. Ryder, B. Weidmann, D. Patel, J. Trias, R. Whitea and Z. Yuana. (2003). Substituted Hydroxamic Acids as Novel Bacterial DeformylaseInhibitor-Based Antibacterial Agents, *Bioorganic & Medicinal Chemistry Letters*, 13: 4223–4228.

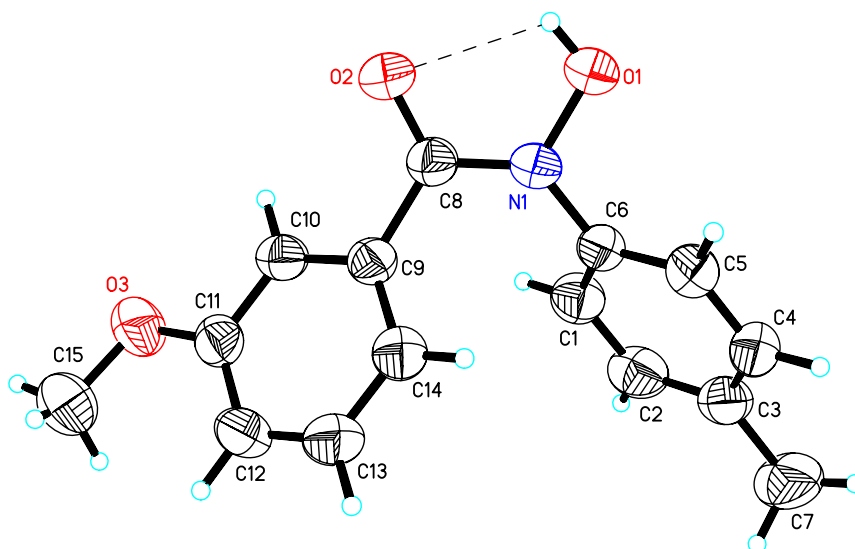
Zhou, Y., T., S. Ren, J. Yu and Z. Xia, (2005). Synthesis, crystal structure and in vitro antitumor activity of di-n-butyltin 40-(7-oxabicyclo [2,2,1]-5-heptane-2,3-dicarboximide)benzoates, *Journal of Organometallic Chemistry*, 69: 2186–2190.



Scheme 1.



Scheme 2.



Scheme 3.

Table 1. Physical data for preparation ligand and the complexes prepared.

Compound	Colour	Yield %	M.P(°C)	C	Found H	(Calad.)(%) N	Sn
HL	Yellow	85	137-138	69.46 (70.02)	5.13 (5.88)	4.90 (5.44)	-
Ph ₂ SnL ₂	Yellow	67	142-143	62.17 (64.22)	3.90 (4.88)	3.09 (3.57)	14.01 (15.11)
Bu ₂ SnL ₂	Yellow pale	71	189-190	60.89 (61.22)	5.78 (6.22)	3.14 (3.76)	15.22 (15.92)
Me ₂ SnL ₂	Brown	69	122-123	57.49 (58.12)	4.98 (5.18)	3.85 (4.24)	16.89 (17.95)

Table 2. Infrared Spectral Data for the ligand and its complexes

Compound	ν (O-H) cm ⁻¹	ν (C=O) cm ⁻¹	ν (C-N) cm ⁻¹	ν (N-O) cm ⁻¹	ν (Sn-C) cm ⁻¹	ν (Sn-O) cm ⁻¹
HL	3251	1617	1429	953	-	-
Ph ₂ SnL ₂	-	1724	1442	922	569	443
Bu ₂ SnL ₂	-	1691	1428	927	573	454
Me ₂ SnL ₂	-	1693	1430	934	545	455

Table 3. ^1H NMR spectral data (δ ,ppm) of the ligand and complexes

Compound	-OH(s)	Aromatic	-O-CH ₃ (s)	-CH ₃ (s)
HL	10.64	8.48-7.27	3.52	3.74
Ph ₂ SnL ₂	-	8.12-7.16	3.52	3.71
Bu ₂ SnL ₂	-	8.44-7.21	3.79	3.81
Me ₂ SnL ₂	-	8.14-7.39	3.79	3.79

Table 4. ^{13}C NMR spectral data (δ ,ppm) of the ligand and complexes

Compound	C-N	Aromatic	O-C, Ph-C	^{119}Sn
HL	158.61	113.67 -139.73	55.24	-
Ph ₂ SnL ₂	159.25	113.80-132.19	55.27	-404.75
Bu ₂ SnL ₂	159.44	114.13-133.49	55.26	-382.85
Me ₂ SnL ₂	159.18	113.77-129.95	55.23	-443.56

Table 5. Crystal data and structure refinement *N*-tolyl *m*-methoxybenzohydroxamic acid

Empirical formula	C ₁₅ H ₁₅ N O ₃	
Formula weight	257.28	
Temperature	298(2) K	
Wavelength	0.71073 Å	
Unit cell dimensions	a = 11.326(2) Å b = 7.9503(17) Å c = 15.560(3) Å	alpha = 90 deg. beta = 106.369(4) deg. gamma = 90 deg.
Volume	1344.3(5) Å ³	
Z, Calculated density	4, 1.271 Mg/m ³	
Absorption coefficient	0.089 mm ⁻¹	
F (000)	544	
Crystal size	0.47 x 0.36 x 0.27 mm	
Theta range for data collection	1.87 to 26.00 deg.	
Limiting indices	-7 ≤ h ≤ 13, -9 ≤ k ≤ 9, -19 ≤ l ≤ 15	
Reflections collected/unique	7258/2636 [R (int) = 0.0232]	
Completeness to theta	26.00	99.8 %
Refinement method	Full-matrix least-squares on F ²	
Data / restraints / parameters	2636 / 0 / 172	
Goodness-of-fit on F ²	1.158	
Final R indices [I > 2σ(I)]	R1 = 0.0588, wR2 = 0.1212	
R indices (all data)	R1 = 0.0767, wR2 = 0.1286	
Largest diff. peak and hole	0.176 and -0.164 e.Å ⁻³	

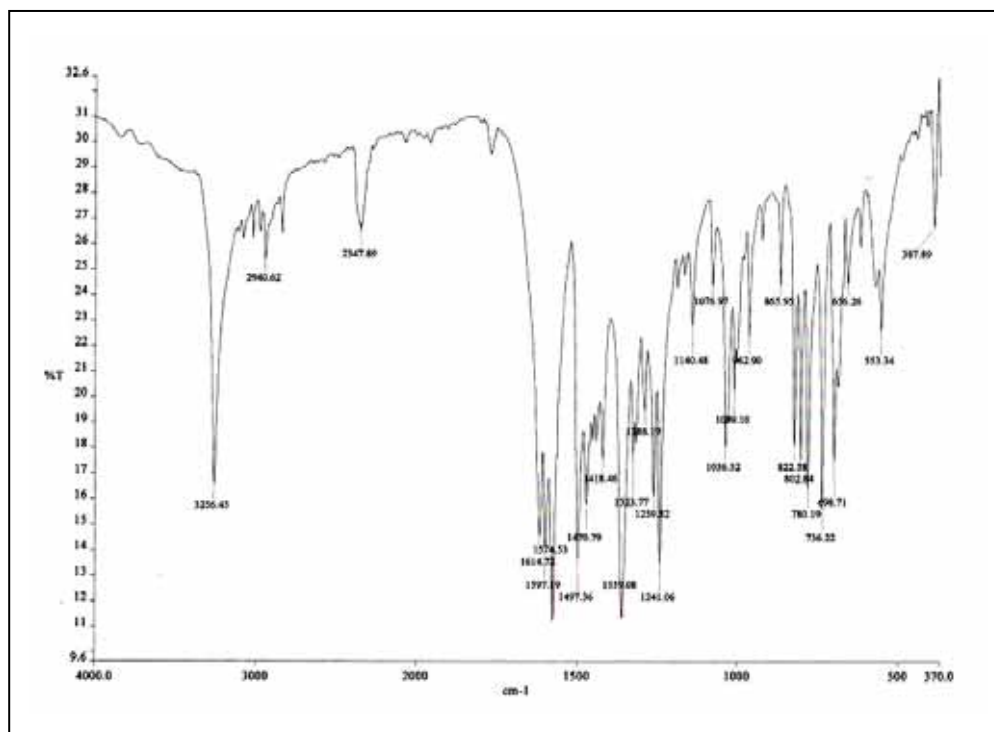
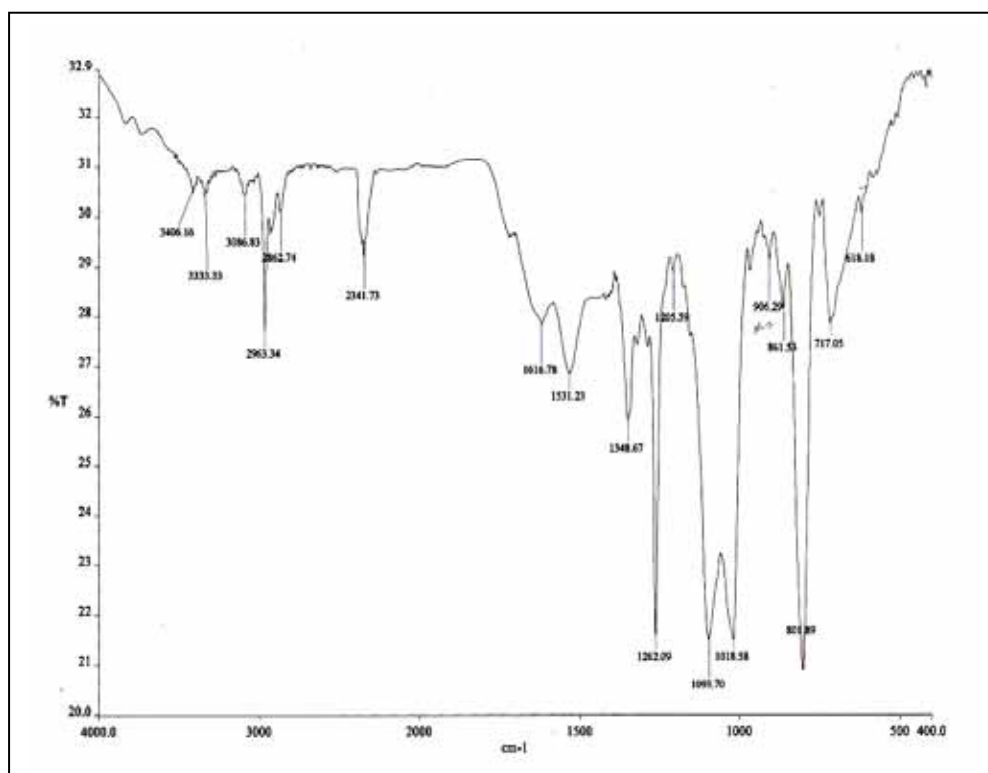
Table 6. Bond lengths [Å] and angles [deg] for *N*-tolyl *m*-methoxybenzohydroxamic acid

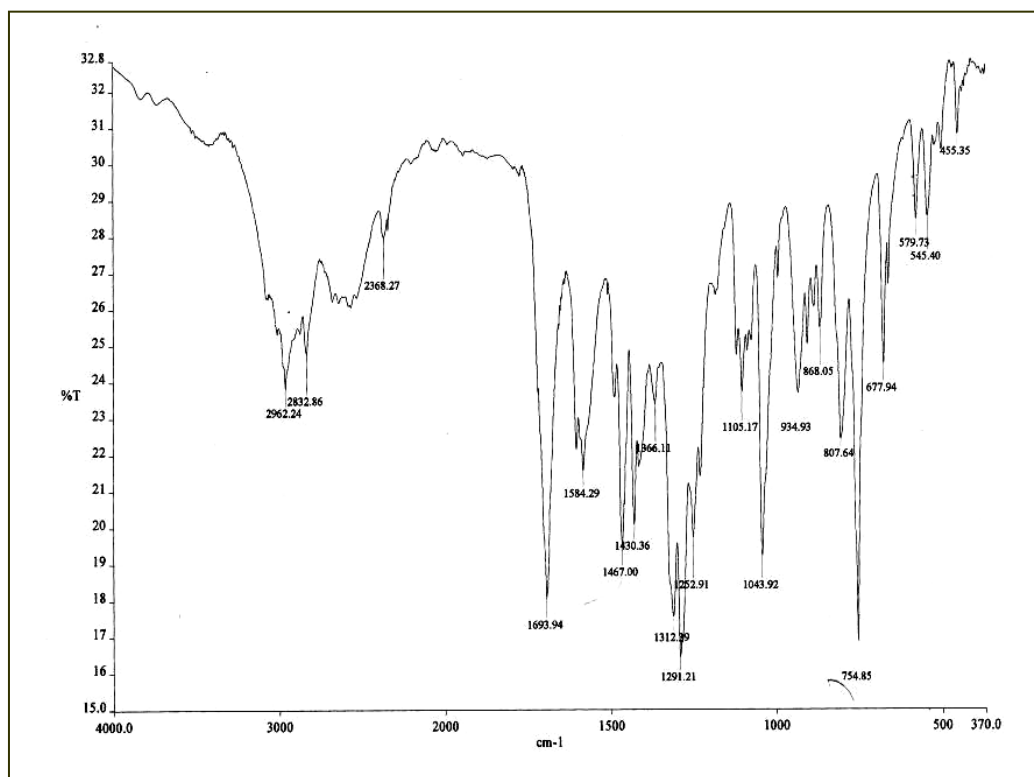
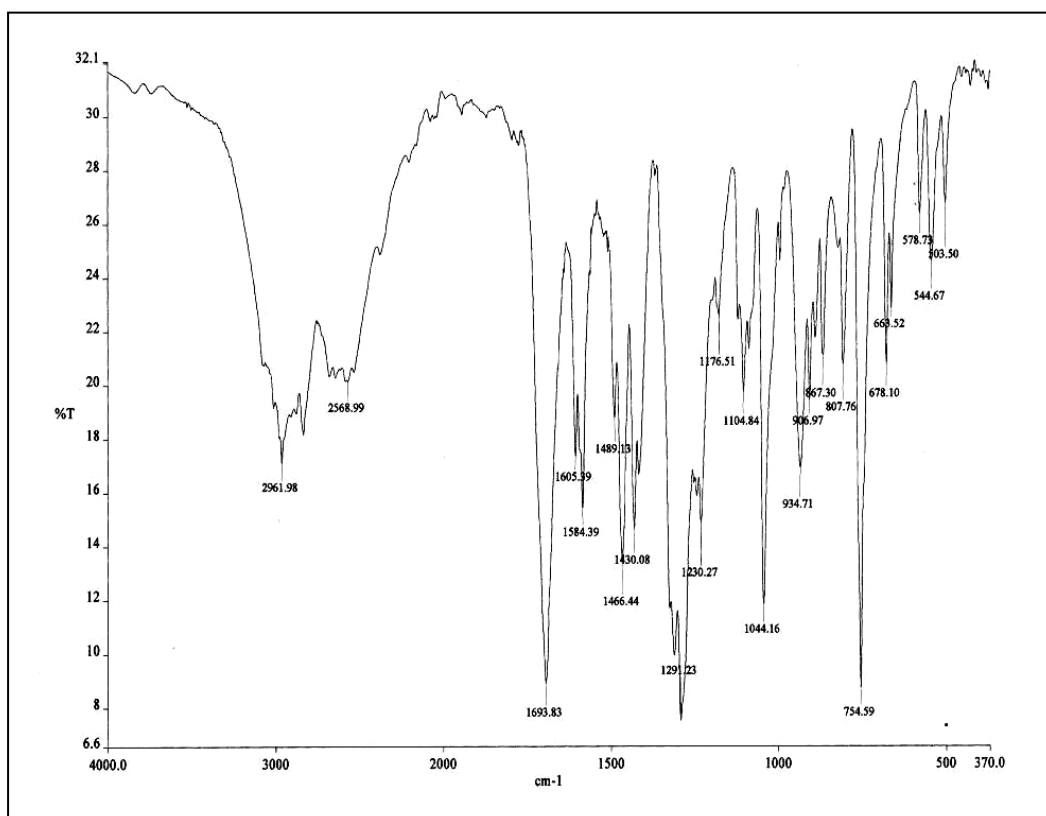
O(1)-C(2)	1.416(3)	C(4)-C(3)-C(2)	120.2
O(1)-C(7)	1.236(2)	C(4)-C(3)-H(3B)	120.2
O(2)-C(8)	1.4007(19)	C(2)-C(3)-H(3B)	121.4(2)
O(3)-N(1)	0.8200	C(5)-C(4)-C(3)	119.3
O(3)-H(3A)	1.331(2)	C(5)-C(4)-H(4A)	119.3
N(1)-C(8)	1.425(2)	C(3)-C(4)-H(4A)	119.31(19)
N(1)-C(9)	1.379(3)	C(4)-C(5)-C(6)	120.3
C(1)-C(6)	1.383(3)	C(4)-C(5)-H(5A)	120.3
C(1)-C(2)	0.9300	C(6)-C(5)-H(5A)	119.59(18)
C(1)-H(1A)	1.385(3)	C(1)-C(6)-C(5)	117.03(17)
C(2)-C(3)	1.378(3)	C(1)-C(6)-C(8)	123.03(17)
C(3)-C(4)	0.9300	C(5)-C(6)-C(8)	109.5
C(3)-H(3B)	1.373(3)	O(1)-C(7)-H(7A)	109.5
C(4)-C(5)	0.9300	O(1)-C(7)-H(7B)	109.5
C(4)-H(4A)	1.386(3)	H(7A)-C(7)-H(7B)	109.5
C(5)-C(6)	0.9300	O(1)-C(7)-H(7C)	109.5
C(5)-H(5A)	1.493(3)	H(7A)-C(7)-H(7C)	109.5
C(6)-C(8)	0.9600	H(7B)-C(7)-H(7C)	120.34(17)
C(7)-H(7A)	0.9600	O(2)-C(8)-N(1)	120.66(17)
C(7)-H(7B)	0.9600	O(2)-C(8)-C(6)	118.92(17)
C(7)-H(7C)	1.377(3)	N(1)-C(8)-C(6)	120.52(18)
C(9)-C(14)	1.378(3)	C(14)-C(9)-C(10)	118.90(17)
C(9)-C(10)	1.380(3)	C(14)-C(9)-N(1)	120.55(17)
C(10)-C(11)	0.9300	C(10)-C(9)-N(1)	119.1(2)
C(10)-H(10A)	1.387(3)	C(9)-C(10)-C(11)	120.4
C(11)-C(12)	0.9300	C(9)-C(10)-H(10A)	120.4
C(11)-H(11A)	1.381(3)	C(11)-C(10)-H(10A)	121.6(2)
C(12)-C(13)	1.505(3)	C(10)-C(11)-C(12)	119.2
C(12)-C(15)	1.379(3)	C(10)-C(11)-H(11A)	119.2
C(13)-C(14)	0.9300	C(12)-C(11)-H(11A)	117.72(19)
C(13)-H(13A)	0.9300	C(13)-C(12)-C(11)	121.5(2)
C(14)-H(14A)	0.9600	C(13)-C(12)-C(15)	120.8(2)
C(15)-H(15A)	0.9600	C(11)-C(12)-C(15)	121.6(2)
C(15)-H(15B)	0.9600	C(14)-C(13)-C(12)	119.2
C(15)-H(15C)	117.77(19)	C(14)-C(13)-H(13A)	119.2
C(2)-O(1)-C(7)	109.5	C(12)-C(13)-H(13A)	119.37(19)
N(1)-O(3)-H(3A)	117.34(15)	C(9)-C(14)-C(13)	120.3
C(8)-N(1)-O(3)	130.83(16)	C(9)-C(14)-H(14A)	120.3
C(8)-N(1)-C(9)	111.54(14)	C(13)-C(14)-H(14A)	109.5
O(3)-N(1)-C(9)	121.02(19)	C(12)-C(15)-H(15A)	109.5
C(6)-C(1)-C(2)	119.5	C(12)-C(15)-H(15B)	109.5
C(6)-C(1)-H(1A)	119.5	H(15A)-C(15)-H(15B)	109.5
C(2)-C(1)-H(1A)	115.84(18)	C(12)-C(15)-H(15C)	109.5
O(1)-C(2)-C(1)	125.03(19)	H(15A)-C(15)-H(15C)	109.5
O(1)-C(2)-C(3)	119.12(19)	H(15B)-C(15)-H(15C)	109.5
C(1)-C(2)-C(3)	119.6(2)		

Symmetry transformations used to generate equivalent atoms:

Table 7. Hydrogen bonds geometry for *N*-tolyl *m*-methoxybenzohydroxamic acid [Å° and deg.].

No	D—H...A	D—H	H...A	D...A	D—H...A	Symmetry code(i)
1	O1—H1...O2 ⁱ	0.86	1.99	2.699	139	-x+1,-y+1,z+1.

Figure 1. Infrared Spectra of *N*-tolyl *m*-methoxybenzohydroxamic acidFigure 2. Infrared Spectra of dibutyltin (IV) bis(*N*-tolyl *m*-methoxybenzohydroxamate)

Figure 3. Infrared Spectra of dimethyltin (IV) bis (*N*-tolyl-*m*- methoxybenzohydroxamate)Figure 4. Infrared Spectra of diphenyltin (IV) bis (*N*- tolyl *m*- methoxybenzohydroxamate)

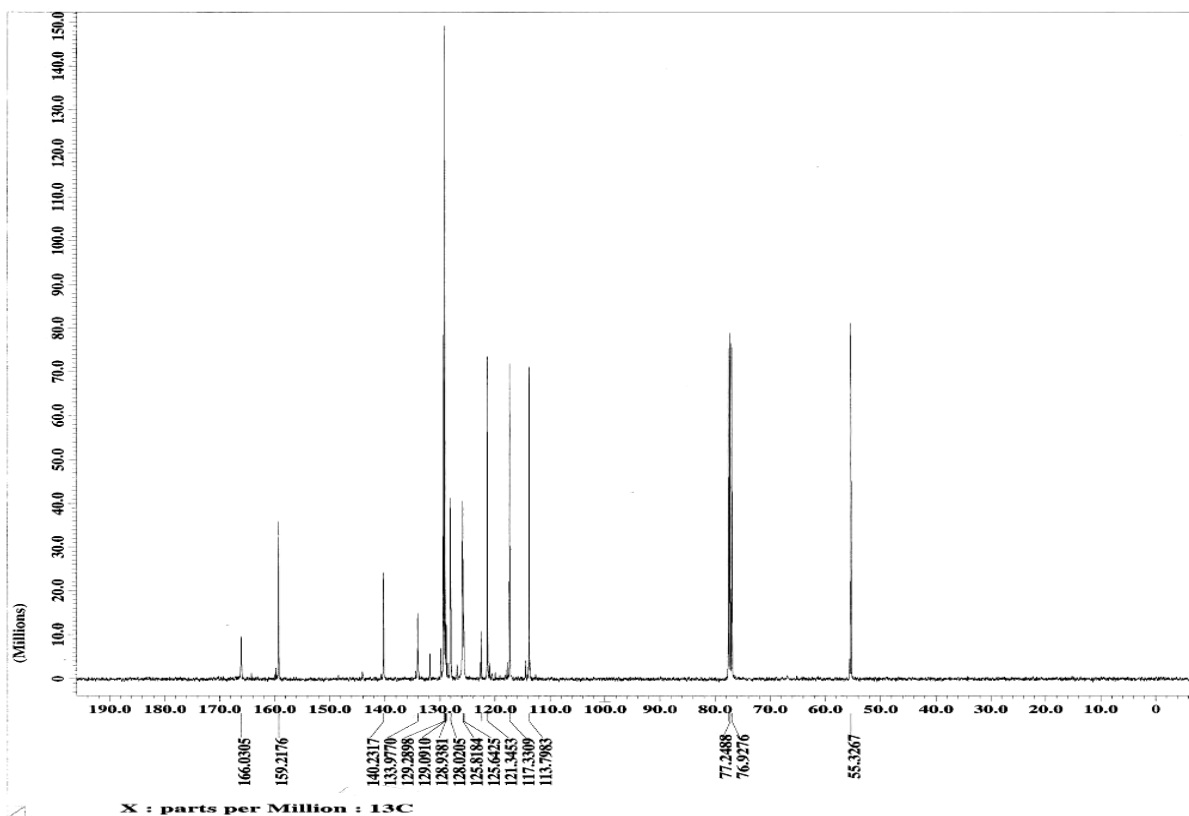


Figure 5. ^{13}C NMR spectrum of *N*-tolyl *m*-methoxybenzohydroxamic acid

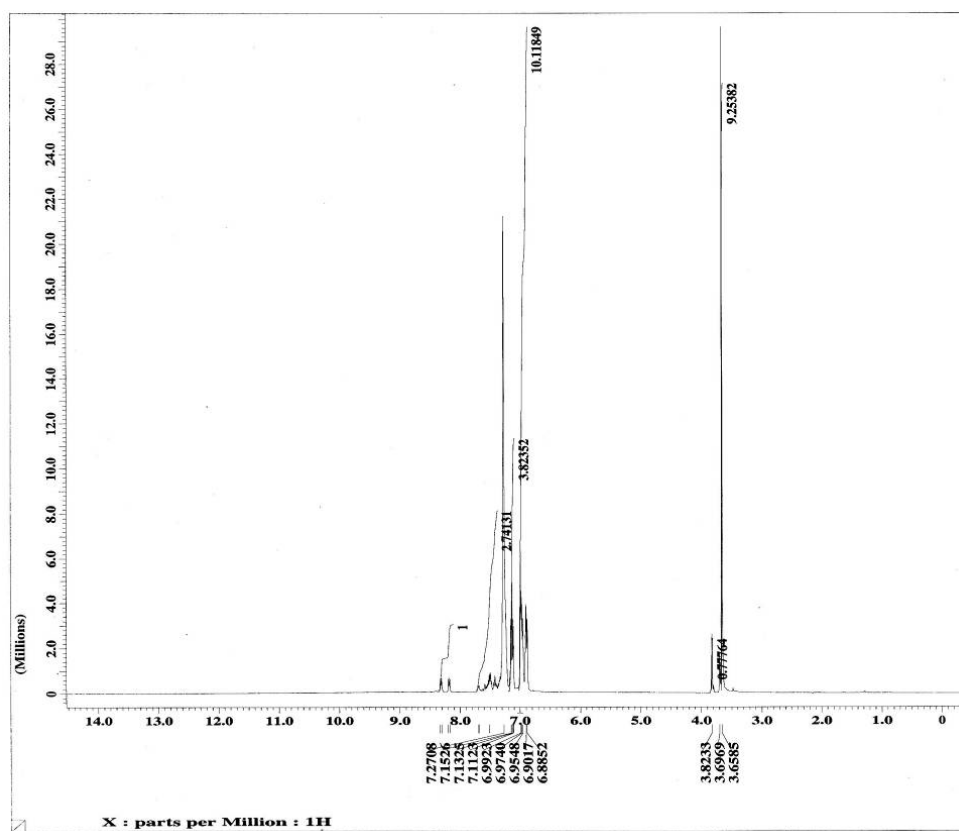


Figure 6. ^1H NMR spectrum of *N*-tolyl *m*-methoxybenzohydroxamic acid

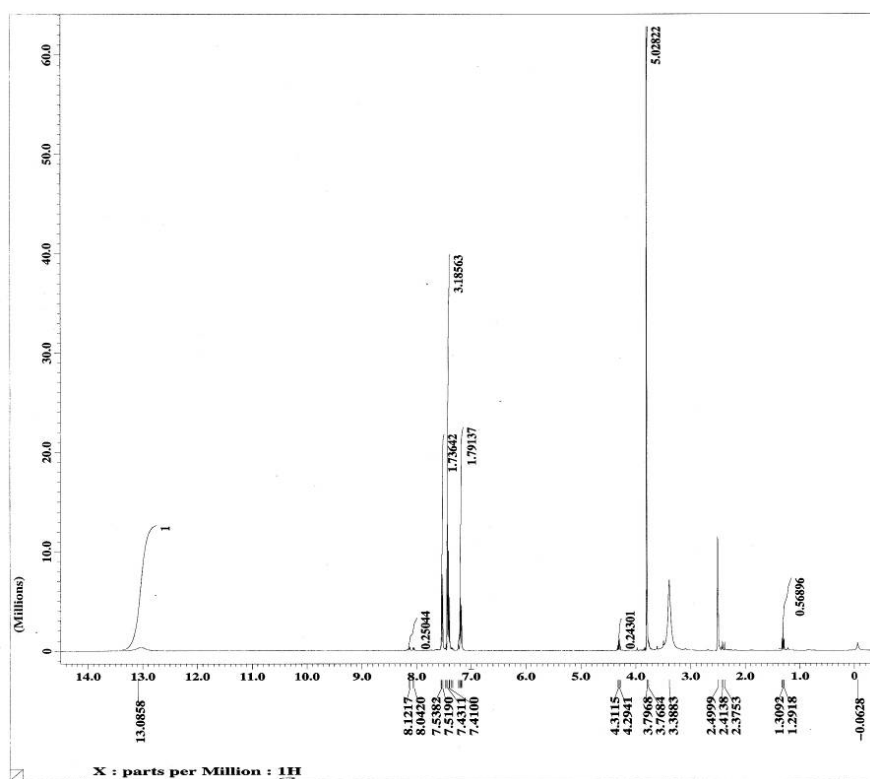


Figure 7. ^1H NMR spectrum of diphenyltin(IV) bis(*N*-tolyl *m*-methoxybenzohydroxamate)

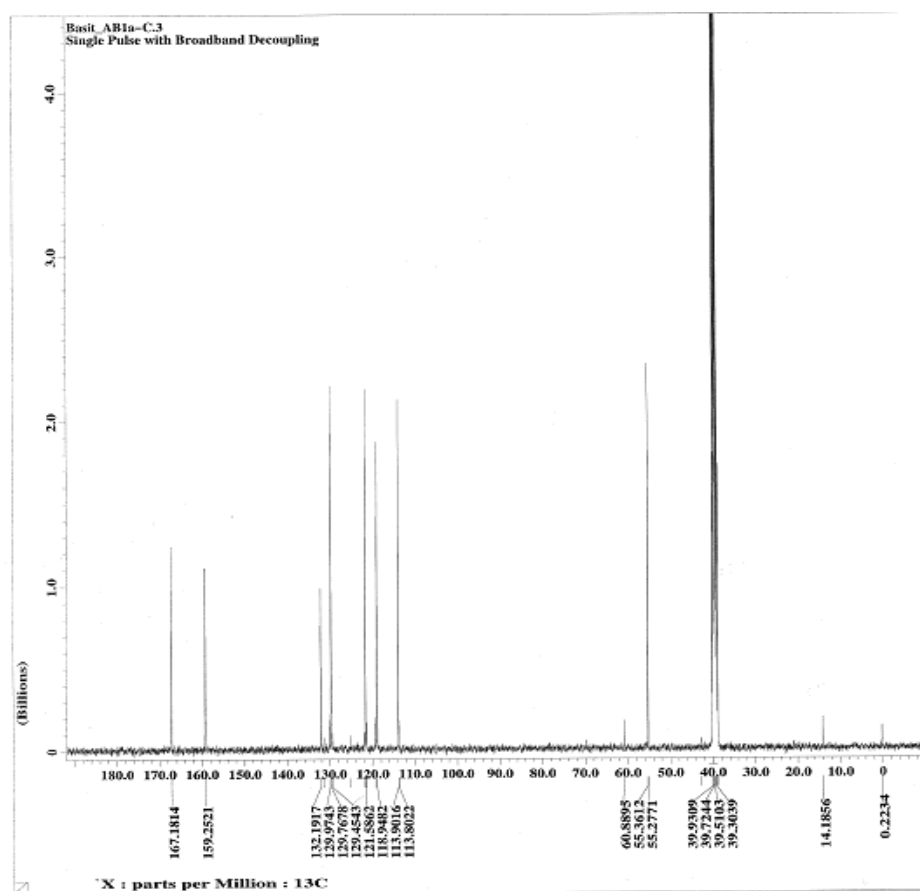
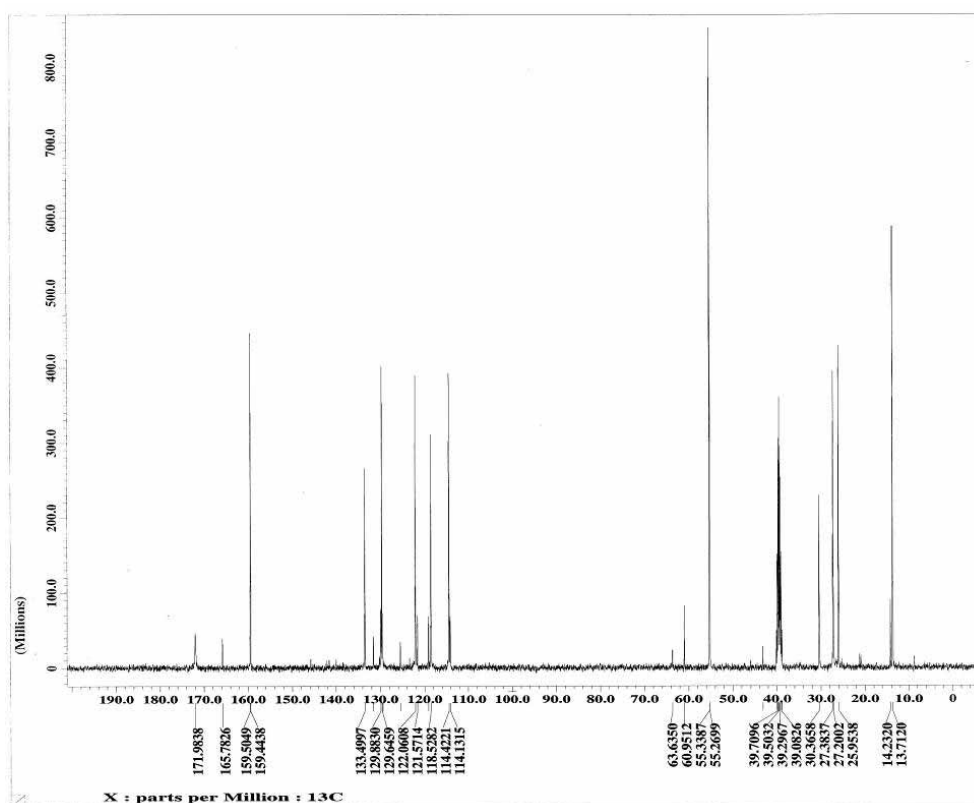
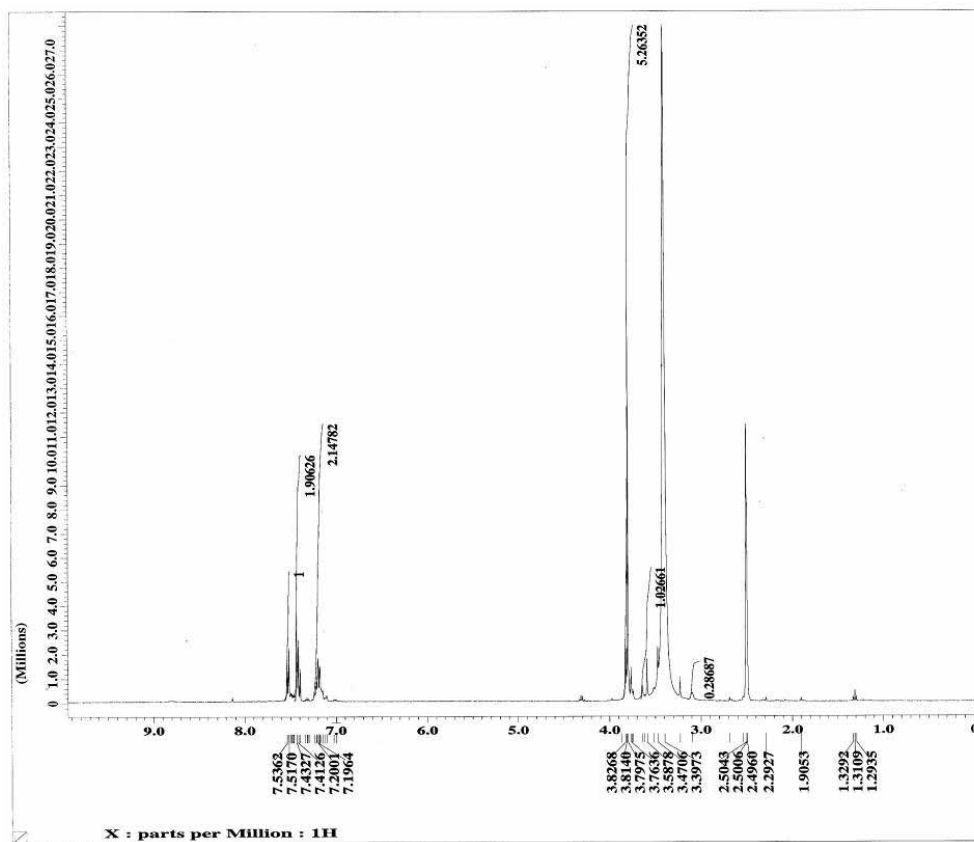
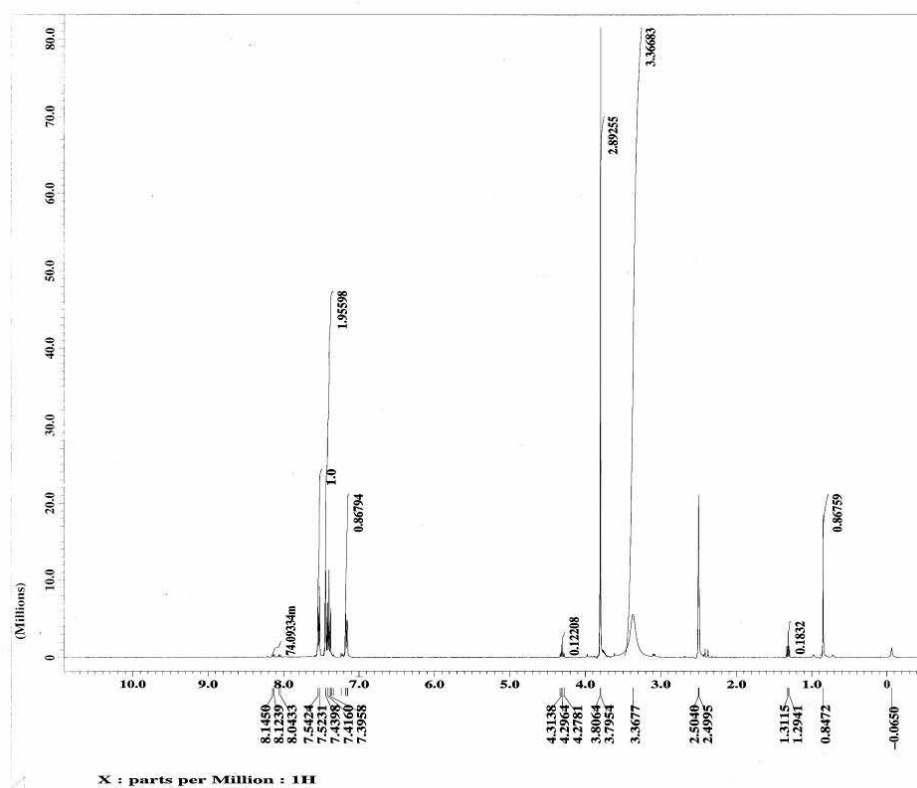
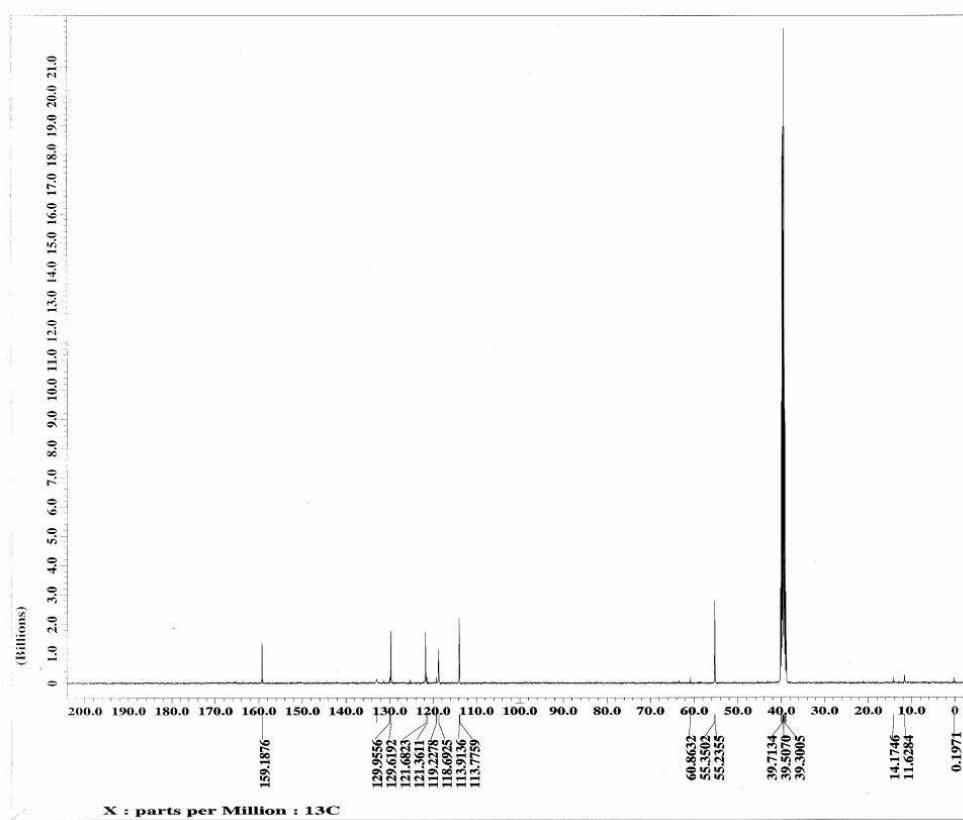


Figure 8. ^{13}C NMR spectrum of diphenyltin(IV) bis(*N*-tolyl *m*-methoxybenzohydroxamate)

Figure 9. ^{13}C NMR spectrum of dibutyltin (IV) bis(*N*-tolyl *m*-methoxybenzohydroxamateFigure 10. ^1H NMR spectrum of dibutyltin (IV) bis(*N*-tolyl *m*-methoxybenzohydroxamate

Figure 11. ^1H NMR spectrum of dimethyltin (IV) bis(*N*-tolyl *m*-methoxybenzohydroxamate)Figure 12. ^{13}C NMR spectrum of dimethyltin (IV) bis(*N*-tolyl *m*-methoxybenzohydroxamate)



Studies on Thermal, Mechanical and Morphological Behaviour of Caprolactam Blocked Methylenediphenyl Diisocyanate and Bismaleimide Modified Epoxy Matrices

Daofang Shi

Tianjin Polytechnic University

NO.63 Cheng Lin Zhuang Road, Tianjin 300160, China

E-mail:sdf_1103@126.com

Mingkang An

Tianjin Polytechnic University

NO.63 Cheng Lin Zhuang Road, Tianjin 300160, China

E-mail:amk_8496@126.com

Guojun Wang

Tianjin Polytechnic University

NO.63 Cheng Lin Zhuang Road, Tianjin 300160, China

E-mail:wangguojun1001@163.com

Abstract

Diglycidyl ether of bisphenol A epoxy resin (DGEBA) was toughened with 5%, 10% and 15% (by wt) of caprolactam blocked methylenediphenyl diisocyanate (CMDI) using 4,4'-diaminodiphenylmethane (DDM) as curing agent. The toughened epoxy resin was further modified with chemical modifier N, N'-bismaleimido-4,4'-diphenylmethane (BMI). Caprolactam blocked methylenediphenyl diisocyanate was synthesized by the reaction of caprolactam with methylenediphenyl diisocyanate in presence of carbon tetrachloride under nitrogen atmosphere. Thermal properties of the developed matrices were characterized by means of differential scanning calorimetry (DSC), thermo gravimetric analysis (TGA), heat distortion temperature (HDT) and dynamic mechanical analysis (DMA). Mechanical properties like tensile strength, flexural strength and impact strength were tested as per ASTM standards. The glass transition temperature (T_g) and thermal stability were decreased with increase in the percentage incorporation of CMDI. The thermomechanical properties of caprolactam blocked methylenediphenyl diisocyanate toughened epoxy resin were increased by increasing the percentage incorporation of bismaleimide. The values of impact strength for epoxy resin were increased with increase in the percentage concentration of CMDI. The homogeneous morphology of CMDI toughened epoxy resin and bismaleimide modified CMDI toughened epoxy resin system was ascertained from scanning electron microscope (SEM).

Keywords: Epoxy resin, CMDA, BMI, Glass transition temperature, Thermal stability and impact strength

1. Introduction

Epoxy resin is a versatile and widely accepted matrix material for the fabrication of advanced composites, hardware components, electronic circuit board materials, radomes and missile equipment components because of its excellent bonding, physico-chemical, thermal, mechanical, dielectric and aging characteristics (Leon Yu T, 2000, p.257). To improve working performance of epoxy resin suitable for advanced engineering applications, the toughening of epoxy resin with by blending with flexible polymers and elastomers. However, they improved its impact properties with appreciable loss of tensile and thermal properties. Hence, selection of suitable polymeric materials is essential to

improve the impact strength with retaining stiffness, glass transition temperature and thermal stability of the epoxy matrix.

In earlier studies the significant improvement in thermo mechanical, dielectric and aging characteristics have been achieved by using siloxane (Suresh Kumar R, 2006, p.668), cyanate ester (Dinakaran K, 2003, p.1596) and polysulphone (Rajasekaran R, 2007, p.911) as chemical modifiers for epoxy resin.

To make further advancement in this direction the present work is under taken to use caprolactam blocked methylenediphenyl diisocyanate as toughening agent and bismaleimide as chemical modifier for epoxy resin. Propriate chemical modifiers are essential. The toughness of the epoxy resin has been increased by blend

Caprolactam blocked methylenediphenyl diisocyanate is expected to possess better combinations of thermo mechanical properties suitable for the fabrication of polymer composites because of their flexible structure (-NH-CO-) formed during in situ reaction of cyclic aliphatic caprolactam with aromatic diisocyanate. Several blocked diisocyanates like ketoxime, dimethylpyrazole and caprolactam blocked aromatic diisocyanates (Subramani S, 2004, p.329) have already been developed and used for the synthesis of chain extended polyurethanes.

Blocked diisocyanate with flexible linkage (-NH-CO-) is expected to function as the best thermoplastic toughener for epoxy resin, because of its versatile behavior of flexibility. It was observed that the introduction of CMDI into epoxy resin improved its mechanical properties with little loss of glass transition temperature. To retain and to improve the glass transition temperature of CMDI (Han HL, 1998, p.2635) toughened epoxy system to an appreciable extent, bismaleimide (Guozheng Liang, 1998, p.1623) is used as a chemical modifier in the present work owing to its superior thermo mechanical properties.

Hence, in the present work an attempt has been made to improve both toughness and thermo mechanical behavior of epoxy resin without an appreciable loss in strength properties by forming an inter-crosslinked network of caprolactam blocked methylenediphenyl diisocyanate toughened epoxy system and bismaleimide (4,4'-bismaleimidodiphenylmethane).

2. Experimental

2.1 Materials

The commercially available epoxy resin (diglycidylether of bisphenol A, DGEBA) having epoxy equivalent about 180–190, 4, 4'-diaminodiphenylmethane (DDM) curing agent. BMI was obtained from Hubei. CMDI was obtained from Shandong.

2.2 Preparation of caprolactam blocked diisocyanate epoxy resin bismaleimide blend

Fixed amount of epoxy resin, varying amounts (5%, 10% and 15%) of caprolactam blocked methylenediphenyl diisocyanate (by wt%) were thoroughly blended at 90 °C for 10 min with constant stirring. The calculated amounts (4%, 8% and 12%) of BMI (by wt %) were dissolved in the above blend at 100 °C under vigorous stirring. After complete dissolution, the stoichiometric amount of diaminodiphenylmethane (with respect to epoxy) was added and the

2.3 Test methods

2.3.1 Thermal properties

Glass transition temperature (T_g) of the samples was determined using a DSC Netzsch (TA instruments, USA) in the temperature range between 50 °C and 250 °C at a heating rate of 10 °C per min in nitrogen atmosphere. Thermo-gravimetric analysis (TGA) was carried out using a Thermal Analyst 2000 (TA instruments, USA) at a heating rate of 10 °C per min in nitrogen atmosphere. Dynamic mechanical behavior of the samples was measured using a DMA Netzsch 242 at a heating rate of 10 °C per min from 30 to 300 °C. The heat deflection temperature (HDT) of the samples was tested as per ASTM D648 - 72.

2.3.2 Mechanical properties

The tensile (stress–strain) properties were determined using INSTRON (Model 6025 UK) as per ASTM D 3039 at 10 mm/min cross-head speed using specimen with a width of 25 mm, length of 200 mm and thickness of 3 mm. The flexural (strength and modulus) properties were measured (INSTRON, Model 6025 UK) as per ASTM D 790 using specimen with dimensions 3 mm in depth, 10 mm in width and 90 mm in length at 10 mm/min cross-head speed. The unnotched Izod impact strength of each sample was studied as per ASTM D 256. Five sample specimens were tested for each analysis.

2.3.3 Morphology

Surface morphology of fractured surface of the samples was performed using scanning electron microscope (SEM; JEOL JSM Model 6360). The fractured surface of the samples was coated with platinum before scanning.

3. Results and discussion

3.1 Thermal properties

The glass transition temperature (T_g) of unmodified epoxy, caprolactam blocked methylenediphenyl diisocyanate toughened epoxy systems and bismaleimide incorporated caprolactam blocked methylenediphenyl diisocyanate toughened epoxy systems are presented in Table 1. The value of the glass transition temperature of the epoxy system is decreased with increasing concentration of caprolactam blocked methylenediphenyl diisocyanate. For example, the T_g values obtained for 5%, 10% and 15% caprolactam blocked methylenediphenyl diisocyanate toughened epoxy systems are 162 °C, 154 °C and 148 °C, respectively, when compared with that of 165 °C obtained for unmodified epoxy system. This may be explained due to the chain lengthening and flexibility behaviour of -NH-CO- linkage formed during the reaction of aliphatic cyclic caprolactam with aromatic diisocyanates, which in turn decreased the effective crosslink density. This creates excess free volume in the matrix system and leads to reduction in the values of T_g , since T_g is associated with mobility of the molecules (Table 1) and which undergo co-operative motions i.e., segmental motion above T_g . The introduction of bismaleimide into caprolactam blocked methylenediphenyl diisocyanate (CMDI) toughened epoxy systems has increased the values of T_g when compared to CMDI toughened epoxy systems. The values of T_g for 4%, 8% and 12% BMI incorporated 10% caprolactam blocked methylenediphenyl diisocyanate toughened epoxy system are increased to 160 °C, 168 °C and 173 °C, respectively (Table 1) when compared with CMDI toughened epoxy system without BMI incorporation. This may be explained due to the homopolymerization of BMIs rather than the Michael addition reaction confirmed from our earlier studies, since the Michael addition reaction reduces the crosslink density due to chain extension. The single T_g value obtained for both the BMI modified epoxy and CMDI toughened epoxy systems confirms the formation of intercrosslinking network between epoxy and caprolactam. The values of HDT obtained for epoxy, caprolactam blocked methylenediphenyl diisocyanate toughened epoxy systems are presented in Table 1. From Table 1, it is evident that the values of HDT are decreased with increasing caprolactam blocked methylenediphenyl diisocyanate concentration due to lowering crosslink density and in turn reduced the values of heat distortion temperature.

3.2 Thermogravimetric analysis

The incorporation of caprolactam blocked methylenediphenyl diisocyanate into epoxy resin decreased the thermal stability and lowered the degradation temperature according to the rise in percentage concentration (Table 2). For example, the temperature required for 20%, 40% and 60% weight losses of unmodified epoxy system are 375 °C, 393 °C and 422 °C, respectively, whereas the temperatures required to attain the same percentages of weight losses for 10% caprolactam blocked methylenediphenyl diisocyanate toughened epoxy system are decreased to 352 °C, 368 °C and 392 °C, respectively (Table 2). A similar trend is observed for 5% and 15% CMDI toughened epoxy systems. This may be explained due to the presence of thermally weak flexible linkage (-NH-CO-) in the epoxy backbone. The introduction of bismaleimide into caprolactam blocked methylenediphenyl diisocyanate toughened epoxy system increased the degradation temperature. The temperatures required for 20%, 40% and 60% weight losses of 8% BMI incorporated 10% CMDI toughened epoxy system are increased to 383 °C, 413 °C and 427 °C, respectively, when compared to those of unmodified epoxy resin occurred at 375 °C, 393 °C and 422 °C, respectively (Table 2). This is explained due to the formation of inter-crosslinking network between epoxy resin and bismaleimide and the rigid heterocyclic ring structure of bismaleimide.

3.3 Mechanical properties

The observed values for tensile and flexural properties of unmodified epoxy, caprolactam blocked methylenediphenyl diisocyanate toughened epoxy are presented in Table 3. The introduction of 5%, 10% and 15% caprolactam blocked methylenediphenyl diisocyanate (by wt%) into epoxy resin enhanced the values of tensile strength by 3%, 12%, 20%, respectively, when compared with that of unmodified epoxy resin. Similarly the values of flexural strength of 5%, 10% and 15% of CMDI blocked epoxy resin systems are increased to 4%, 13% and 20%, respectively, when compared with that of unmodified epoxy system, due to the formation of an interpenetrating network between the molecular chains of epoxy and caprolactam blocked methylenediphenyl diisocyanate. Further, the incorporation of 4%, 8%, 12% bismaleimide into 10% CMDI toughened epoxy resin increased the values of tensile strength by 18%, 27%, 33%, respectively, and flexural strength by 18%, 24%, 32%, respectively, when compared with that of unmodified epoxy system due to the formation of the network structure between bismaleimide and epoxy resin. A trend similar to this was observed in the cases of tensile modulus and flexural modulus (Table 3).

The incorporation of 5%, 10% and 15% of CMDI into the epoxy system improved the impact strength to an appreciable extent by 23%, 59%, 74%, respectively, when compared with that of unmodified epoxy system. The improvement in impact behaviour may be explained due to the influence of long molecular chain with flexible group (-NH-CO-) present in the caprolactam blocked methylenediphenyl diisocyanate skeleton. In contrast, the incorporation of bismaleimide in both epoxy and caprolactam blocked methylenediphenyl diisocyanate toughened epoxy resin decreased the values of impact strength when compared with that of unmodified epoxy system and 10% CMDI toughened epoxy resin. The

decrease in the values of impact strength is due to the restricted chain mobility resulted from the formation of network structure and consequent reduction in free volume. However, a significant improvement in the values of impact strength (51%, 46% and 36%) is observed for 10% CMDI toughened epoxy system incorporated with 4%, 8% and 12% BMI when compared with that of unmodified epoxy system (Table 3). The mechanical properties of epoxy-BMI modified with different modifiers (DGTPDMS, PS and PES) are compared with BMI modified CMDI toughened epoxy system (Table 4a, b and c).

3.4 Dynamic mechanical analysis

The ability of a polymeric material to withstand load at elevated temperatures is one of the key aspects of thermomechanical behaviour required for high performance applications to be studied. Dynamic mechanical analysis is a method that measures the stiffness and mechanical damping of a cyclically deformed material as a function of temperature. The loss tangent is a sensitive indicator of crosslinking. At temperatures above T_g , damping behavior decreases due to increase of crosslinking. Fig. 1 shows the $\tan \delta$ curves of unmodified epoxy, caprolactam blocked methylenediphenyl diisocyanate toughened epoxy and BMI modified CMDI toughened epoxy systems at a heating rate of 10°C per min from 30 to 300°C . The caprolactam blocked methylenediphenyl diisocyanate toughened epoxy system exhibited a higher $\tan \delta$ maximum value and storage modulus than unmodified epoxy resin. This indicated that the caprolactam blocked methylenediphenyl diisocyanate toughened epoxy system has lesser crosslink density than unmodified epoxy system; where as the incorporation of BMI into epoxy has decreased the $\tan \delta$ maximum value and storage modulus, due to the increased crosslink density. This further supports the results obtained from thermal studies (T_g) (Fig.2).

3.5 Morphology

Scanning electron microscope was used to investigate the morphology of matrix systems (Fig. 3). SEM photographs of fractured surfaces of the unmodified epoxy and caprolactam blocked methylenediphenyl diisocyanate toughened epoxy resin systems indicated a smooth, glassy and homogeneous microstructure without any plastic deformation. The homogeneous morphology exhibited by the CMDI toughened epoxy system is due to the good compatibility and inter-crosslinking reaction between the caprolactam blocked methylenediphenyl diisocyanate and epoxy resin.

The SEM micrograph of the fractured surface of a BMI modified epoxy system is almost similar to that of the unmodified epoxy system. This indicates that there are no separate phase domains. Further, a smooth fractured surface is observed with increasing BMI content due to the brittle behavior imparted by BMI. The fractured surface of BMI modified CMDI toughened epoxy system showed a homogeneous morphology according to their percentage concentration.

4. Conclusion

BMI modified epoxy and caprolactam blocked methylenediphenyl diisocyanate toughened epoxy intercrosslinked network with various concentrations of BMI and CMDI were developed. Thermal properties such as glass transition temperature, heat distortion temperature and thermal stability of BMI modified epoxy and caprolactam blocked methylenediphenyl diisocyanate toughened epoxy matrices were compared with that of unmodified epoxy system. The caprolactam blocked methylenediphenyl diisocyanate toughened epoxy system possessed decreased thermal stability, glass transition temperature and heat distortion temperature. The incorporation of bismaleimide into caprolactam blocked methylenediphenyl diisocyanate toughened epoxy has increased the thermal properties such as thermal stability, heat distortion temperature and glass transition temperature. From the data obtained from thermal analysis, it was observed that the BMI homopolymerization reaction predominates over the Michael addition reaction. Data resulted from mechanical studies indicated that the incorporation of caprolactam blocked methylenediphenyl diisocyanate into epoxy, improved the tensile and flexural properties with appreciable extent in impact behavior. Similarly, the incorporation of BMI also increased the tensile and flexural properties according to its percentage content with a little loss in the values of impact strength. The incorporation of CMDI into epoxy increased the water absorption when compared with unmodified epoxy system but decreased in the case of BMI incorporated CMDI toughened epoxy systems. The morphology study indicated that BMI modified epoxy systems showed homogenous microstructure without any plastic deformation. The BMI/CMDI modified epoxy matrix systems possess better thermal stability, dynamic mechanical behavior and better resistance than that of the unmodified epoxy system. These toughened epoxy matrix systems could be used to fabricate advanced composite components of improved toughness with better thermo mechanical behavior for engineering applications.

References

- Dinakaran.K,Suresh Kumar.R,and Alagar M. (2003). Preparation and characterization of bismaleimide-modified bisphenol dicyanate epoxy matrices. *J Appl Polym Sci*, 90, 1596–1603.
- Han, HL, and Li, KY. (1998). Interpenetrating polymer networks of bismaleimide and polyether polyurethane-crosslinked epoxy. *J Appl Polym Sci*, 70, 2635–2645.

Leon Yu T. and Chen Y.S. (2000). Physical aging of epoxy resin blended with poly(ether sulfone): effect of poly(ether sulfone) molecular weight. *J Polym Re. s*, 7, 257–266.

Liang, Guozheng, and Fan, Jing. (1999). Novel modified bismaleimide resins with improved ablativity. *J Appl Polym Sci*, 73, 1623–1631.

Rajasekaran R, and Alagar M. (2007). Mechanical properties of bismaleimides modified polysulfone epoxy matrices. *Int J Polym Mater*, 56, 911–27.

Subramani S, Cheong .I.W, and Kim. J.H.(2004). Chain extension studies of waterborne polyurethanes from methyl ethyl ketoxime/*ε*-caprolactamblocked aromatic isocyanates. *Prog Org Coat*, 51, 329–338.

Suresh Kumar R. and Alagar M.(2006). Studies on mechanical, thermal and morphological of diglycidylether terminated polydimethylsiloxane modified epoxy-bismaleimide matrices. *J Appl Polym Sc*, 101, 668–74.

Table 1. Thermal and water absorption behavior of BMI modified CMDI toughened epoxy hybrid matrices

<i>Epoxy/CMDI/BMI composition</i>	<i>Heat distortion temperature (°C)</i>	<i>Glass transition temperature (°C) from DSC</i>	Glass transition temperature (°C) from DMA
100/00/00	154	165	165
100/05/00	150	162	163
100/10/00	146	154	154
100/15/00	142	148	149
100/00/04	157	167	168
100/00/08	161	172	171
100/00/12	170	180	182
100/10/04	151	160	162
100/10/08	159	168	170
100/10/12	163	173	172

Table 2. Data on thermal stability BMI modified CMDI toughened epoxy hybrid matrices

Epoxy/CMDI/BMI composition	Initial decomposition temperature (°C)	Temperature at characteristic weight loss (°C)		
		20%	40%	60%
100/00/00	355	375	393	422
100/05/00	348	369	380	408
100/10/00	341	352	368	392
100/15/00	332	343	357	377
100/00/04	364	391	411	428
100/00/08	372	398	421	436
100/00/12	383	408	433	445
100/10/04	349	366	388	407
100/10/08	356	383	413	427
100/10/12	367	394	426	433

Table 3. Mechanical properties of BMI modified CMDI toughened epoxy hybrid matrices

Epoxy/CMDI/BMI composition	Tensile strength (MPa)	Tensile modulus (MPa)	Flexural strength (MPa)	Flexural modulus (MPa)	Impact strength (J/m)
100/00/00	66 ± 6	2753 ± 39	115 ± 4	1984 ± 31	105 ± 3
100/05/00	68 ± 4	2770 ± 28	120 ± 6	2071 ± 22	129 ± 5
100/10/00	74 ± 7	2863 ± 21	130 ± 2	2162 ± 18	167 ± 4
100/15/00	79 ± 3	2912 ± 23	138 ± 7	2210 ± 26	183 ± 2
100/05/04	73 ± 3	2974 ± 23	128 ± 3	2143 ± 23	126 ± 4
100/05/08	80 ± 4	3088 ± 14	137 ± 1	2247 ± 18	121 ± 2
100/05/12	85 ± 7	3194 ± 27	147 ± 7	2335 ± 44	115 ± 7
100/10/04	78 ± 2	3053 ± 33	136 ± 3	2198 ± 19	159 ± 4
100/10/08	84 ± 4	3164 ± 24	143 ± 4	2283 ± 27	153 ± 2
100/10/12	88 ± 7	3260 ± 28	152 ± 2	2386 ± 12	143 ± 7
100/15/0	81 ± 3	43117 ± 23	144 ± 3	2237 ± 33	177 ± 4
100/15/08	86 ± 6	3221 ± 14	150 ± 5	2318 ± 14	169 ± 2
100/15/12	91 ± 2	3314 ± 18	157 ± 2	2424 ± 28	160 ± 7
100/00/04	71 ± 5	2920 ± 17	123 ± 3	2091 ± 14	96 ± 6
100/00/08	77 ± 8	3026 ± 22	131 ± 2	2206 ± 23	91 ± 4
100/00/12	83 ± 3	3144 ± 27	143 ± 4	2307 ± 29	86 ± 7

Table 4a. Epoxy modifications using different modifiers – a comparison

<i>Polymer systems (100/10/12)</i>	<i>Tensile strength (MPa)</i>	<i>Flexural strength (MPa)</i>	Impact strength (J/m)
Epoxy/CMDI/BMI	88 ± 7	152 ± 2	143 ± 7
Epoxy/DGTPDMS/ BMI	71 ± 3	97 ± 5	96 ± 1
Epoxy/PS/BMI	70 ± 4	124 ± 5	119 ± 3
Epoxy/PES/BMI	70 ± 5	119 ± 5	120 ± 7

CMDI – Caprolactam blocked methylenediphenyl diisocyanate.

DGTPDMS – Diglycidyl ether terminated poly(dimethyl siloxane).

PS – Polysulfone.

PES – Polyethersulfone.

Table 4b. Epoxy modifications using different modifiers – a compariso

<i>Polymer systems (100/10/12)</i>	<i>Heat Distortion Temperature (°C)</i>	Glass transition temperature (°C)
Epoxy/CMDI/BMI	163	173
Epoxy/DGTPDMS/BMI	155	167
Epoxy/PES/BMI	157	179

Table 4c. Epoxy modifications using different modifiers – a comparison

<i>Polymer systems (100/10/12)</i>	<i>Initial decomposition temperature (°C)</i>	Temperature at characteristic weight loss (°C)		
		20%	40%	60%
Epoxy/CMDI/BMI	367	394	426	433
Epoxy/DGTPDMS/BMI	380	414	454	470
Epoxy/PES/BMI	347	378	412	426

CMDI – caprolactam blocked methylenediphenyl diisocyanate.

DGTPDMS – diglycidyl ether terminated poly(dimethyl siloxane).

PS – polysulfone.

PES – polyethersulfone.

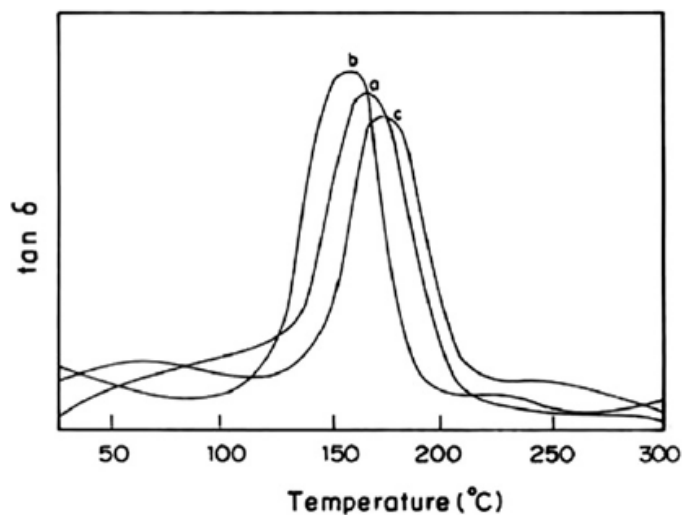


Figure 1. Variation of $\tan \delta$ as a function of temperature (a) unmodified epoxy, (b) caprolactam blocked methylenediphenyl diisocyanate (10%) toughened epoxy system and (c) bismaleimide (8%) modified caprolactam blocked methylenediphenyl diisocyanate (10%) toughened epoxy system.

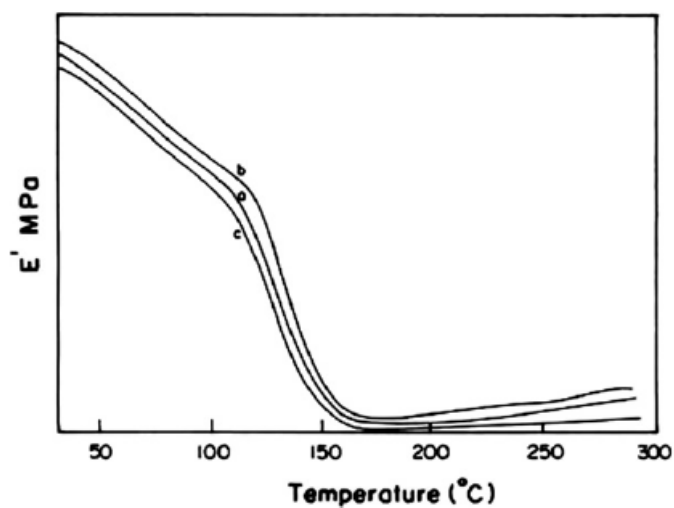


Figure 2. Variation of storage modulus as a function of temperature (a) unmodified epoxy, (b) caprolactam blocked methylenediphenyl diisocyanate (10%) toughened epoxy system and (c) bismaleimide (8%) modified caprolactam blocked methylenediphenyl diisocyanate (10%) toughened epoxy system.

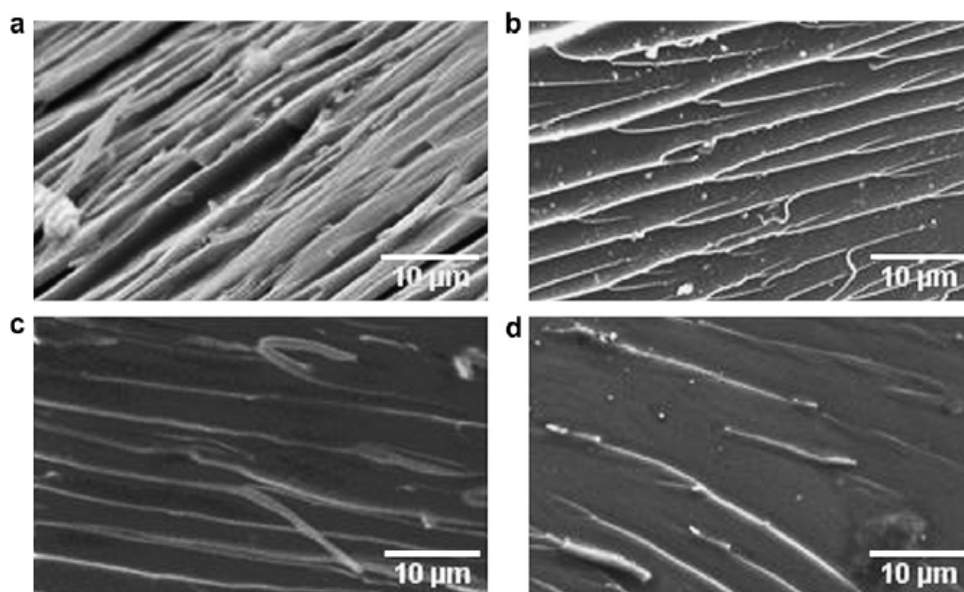


Figure 3. SEM micrographs of (a) unmodified epoxy, (b) caprolactam blocked methylenediphenyl diisocyanate (10%) toughened epoxy system, (c) bismaleimide (8%) modified epoxy system and (d) bismaleimide (8%) modified caprolactam blocked methylenediphenyl diisocyanate (10%) toughened epoxy system.



Evaluate the Effectiveness of the Natural Cosmetic Product Compared to Chemical-Based Products

Qiushi Chen

Biological & Chemical Sciences School

UQ, Brisbane, 4072, Australia

Tel: 61-41-433-0749 E-mail: cleantea100@126.com

Abstract

Based on the differences between natural cosmetics and chemical-based products, this essay demonstrates advantages and disadvantages of the natural cosmetic and the chemical-based product respectively. The natural cosmetic has grown to be a great trend in recent years, the future developing tendency of cosmetic industry should be more environmentally-friendly. Moreover, this essay is prepared in an attempt to give people an advice on choosing cosmetics.

Keywords: Effectiveness, Natural cosmetics, Chemical-based products

1. Introduction

As the old Chinese saying: "Everyone loves beauty". Human have constant pursuit of cosmetics since ancient times. Han, a Chinese ancient document, had mentioned blacken eyebrows since 2000 years ago, and the cosmetic also plays a momentous role in the daily life. Furthermore, in the USA, Europe and Japan, different definitions of cosmetics are used. The Food, Drug, and Cosmetic Act in 1938 have classified cosmetics into 13 categories (Stehlin, D., 1991). According to the Act, a cosmetic is defined as an article intended to be rubbed, poured, sprinkled, or sprayed on, introduced into, or otherwise applied to the human body or any part thereof for cleansing, beautifying, promoting attractiveness, or altering the appearance without affecting structure or function (Elsner, P., &Maibach, H.I., 2005). Now cosmetics could be divided into two parts: natural cosmetics and chemical-based cosmetics. The essay will firstly introduce the natural cosmetic and focus on its advantages and disadvantages. Secondly, the essay will talk about chemical-based ones.

2. Natural cosmetics

Firstly, the natural cosmetic has grown to be a remarkable trend Nowadays,. For example, Earth Care in UK built strong competitive advantage and grew really fast since it started its new business plan (Johri, L.M., & Sahasakmontri, K., 1998). We understand and get pleasure from delicate balance of the nature and try our best to keep melody in existence at the same level. So we need to use more pure cosmetics which are nourishing us and not able to blight the natural world.

2.1 Strong points

Here are the advantages of natural cosmetics followed:

2.1.1 It is obvious that natural cosmetics have more pure raw materials, and it is not able to cause less harm to the earth. This is the reason why more environmentally-friendly companies are emerging (Johri, L.M., & Sahasakmontri, K., 1998). According to Elsner, P., &Maibach, H.I. (2005), "natural is good and synthetic is bad" for many consumers, so merchants would spare no efforts to do everything possible to meet the need of customers. Now residents are also more concerning about environment than before; furthermore, the government has put many environmental measures into action (Johri, L.M., & Sahasakmontri, K., 1998).

2.1.2 Natural cosmetics would cause fewer side effects than chemical-based cosmetics. I did a simple survey about cosmetic users and cause of side effects to the skin. 87.1% of the people use cosmetics (see Figure 1), and 94% of users believe that the chemical-based cosmetic would cause side effects while only 6% hold an opinion that natural cosmetics may cause side effects(Figure 2).

2.2 Weak points

Nevertheless, natural cosmetics also have some unfavorable conditions:

2.2.1 Natural cosmetics may contain plant-derived materials benefic to microbial growth and only a few traditional preservatives or no preservatives at all, so they usually have short shelf-life (Stehlin, D., 1991).

2.2.2 They are always having higher prize. You could see curve chart 2 above, 87.1% informants insist on that the chemical-based cosmetic is cheaper than the natural cosmetic.

3. chemical-based products

Secondly, I would like to introduce the next part, which is about chemical-based cosmetics.

3.1 advantages

As everyone knows they have flourished for a long time. We have obviously seen what synthetic cosmetics have done to people: we may show signs of becoming a dried out flower without that. Their superiority comes behind:

3.1.1 Long shelf-life. According to Stehlin, D. (1991), chemical-based products contain preservatives which could hinder the growth of microbial, so they would have a longer shelf-life than the natural ones.

3.1.2 Many components and functions (including positive and negative). The variety of materials which have been incorporated in cosmeceuticals is staggering, including vitamins, antioxidants, minerals, herbs, hormones, anti-inflammatories, mood-influencing fragrances (aromatherapy), and even such exotica as placenta, amniotic fluid, ad infinitum (Elsner, P., & Maibach, H.I. (Eds.), 2005). The antioxidant is a kind of oxidation retarders which prevent your skin becoming senile; nevertheless, vitamin E is a potent sensitizer which could cause both delayed allergic contact dermatitis and immediate hives (Stehlin, D., 1991).

3.2 Disadvantages

However, every coin has two sides; the negative aspects are also apparent:

3.2.1 If used improperly, the chemical material may cause serious result. According to Stehlin, D. (1991), the agency could not take many effects on allergic or irritation problems. It depends on the people who use the cosmetic to prevent the product that caused the reaction and any other products that have the offending ingredient. One of the riskiest things a woman can do is put on mascara while she is driving, says McEwen. "You hit a bump and you scratch your eyeball," he explains. "Once you have scratched your eyeball, you have all kinds of possibilities of contamination. We are not talking about disease germs here. We are talking about normal bacteria that are all over the air. Those get into that kind of a cut, and without proper medical attention you can go blind." (Stehlin, D., 1991).

3.2.2 The waste is harmful to our environment. The environmental risk of pharmaceuticals and personal care products (PPCPS) in wastewater, surface water and drinking water is not optimistic. PPCPS includes various kinds of prescription drugs and non-prescription drugs (such as antibiotics, steroids, painkillers, blood pressure drugs, contraceptives, hypnotics, diet pills, etc.), soap, shampoo, toothpaste, perfume, skin care, sunscreen, hair spray, Hair gel, and so on. Drugs will not be fully absorbed by the human body after eating; the left which have not been absorbed would enter the city sewage system with excrement. If these could not be deal with properly, they would also endanger human being through the water and food (Ternes, T.A., & Joss A., 2006).

3.2.3 Because there are more preservatives in synthetic cosmetics, they may cause some allergic reaction. According to a study of cosmetic reactions conducted by the North American Contact Dermatitis Group, preservatives are the second most common cause of allergic and irritant reactions to cosmetics (Stehlin, D., 1991). In a word, more preservatives exist, more risk we have.

4. Conclusion

Through the above analysis, I believe that the positive aspects of natural cosmetics overweigh advantages of chemical-based products; meanwhile, they have fewer negative aspects than chemical-based products. I prefer the natural to the synthetic.

Natural cosmetics are safer for people and friendlier to the nature, so are a little bit better than chemical-based products. I tend to recommend cosmetics, not only for ourselves, but also for future generations.

References

Elsner, P., & Maibach, H.I. (Eds.). (2005). *Cosmeceuticals and Active Cosmetics: Drugs versus Cosmetics* (2nd Ed.). New York: Taylor & Francis.

Johri, L.M., & Sahasakmontri, K. (1998). Green marketing of cosmetics and toiletries in Thailand. *Journal of Consumer Marketing*, 15 (3), 265-281.

Stehlin, D. (1991). *Cosmetic Safety: More Complex than at First Blush*. U. S. Food and Drug Administration. [Online]

available: <http://www.cfsan.fda.gov/~dms/cos-safe.html>.2007.01.19

Ternes, T.A., & Joss A. (Eds.). (2006). Human pharmaceuticals, hormones and fragrances : the challenge of micropollutants in urban water management. London: IWA Publishing.

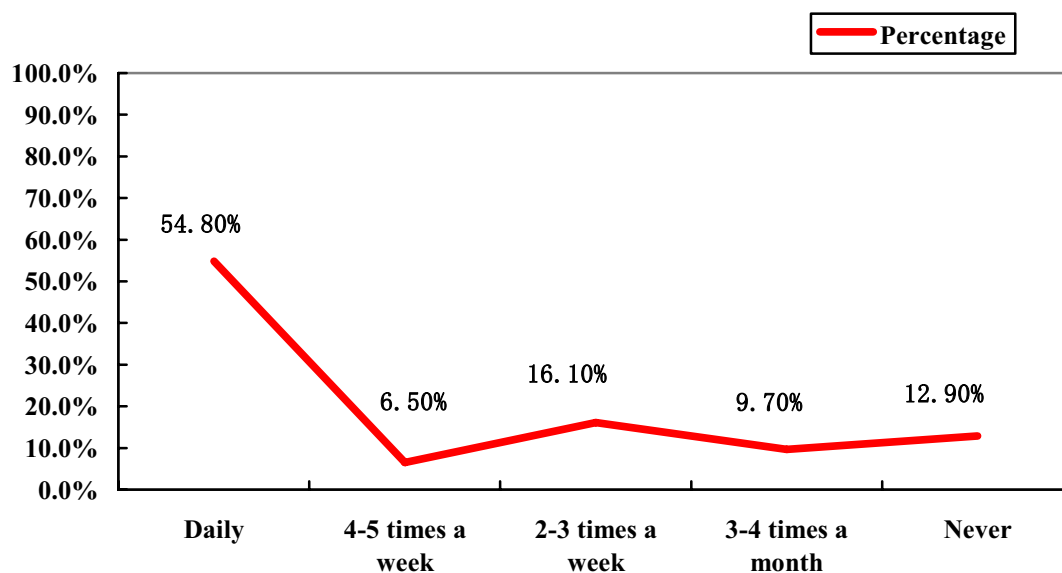


Figure 1. A simple survey about the frequency of use of cosmetics

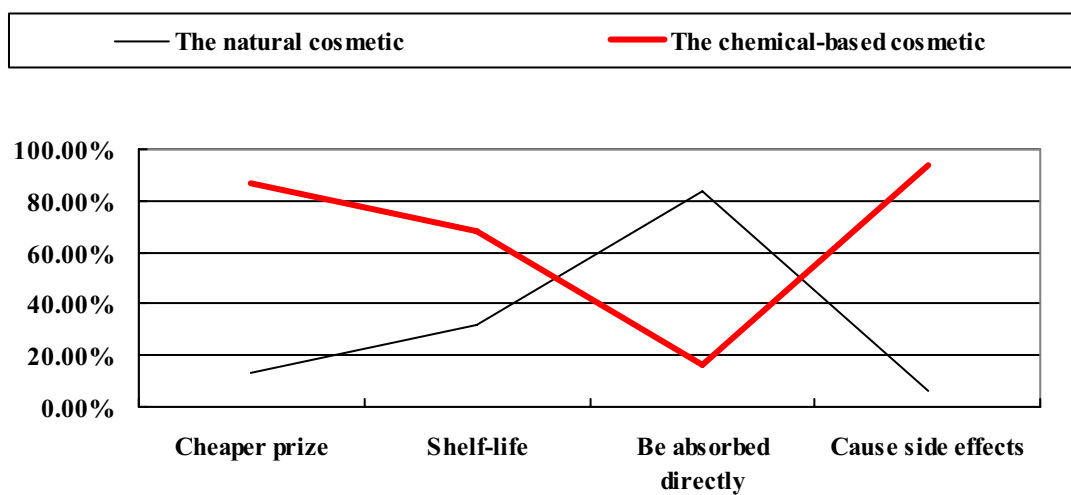


Figure 2. A simple survey about natural cosmetics and chemical-based cosmetics



Preparation and Characterization of Nonwoven Polypropylene Fabric Irradiation-grafted with Acrylic Acid as Weakly Acidic Cation Exchange Fiber

Li Wei, Junfu Wei, Feng Yuan & Jing Dong

Tianjin Polytechnic University

Tianjin Municipal Key Lab of Fiber Modification and Functional Fibers

Tianjin 300160, China

College of Material Science and Chemical Engineering

Tianjin Polytechnic University, Tianjin 300160, China

E-mail: wlily721@163.com

Abstract

Graft polymerization of acrylic acid onto nonwoven polypropylene (PP) fabric was carried out by a preirradiation method using a ^{60}Co gamma radiation source. Results showed that 2,2'-Azobisisobutyronitrile (AIBN), its concentration was 0.2%, was very important during the grafting polymerization without removal of polymerization inhibitor of AA. The most favorable grafting polymerization conditions were that the total preirradiation dose was under 60 kGy, the monomer concentration was lower than 30%, and the bath ratio was 1:200. FT-IR spectroscopy, surface morphology (SEM), wide angle X-ray diffraction (WAXD) spectra of the original PP and the grafted PP were also studied.

Keywords: Polypropylene, Graft, Preirradiation

People have paid more and more attention to the environment protection because of the increasing environmental pollution all over the world. Hence, environmentally clean radiation technologies, such as the radiation induced grafting polymerization, have been an efficient and convenient method for modification of polymeric substrates since the second half of last century. Meanwhile ion exchange fibers have played an more important role in removal of heavy metals from wastewater and acidic gas in recent years, due to their large specific surface areas and high adsorption rates. So the synthesis of these ion exchange fibers by using radiation-induced graft polymerization, have attracted the attention of many investigators (Okamoto, 1984, Yun, L, 1994, et al.). The weakly acidic cation exchange fiber in this study is nonwoven polypropylene (PP) fabric with radiation induce-grafted acrylic acid (AA). PP is a diffusely used material because of its outstanding mechanical properties and cost-effectiveness. This type of ion exchangers with carboxy group is widely used to remove heavy metals from seawater, and ammonia, amines, and alkali aerosols from atmosphere. And the previous research has been mainly focused on the basal conditions of reaction, such as solvent type, comonomer compositions, the total irradiation dose, dose rate and so on, and its applications. Although the preparation of the monofunctional group carboxylate cation exchanger based on strong, chemically inert, and nontoxic fiber has been carried out, the process should be made as perfect and effective as possible.

In generally, grafting polymerization is carried out by three different methods; (I) direct irradiation of fiber in monomer solution (II) vapor phase irradiation method (III) preirradiation. Several procedures for preparing PP fibers with grafted AA are known (U Zhun Zhui, 1963). Tsetlin *et al.* (Malakhova, L.I., 1972) prepare these fibers by direct irradiation under AA vapor at reduced pressure. This indicates that maintaining reduced pressure of AA in an installation exposed to gamma radiation is a complicated problem. And the problem of efficient removal of the heat of the grafting under these conditions is very complex. Besides, removal of the polymerization inhibitor in AA is a slow process, and the irradiation-grafting polymerization could not be generated when the polymerization inhibitor exists in AA solution. From this standpoint, we discover that a small quantity of 2,2'-Azobisisobutyronitrile (AIBN), which is mixed in the

aqueous solutions, could get the degree of grafting reach to 50% upwards and the molecular weight of residual polyacrylic acid in solution could be reached to about 2000-8000, these low molecular weight polymers are traditionally used as dispersants (Das, 2003). The modification of PP by using AIBN in grafting polymerization after preirradiation has seldom been reported. This has stimulated our interest in developing a simply and effective approach to utilize this method for PP modification. And it will be a great improvement in industrialized production of this type of IEF. At the same time, we put a small amount of sulfuric acid into the reactive aqueous solutions on account of the addition of a small amount of sulfuric acid to the reaction mixture resulted in a significant acceleration of the degree of grafting.

The aim of this work is to prepare a cation exchange fiber by γ - preirradiation-induced grafting of acrylic acid onto nonwoven polypropylene fabric, and evaluate the feasibility for the residual polyacrylic acid in solution as dispersants. The influence of experimental conditions such as the total dose, storage time after preirradiation, the monomer concentration, and the bath ratio on the degree of grafting will be discussed, meanwhile the change of crystallinity of the original PP, the preirradiated PP and the grafted PP will be revealed.

1. Experimental

The grafting polymerization of acrylic acid (AA) onto nonwoven polypropylene material was carried out by preirradiation method using a ^{60}Co gamma radiation source at different total radiation dose. The nonwoven PP fabric with density of 22 g cm^{-2} is used as substrate materials produced by China nonwoven Co. Ltd in Xianghe, (Hebei, P.R. China); Acrylic acid (AA) of purity more than 99.5% (Tianjin, P.R. China) was used as a grafting monomer without any further purification, other chemicals were analytic reagent and used as received.

The structure of nonwoven fabric was characterized by VECTOR22 IR-spectrometer (Germany, BRUKER Co.) and its surface was examined by QUANTA200-scanning electron micron microscope (Holand, FEI Co.). Besides, the crystal structure was revealed by D8DISCOVER-WAXD measurements (Germany, BRUKER Co.).

The fabric was preirradiated at room temperature without using additional equipment in irradiation zone. The dose rate was 0.56 Gys^{-1} . The total radiation dose ranged from 20 to 100 kGy. The polymerization was carried out within 7 days after preirradiation.

The graft polymerization was carried out in aqueous solutions of AA. The AA concentration ranged from 10 to 35%. The bath ratio (the wt ratio of solid and liquid phases) ranged from 1:300 to 1:50. The reactant mixtures in the glass flask were aerated by bubbling nitrogen gas for 5-7 min. Then Mohr's salt ($2.5 \times 10^{-3}\text{ mol/L}$) was added to the reaction medium to minimize the homopolymerization of AA during the radiation grafting process. The additive AIBN was always 0.2%. The nonwoven PP fabric after grafted AA was removed in hot distilled water. The products were then dried in a vacuum oven for 8 h at 333 K and weighed. The degree of grafting (G) was defined as (Yu, V, 2005):

$$G (\%) = [(w_g - w_0) / w_0] \times 100\%$$

Where w_g and w_0 represent the weights of initial and grafted fibers, respectively.

The influence of various parameters on the grafting copolymerization, such as reaction temperature, additives, preirradiation dose, reaction time, monomer concentration, and bath ratio on the degree of grafting was studied.

Agitate the nonwoven PP ion exchange fabric (degree of grafting: 44%) in 50ml HCl solution (0.5mol/L) for 10 minutes, then washed through Buchner funnel with deionized water until the eluate reached neutral. Wash the burette with a little water and poured 25ml NaCl solution (1mol/L) into it, some salt became pyrolysis. Titrate the ion exchange fabric with NaOH solution (0.1mol/L) while agitating. Test the PH value at regular intervals until it reached 10 with a glass-electroded PH meter. Draw the titration curves with the volume of NaOH consumed by per mass unit as the X-axis and the relevant PH value as the Y-axis.

2. Results and Discussion

Grafting was predominantly controlled by both concentration of trapped radicals and monomer diffusibility in the polymer matrix. For the samples irradiated at a dose under 80 kGy, grafting was proceeding every day within one week. The reaction was carried out at 343 K, which favored the degradation of hydroperoxides. The composition of irradiated nonwoven PP fabric stored for 30 days approached to that of unirradiated samples (Medyak, 2001). In the study, when the storage time after irradiation exceeded seven days, the degree of grafting tended to zero. This demonstrated that the concentration of free radicals become very little.

It can be seen from Fig.1. That the degree of grafting AA in this curve increased as the absorbed dose increased from 30 kGy to 80 kGy, but it then decreased from 80 kGy to 100 kGy, because the degree of grafting, in the preirradiation process, rested with the concentration of peroxides. The degree of grafting reached the peak when the irradiation total dose was 80 kGy. Liquid-phase grafting polymerization of AA on nonwoven polypropylene fabric after preliminary gamma irradiation was studied as influenced by the ratio of the concentration peroxides formed during gamma (^{60}Co) irradiation of polypropylene in the air. Therefore, as the total radiation dose increased, the concentration of peroxide increased and so did the degree of grafting. But the homopolymerization of acrylic acid would prick up if the total

radiation dose was too big, which was not favorable for the use of ion exchange fiber. So, we usually controlled the total radiation dose under 60 kGy.

It can be seen from Fig.2 that the degree of grafting increased as the monomer concentration increased. When the AA concentration was lower than 30%, the grafting polymerization proceeded satisfactorily with the appropriate degree of grafting. When the AA concentration was greater than, or equal to 50% in solutions, the homopolymer yield increased along with a sharp rise in the degree of grafting. In this case, it was difficult to wash out gelatinous polyacrylic acid from the grafted nonwoven PP fabric.

As seen from Fig.3, when the bath ratio was from 1:50 to 1:200, the degree of grafting increased, and then it decreased with the continue increasing of the bath ratio. The concentration of acrylic acid monomer in the system and concentration of peroxide in the system may be the two factors that influence on the change of degree of grafting with the bath ratio. When the bath ratio was low, the amount of acrylic acid was the major influence factor on the degree of grafting. As the bath ratio increased, the amount of acrylic acid in solution increased and thus the degree of grafting increased. But when the bath ratio reached a certain value, the degree of grafting became to be determined by the comparative concentration of peroxides in the system instead of the amount of acrylic acid. As the bath ratio continued to increase, the comparative concentration of peroxides decreased which led to decrease of grafting active center concentration and therefore led to decrease of degree of grafting.

Fig.4 showed the IR spectra of the original (curve 1) and the grafted nonwoven PP (curve 2) fabric. There were strong adsorption bands at 1455 cm^{-1} and 1372 cm^{-1} , corresponding to the bending vibrations of CH_2 for both PP and the grafted PP fabric. Compared to the original fabric spectrum, the appearance of the new bands at 1730 cm^{-1} and $3500\text{-}2900\text{ cm}^{-1}$ O-H was due to the stretching vibrations of $\text{C}=\text{O}$, and at $1470\text{-}1410\text{ cm}^{-1}$ corresponding to the bending vibration of O-H.

That was an evidence of AA had grafted onto the nonwoven PP fabric after the preirradiation and grafting polymerization.

Fig.5 (a), (b) and (c), (d) compared the original fabric with grafted fabric surface at different amplificatory times. The diameter of fiber increased obviously after grafting polymerization, and the smooth surface of the original PP turned into rough. The branch of polyacrylic acid grafted onto the PP randomly during the irradiation and most of them were vertical to the axis of fiber. A heterogeneous grafting layer liking brush structure were formed on the surface of fiber after grafted, resulting in that the fiber became thickness and coarse. That was an evidence of AA had been grafted onto the PP nonwoven fabric during the reaction.

The theoretical static exchange capacities (SEC) of carboxylate ion exchangers were calculated from the degree of AA grafting to the PP fabric. The theoretical SEC for cations agreed well with the experimental values. The difference between the theoretical and experimental SEC was no higher than 12% ($\text{SEC}^{\text{t}} = 4.2$ and $\text{SEC}^{\text{e}} = 3.7\text{ mmol/g}$) at (44 wt %) degree of AA grafting to the PP fabric. This suggested the absence of cross-linking during the grafting and accessibility of all carboxyl groups in the grafted fabric.

Fig.7. presented a plot of scattered intensity as a function of scattering angle (2θ). From this plot, the α -PP crystalline reflections of the original PP can be indexed as the (110) at $2\theta=14.45$, the (040) at $2\theta=17.15$, the (130) at $2\theta=18.80$. The α -PP crystalline reflections of the preirradiated PP can be indexed as the (110) at $2\theta=14.30$, the (040) at $2\theta=16.75$, the (130) at $2\theta=18.35$. The α -PP crystalline reflections of the grafted PP can be indexed as the (110) at $2\theta=14.25$, the (040) at $2\theta=16.75$, the (130) at $2\theta=18.40$.

To reveal the impact of preirradiation and grafting modification on the crystal structure or crystallite size of PP, WAXD measurements were performed. The crystallite size (D) vertical to the lattice plane (hkl) could be obtained according to the Scherrer's equation (Alexander LE, 1969):

$$D = k\lambda/\beta\cos\theta$$

Where k was the factor of the crystal figure, taking $k=0.89$. λ was the wavelength of the X-ray ($\lambda=1.54056\text{ \AA}$, taking $\text{\AA}=0.1\text{ nm}$), and θ was the diffraction angle. β was equal to $(B^2 - b_0^2)^{1/2}$, where B was the width at half-tallness of the diffraction peak and b_0 was the broadening factor of the instrument. If we took no account of the lattice distortion, the equation could be simplified as follows:

$$D = K\lambda/\beta\cos\theta = 0.89 \times 1.54056 \times 57.3 / B \cos\theta$$

The results of WAXD for the original PP, the preirradiated PP and the grafted PP fabric were shown in Table 1. In Table 1, I was the intensity of the crystalline peaks and B was the peak width at half height, d_{hkl} was the space between lattice planes (hkl).

As shown in Fig.6, the plot of the original PP indicated that the nonwoven polypropylene fabric in this study was melting spinning elicited from boiling pentane. Three curves exhibited scattering angles under these conditions, indicating the α -phase monoclinic structure (Guan Y, 2003). The d spacing of the original PP and the preirradiated PP

had a little changed while D increases. But the d spacing of the preirradiated PP and the grafted PP had slightly changed while D decreases. The results can be explained by the heterogeneous nucleation induced by AA. The nucleation accelerated the crystallization in which the growth of grains was restricted for their crushing each other in the course of their growing. The over-dosing of AA onto the backbones of PP tended to increase the crystallite size.

3. Conclusions

(1) Preirradiation-induced graft polymerization of AA onto nonwoven polypropylene fabric was carried out effectively by a preirradiation method using a ^{60}Co gamma radiation source at 343 K with adding 0.2% of AIBN without removal of polymerization inhibitor of AA.

(2) The most favorable grafting polymerization conditions were that the total preirradiation dose was under 60 kGy, the monomer concentration was lower than 30%, and the bath ratio was 1:200.

(3) The FT-IR and SEM of the grafted PP showed that carboxyl group was successfully introduced onto nonwoven polypropylene.

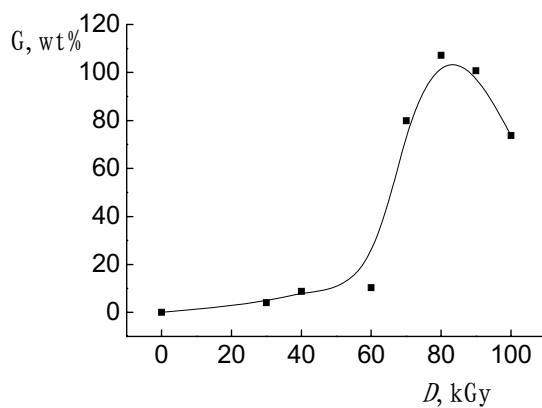
(4) The WAXD spectra of the original PP, the preirradiated PP and the grafted PP indicated that the over-dosing of AA onto the backbones of PP tended to increase the crystallite size.

References

- Alexander LE. (1969). X-ray Diffraction Methods in Polymer Science: New York.
- Bondar, Y., Kim, H.J., Lim, Y.J., Kravets, L. (2003). Cation-Exchange Fabric Prepared by Electron Beam-Induced Graft Copolymerization of Binary Monomer Mixture. *Macromolecular Symp.* 202: 167-178.
- Das, Kalyan, K., Somasundaran, P. (2003). Flocculation-Dispersion Characteristics of Alumina Using a Wide Molecular Weight Range of Polyacrylic Acids. *Coll. and Surf. A: Physicochemical and Engineering Aspects.* 223(1-3): 17-25
- Guan Y, Wang SZ, Zheng AN, (2003). *Journal of Applied Polymer Science.* 88:872.
- Gupta, B., Jain, R., Anjum, N., Singh, H. (2006). Preirradiation Grafting of Acrylonitrile onto Polypropylene Monofilament for Biomedical Applications: I. Influence of Synthesis conditions. *Radi. Phys. and Chem.* 75 (1): 161-167.
- Jain, R., Gupta, B., Anjum, N., Revagade, N., Singh, H. (2004). Preparation of Antimicrobial Sutures by Preirradiation Grafting of Acrylonitrile onto Polypropylene Monofilament. II. Mechanical, Physical and Thermal characteristics. *Jour. of Appl. Poly. Scie.* 93 (3-5): 1224-1229.
- Le Thuaut, P., Martel, B., Crini, G., Maschke, U., Conqueret, X., Morcellet, M. (2000). Grafting of Cyclodextrins onto Polypropylene Nonwoven Fabrics for the Manufacture of Reactive Filters. I. Synthesis Parameters. *Janu. of Appl. Poly. Scie.* 77 (10): 2118-2125.
- Malakhova, L.I., Vlasov, A.V., Mikhailov, N.V., and Tsetlin, B.L. (1972). *Vysokomol Soedin, Ser A.* 14(4): 751-755.
- Medyak, G. V., Shunkevich, A. A., Polikarpov, A. P., Soldatov, V. S. (2001). Features of Preparation and Properties of FIBAN K-4 Fibrous Sorbents. *Russ. Jour. of Appl. Chem.*, 74(10): 1658-1633.
- Okamoto, J., Sugo, T., Katakai, A., Omichi, H. (1984). Complex-forming Polymer Prepared by Electron Beam Radiation-induced graft polymerization. *Radi. Phys. and Chem.* 25 (1-3): 333-342.
- U Zhun Zhui, Stasyuk, Kh.A., Kocherginskaya, L.A., et. al., (1963). *Chemisorption Fibers.* 5: 12-15.
- Wei, J.F., Wang, Z.P., Zhang, J., Wu, Y.Y., Zhang, Z.P., Xiong, C.H.. (2005). The Preparation and the Application of Grafted Polytetrafluoroethylene Fiber as a Cation Exchanger for Adsorption of Heavy Metals. *Reactive and Functional polymers*, 65(1-2): 127-134.
- Yu. V. Bondar', Hong Je Kim, and Yong Jin Lim. (2005). *Russian Journal of Applied Chemistry*, 78(5): 811-814.
- Yuan, S., Wang, Y., Lan, S., Lu, Y., Zeng, H. (1998). Study on the Physical Chemical Properties of FFA-I Ion Exchange Fiber. *Chin. Jour. of Reac. Poly.* 7 (2):54-60.
- Yun, L., Zhu, Z., Hanmin, Z. (1994). Studies on Preparation and Ion-exchange Properties of Weakly Acidic Cation Exchange Fiber by Preirradiation-induced Graft Copolymerization with Electron Beam. *Jour. of Appl. Poly. Scie.* 53 (4): 405-410.

Table 1. Crystal parameters of the original PP, the preirradiated PP and the grafted PP from WAXD

sample	<i>hkl</i>	2θ	d_{hkl} (Å)	I(cps)	<i>B</i> (o)	<i>D</i> (Å)
PP	110	14.45	6.12	148	1.10	71.99
	040	17.15	5.16	154	2.40	33.11
	130	18.80	4.72	123	4.70	16.94
Preirradiated PP	110	14.30	6.19	468	0.80	98.97
	040	16.75	5.29	515	1.00	79.41
	130	18.35	4.83	288	1.60	49.74
Grafted PP	110	14.25	6.21	645	1.10	71.98
	040	16.75	5.29	600	1.40	56.72
	130	18.40	4.82	342	1.80	44.22

Figure 1. The degree of grafting G vs. the total radiation dose D

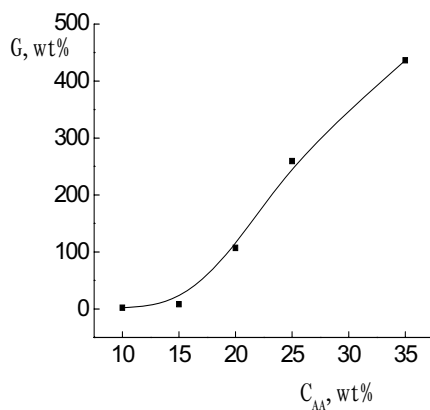


Figure 2. The curve of degree of AA grafting G vs. the AA concentration C_{AA} (polymerization at 348 K for 2 h)

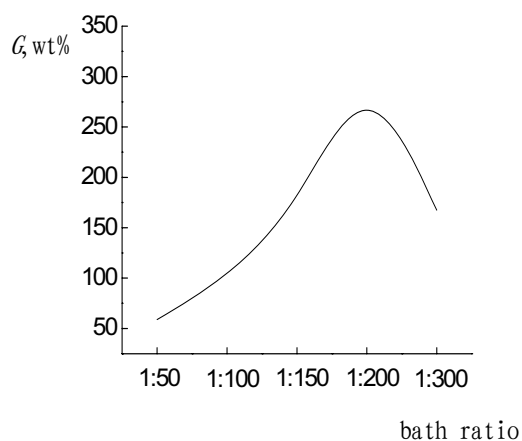


Figure 3. The degree of grafting from a 20% solution at 348 K for 2 h vs. the bath ratio

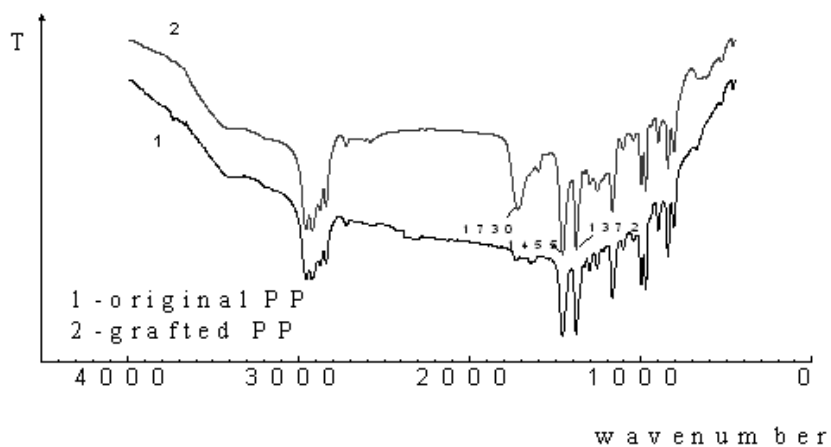
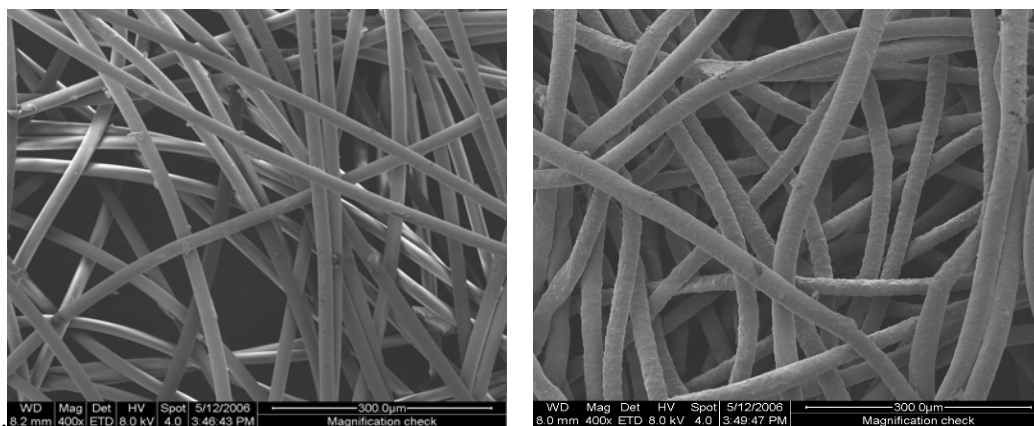
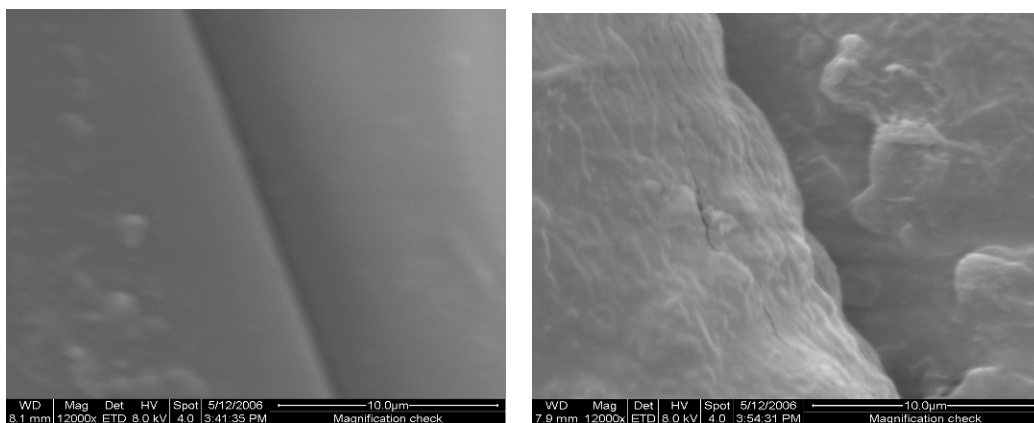


Figure 4. The IR spectra of (1) the original and (2) the grafted PP nonwoven



(a) The original PP nonwoven (400 times)

(b) The grafted PP nonwoven (400 times)



(c) The original PP nonwoven (12000 times)

(d) The grafted PP nonwoven (12000 times)

Figure 5. SEM micrograph of the original PP and the grafted PP nonwoven

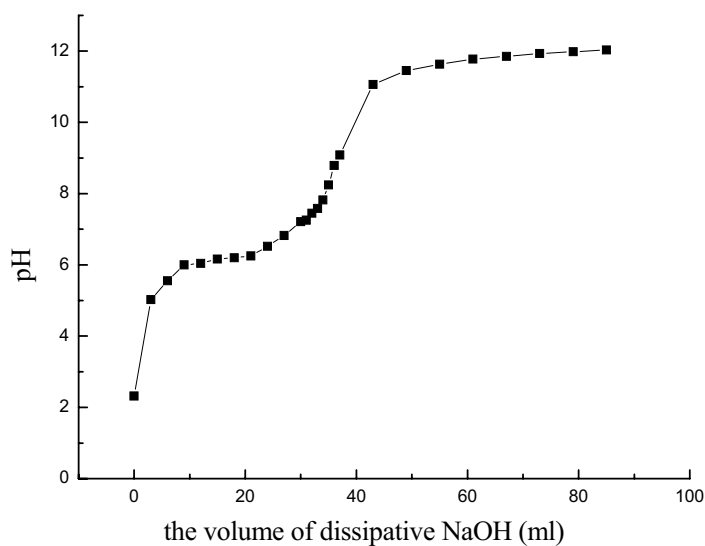


Figure 6. The experimental SEC of 44 wt % degree of grafting PP fabric

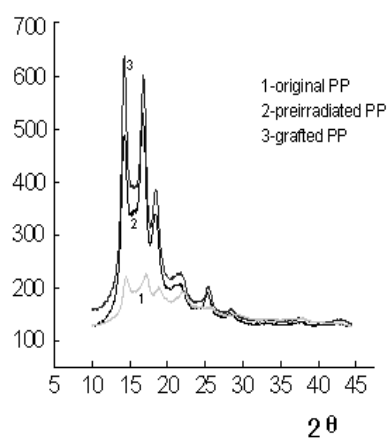


Figure 7. The WAXD spectra of (1) the original, (2) the preirradiated and (3) the grafted nonwoven PP fabric



Study on Chemical Composition of *Nauclea Officinalis* Leaves

Kui Su

Food College of Shihezi University

Shihezi, Xinjiang 832000, China

Oceanography College of Hainan University

Haikou, Hainan 570228, China

E-mail: lsx20030404@163.com

Min Gong & Jing Zhou

Food College of Shihezi University

Shihezi, Xinjiang 832000, China

Shiming Deng (Corresponding author)

Oceanography College of Hainan University

Haikou, Hainan 570228, China

The research is financed by the National Key Technology R & D Program. No. 2007BAI27B04 (Sponsoring information)

Abstract

Objective: The chemical composition of *Nauclea officinalis* leaves is analyzed to offer a theoretical base for its application. Method: Separate *Nauclea officinalis* leaves by solvent extraction and silica gel column, and characterize the product structure through analysis on physical properties and spectrum. Results and conclusions: 7 compounds have been separated from liposoluble part of *Nauclea officinalis* leaves, 5 compounds among them have been characterized, which in turn are β -sitosterol palmitate (1), stigmast-4-en-3-one (2), β -sitosterol (3), 24-en-cycloartenone (4) and bis (2-ethylhexyl) phthalate (5), wherein (1) and (4) are separated from *Nauclea officinalis* leaves for the first time.

Keywords: *Nauclea officinalis* leaves, Chemical composition, Determination of structure, Steroid

Nauclea officinalis Merr. Chun, a tree placed in Genus *Nauclea* of Family *Rubiaceae*, is found widely in Guangdong, Guangxin, Yunnan and etc. in China. Its branch, stem and root, gatherable throughout the year, are cut into small pieces and dried for the medical purpose. It is cold natured, tastes bitter, and can be used for treating exogenous fever, acute tonsillitis, laryngopharyngitis, bronchitis, pneumonia, enteritis, dysentery, acute jaundice, stomachache and etc (Deng, Shiming, 2006, p. 149). *Nauclea officinalis* is widely cultivated in Hainan. The existing Chinese medicines of this type distributed in the market are *Nauclea Officinalis* Injection and *Nauclea Officinalis* Extract Tablet, both from *Nauclea officinalis* bark. However, gathering bark is destructive to *Nauclea officinalis*. It is proved by the preliminary experiment and anti-microbial activity experiment that the composition of *Nauclea officinalis* leaves is similar to that of *Nauclea officinalis* bark, and there are plenty of leaves on *Nauclea officinalis*, therefore, the chemical composition of *Nauclea officinalis* leaves is systematically analyzed in this study for sustainable development and exploitation of *Nauclea officinalis*. 7 compounds are separated from liposoluble part of *Nauclea officinalis* leaves, 5 compounds among them have been characterized, which in turn are β -sitosterol palmitate (1), stigmast-4-en-3-one (2), β -sitosterol (3), 24-en-cycloartenone (4) and bis (2-ethylhexyl) phthalate, wherein (1) and (4) are separated from *Nauclea officinalis* leaves for the first time.

1. Materials and instruments

Materials for column chromatography: silica gel of 100~200/200~300 mesh from Qingdao Haiyang Chemical Co., Ltd;

Materials for thin-layer chromatography: silica gel G/60H/GF254 from Qingdao Haiyang Chemical Co., Ltd; Gel: Sephadex LH-20 from Amersham Biosciences of Sweden. All reagents here are technical pure and used after rerun.

^1H NMR and ^{13}C NMR are measured respectively at 400.13 MHz and 100.6 MHz on Bruker AM-400.0 NMR spectrometer with TMS as internal standard. ZF-6 triple-purpose UV analyzer is provided by Jiapeng Tech. Co., Ltd. in Shanghai.

Nauclea officinalis leave is provided by *Nauclea officinalis* Farm of Jinguang Pharmaceutical Group in Hainan. The sample is proved to be *Nauclea officinalis* Merr. Chun by Dr. Shiming Deng from the Oceanography College of Hainan University. The voucher specimens are saved in the Oceanography College of Hainan University.

2. Methods and results

2.1 Extraction and separation

Pick up fresh *Nauclea officinalis* leaves, dry in the shade, coarsely grind, and percolate by 95% ethanol for one week, then concentrate by pressure reduction to obtain 1.5 kg extractum of *Nauclea officinalis* leaves. The extractum is in turn extracted with petroleum ether (60-90 °C), chloroform and ethyl acetate. Extract liquors are respectively concentrated by pressure reduction to obtain 300 g petroleum ether extract, 85 g chloroform extract and 85 g ethyl acetate extract, and solvents therefrom are recycled. The left water collections should pass through macroporous adsorptive resin.

300 g petroleum ether extract is combined with about 7 times its weight of silica gel of 200~300 mesh, dryly fill the column and dryly load the sample, separate by gradient elution with petroleum ether/ ethyl acetate (9:1) - ethyl acetate/methanol (1:1) as eluent. Draw small dots on the origin line of the thin layer chromatography (TLC) plate. 3 bands are finally identified as the plate develops. The first band is dryly loaded and separated by gradient elution with petroleum ether / dichloromethane [1:(0~1)] as eluent to get compound 1 (20 mg) and compound 4 (21 mg); the second band is dryly loaded after separation with Sephadex LH-20, and eluted with petroleum ether / dichloromethane to get compound 3 (200 mg); the third band is dryly loaded after separation with Sephadex LH-20, and eluted with dichloromethane / ethyl acetate to get compound 2 (15 mg) and compound 5 (100 mg). The structures of compound 1~5 are shown in figure 1.

2.2 Characterization of structure and physical property

2.2.1 Compound 1

Appearance: White acicular crystal (ethyl acetate).

Melting point: 88-90 °C.

Formula: $\text{C}_{45}\text{H}_{80}\text{O}_2$.

^1H NMR (400 MHz, CDCl_3) δ : 5.38 (1H, d, $J=4.8$ Hz), 4.62 (1H, m), 1.28 [br.s, $(\text{CH}_2)_n$], 1.04 (3H, s), 0.80~0.93 (m, $(\text{CH}_3)_5$), 0.69 (3H, s, CH_3).

^{13}C NMR (100 MHz, CDCl_3) δ : 37.0 (C-1), 27.8 (C-2), 73.7 (C-3), 38.2 (C-4), 139.7 (C-5), 122.6 (C-6), 31.9 (C-7, C-8), 50.0 (C-9), 36.6 (C-10), 21.0 (C-11), 39.8 (C-12), 42.3 (C-13), 56.7 (C-14), 24.3 (C-15), 28.2 (C-16), 56.1 (C-17), 11.8 (C-18), 19.3 (C-19), 36.2 (C-20), 18.8 (C-21), 34.0 (C-22), 26.2 (C-23), 45.9 (C-24), 29.1 (C-25), 19.8 (C-26), 19.0 (C-27), 23.1 (C-28), 12.0 (C-29); Aliphatic chain part: 173.3 (C-1'), 34.7 (C-2'), 25.1 (C-3'), 29.2~29.7 (C-4' ~C-13'), 31.9 (C-14'), 22.7 (C-15'), 14.1 (C-16'). ^{13}C NMR spectrum indicates a signal of carbon and a signal of fatty acyl carbon of β -sitosterol.

Above-mentioned data are in accordance with the reference-reported spectrum data of β -sitosterol palmitate (Dong, Xue, 2008, p. 63-66; Huang, Ping, 2008, p. 271-274). Therefore, it can be concluded that the compound 1 is β -sitosterol palmitate.

2.2.2 Compound 2

Appearance: Colorless oily matter; non-fluorescence at 254 nm under UV lamp after developing on TLC; grey in 10% sulfuric acid-ethanol solution.

Formula: $\text{C}_{29}\text{H}_{48}\text{O}$.

^1H NMR (400.13 MHz, CDCl_3) spectrum indicates six H signals of methyl group in δ 0.71~1.18, an olefinic H signal of 4-double bond at low field range [δ 5.72 (1H, s, H-4)]. Signals at δ 5.72 (1H, s, 4-H) and δ 2.38~1.30 correspond to hydrogen on the backbone and side chain respectively. Assignments of the rest signals are as following: 1.18 (s, 3H, 19- CH_3), 0.92 (d, 3H, $J=6.4$ Hz, 29- CH_3), 0.82~0.84 (9H, m, 3 CH_3 -21, 26, 27), 0.71 (3H, S, CH_3 -18).

^{13}C NMR (100.6 MHz, CDCl_3) spectrum indicates 29 carbon signals in total with 1 carbon signal of carbonyl group at low field range (δ 198.5) and 2 carbon signals of olefinic carbon at δ 122.7/170.5. Therefore, it is determined that compound 2 is a steroid. Assignments of above-mentioned ^{13}C NMR signals are as following: δ 34.8 (t, C-1), 32.8 (t, C-2), 198.5 (s, C-3), 122.7 (d, C-4), 170.5 (s, C-5), 31.9 (t, C-6), 31.0 (t, C-7), 34.6 (d, C-8), 52.7 (d, C-9), 37.5 (s,

C-10), 22.0 (t, C-11), 38.5 (t, C-12), 41.3 (s, C-13), 54.9 (d, C-14), 25.0 (t, C-15), 27.1 (t, C-16), 54.9 (d, C-17), 10.9 (q, C-18), 18.0 (q, C-19), 35.0 (d, C-20), 16.3 (q, C-21), 32.9 (t, C-22), 23.1 (t, C-23), 44.7 (d, C-24), 27.1 (d, C-25), 18.7 (q, C-26), 17.6 (q, C-27), 23.1 (t, C-28), 10.9 (q, C-29).

Above-mentioned data are in accordance with the reference-reported spectrum data of stigmast-4-en-3-one (Xuan, Weidong, 2005). Therefore, it can be concluded that the compound 2 is stigmast-4-en-3-one.

2.2.3 Compound 3

Appearance: White acicular crystal (chloroform); non-fluorescence at 254 nm under UV lamp after developing on TLC; red in 10% sulfuric acid-ethanol solution.

Formula: C₂₉H₅₀O.

¹H NMR (400.13 MHz, CDCl₃) spectrum indicates six H signals of methyl group in δ 0.67~1.00, an olefinic hydrogen signal of 6-double bond at low field range [δ 5.35 (1H, br.s, H-6)]. Signals at δ 5.35 (d, 1H, J=5.2 Hz, 6-H), 3.56 (m, 1H, 3-H) and 2.27~1.49 correspond to hydrogen on the backbone and side chain respectively. Assignments of the rest signals are as following: 1.00 (s, 3H, 19-CH₃), 0.91 (d, 3H, J=6.9 Hz, 29-CH₃), 0.81-0.84 (9H, m, 3CH₃-21, 26, 27), 0.67 (3H, s, CH₃-18).

¹³C NMR (100.6 MHz, CDCl₃) spectrum indicates 29 carbon signals in total with 1 carbon signal of hydroxyl group at medium field range (δ 71.8) and 2 carbon signals of olefinic carbon at δ 140.7/121.7. Therefore, it is determined that compound 3 is a steroid. Assignments of above-mentioned ¹³C NMR signals are as following: δ 37.3 (t, C-1), 31.9 (t, C-2), 71.8 (d, C-3), 40.5 (t, C-4), 140.7 (s, C-5), 121.7 (d, C-6), 31.9 (t, C-7), 31.6 (d, C-8), 50.2 (d, C-9), 36.5 (s, C-10), 21.1 (t, C-11), 39.8 (t, C-12), 42.3 (s, C-13), 56.8 (d, C-14), 24.3 (t, C-15), 28.3 (t, C-16), 56.1 (d, C-17), 11.9 (q, C-18), 19.5 (q, C-19), 36.2 (d, C-20), 18.9 (q, C-21), 33.9 (t, C-22), 26.1 (t, C-23), 45.8 (d, C-24), 29.1 (d, C-25), 19.4 (q, C-26), 19.1 (q, C-27), 23.1 (t, C-28), 12.0 (q, C-29).

Above-mentioned data are in accordance with the reference-reported spectrum data of β-sitosterol (Liu, Zhiping, 2007, p. 140-142). Therefore, it can be concluded that the compound 3 is β-sitosterol.

2.2.4 Compound 4

Appearance: White acicular crystal (chloroform); non-fluorescence at 254 nm under UV lamp after developing on TLC; red in 10% sulfuric acid-ethanol solution.

Formula: C₃₀H₄₈O.

The EI-MS shows characteristic peaks at 440[M]⁺, 424[M-O]⁺, 409[M-O-CH₃]⁺, m/z, 440, 424, 409, 395, 380, 355, 270, 205, 175, 147, 107, 95, 69, 55.

¹H NMR (400.13 MHz, CDCl₃) spectrum indicates two H signals of 19-methylene group in cycloartane triterpenoids at high field range [δ 0.58 (1H, d, J = 4.4 Hz, H-19) and δ 0.78 (1H, d, J=4.3 Hz, H-19)], seven H signals of methyl group in δ 0.88~1.73, and an olefinic hydrogen signal of 24-double bond at low field range [δ 5.10 (1H, br.s, H-24)].

¹³C NMR (100.6 MHz, CDCl₃) spectrum indicates 30 carbon signals in total with 1 carbon signal of ketone group at low field range (δ 216.6) and 2 carbon signals of olefinic carbon at δ 130.9/125.2. Therefore, it is determined that compound 4 is a 9, 19-cycloartane triterpenoids. Assignments of above-mentioned ¹³C NMR signals are as following: δ 216.6 (C-3), 130.9 (C-25), 125.2 (C-24), 52.3 (C-17), 50.2 (C-4), 48.7(C-14), 48.4 (C-5), 47.9 (C-8), 45.3 (C-13), 37.5(C-2), 36.3 (C-22), 35.8 (C-20), 35.5 (C-15), 33.4 (C-1), 32.8 (C-12), 29.5 (C-19), 28.1(C-7), 26.7 (C-16), 25.9 (C-10), 25.8 (C-11), 25.7 (C-27), 24.9 (C-23), 22.1 (C-30), 21.5 (C-6), 21.1 (C-9), 20.7 (C-29), 19.3 (C-18), 18.2(C-28), 18.0 (C-21), 17.6 (C-26).

Above-mentioned data are in accordance with the reference-reported spectrum data of 24-en-cycloartenone (Wang, Wenzhe, 2006, p. 91-92). Therefore, it can be concluded that the compound 4 is 24-en-cycloartenone.

2.2.5 Compound 5

Appearance: Yellow oily matter; from red to purple in 10% sulfuric acid-ethanol solution.

Formula: C₂₄H₃₈O₄.

¹H NMR (400 MHz, CDCl₃) spectrum indicates characteristic peaks at δ 4.12 (2H, m), 1.69 (1H, m), 1.27~1.47 (8H, m), 0.89 (3H, t, J=7.5 Hz), 0.93 (3H, t), 7.74 (1H, m), 7.64 (1H, m).

¹³C NMR (100 MHz, CDCl₃) spectrum indicates characteristic peaks at δ 68.3 (t, C-1), 39.6 (d, C-2), 31.1 (t, C-3), 23.6 (t, C-4), 29.7 (t, C-5), 14.3 (q, C-6), 24.7 (t, C-7), 11.3 (q, C-8), 167.9 (s, C=O), 133.4 (s, C-1'), 129.6 (d, C-2'), 131.9 (d, C-3').

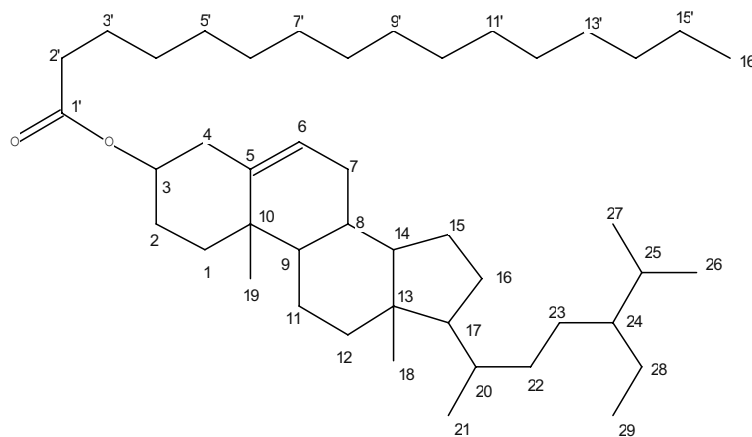
Above-mentioned data are in accordance with the reference-reported spectrum data of bis (2-ethylhexyl) phthalate (Deng, Shiming, 2002, p. 99). Therefore, it can be concluded that the compound 5 is bis (2-ethylhexyl) phthalate.

3. Discussion

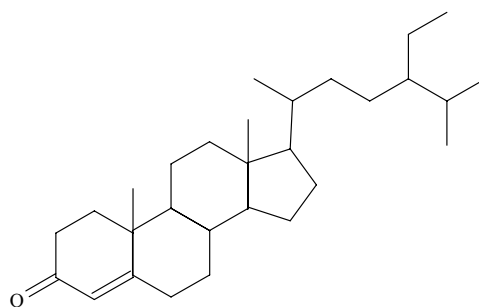
Reports on the chemical composition of *Nauclea officinalis* have been mainly about its bark. However, this paper preliminarily studies the chemical composition of *Nauclea officinalis* leaves, especially its low polar parts. The separated main products are steroid. There have been abundant reports (Jie, Fei, 2006) on *Nauclea officinalis* barks which demonstrate that the main constituents of *Nauclea officinalis* are alkaloid and triterpene. Xuan (2005) reported that the anti-bacterial component in *Nauclea officinalis* is alkaloid. However, this study on the low polar part of ethanol extract from *Nauclea officinalis* leaves indicates no alkaloid in them. Therefore, the issues that if there is great difference in chemical composition between leave and bark of *Nauclea officinalis*, especially if there is the same alkaloid in leave as that in bark, and if the separated compounds in this study have the same anti-bacterial activity should be addressed in the future study.

References

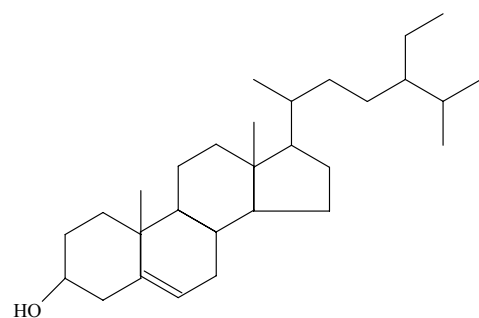
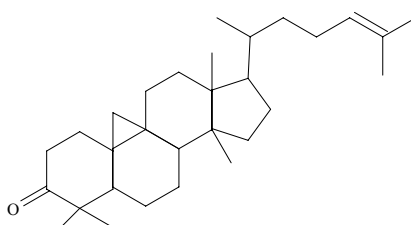
- Deng, Shiming. (2002). Chemical constituents of five medicinal plants. *Doctoral Dissertation from Graduate University of Chinese Academy of Sciences*, 6, 99.
- Deng, Shiming. (2006). *The List of Common Chinese Herbal Medicine in Hainan*. Beijing: Chinese Science and Technology Publisher. p. 149.
- Dong, Xue, Wang, Guorong & Yao, Qingqiang. (2008). Chemical constituents of *Sparganium stoloniferum*. *Acta Pharmaceutica Sinica*, 43(1), 63-66.
- Huang, Ping, Karagianis Gloria, Wei, Shanxin & Waterman Peter G. (2008). Chemical constituents in the heartwood of *Paulownia kawakamii*. *Natural Product Research and Development*, 20(2), 271-274.
- Liu, Zhiping, Cui, Jianguo, Liu, Hongxing, Huang, Chusheng & Zhong, Zhenguo. (2007). Chemical constituents from leaves of *Livistona chinensis*. *Guihaia*, 27(1), 140-142.
- Wang, Wenze, Zhao, Yuqing & Li, Xian. (2006). Chemical constituents from seeds of *Zanthoxylum bungeanum maxim*. *Journal of Shenyang Pharmaceutical University*, 23(2), 91-92.
- Xie, Fei. (2006). Studies on chemical constituents and fingerprints of *Nauclea officinalis*. *MS Dissertation from Shandong University*, 8.
- Xuan, Weidong. (2005). Studies on bioactive constituents of *Nauclea officinalis* and *Ervatamia yunnanensis*. *Doctoral Dissertation of the Second Military Medical University*.



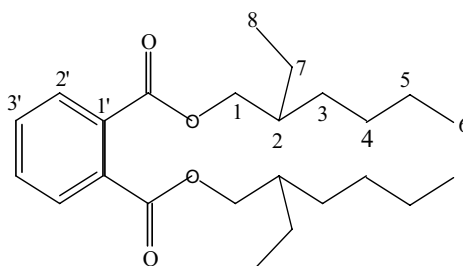
(1) β -sitosterol palmitate



(2) Stigmast-4-en-3-one

(3) β -sitosterol

(4) 24-en-cycloartenone



(5) Bis (2-ethylhexyl) phthalate

Figure 1. Structures of compound 1~5



Research on Antifouling and Easy Decontaminating by a New Method

Xiaojie Liang & Jinbo Yao

Textile College, Tianjin Polytechnic University

Tianjin 300160 China

E-mail: linshaohan2003@163.com

Abstract

Study the effect of blending hydrophilic agent and water and oil repellent agent on cotton fabric property of antifouling and easy decontaminating. The study shows that blending could make the fabric have property of antifouling and easy decontaminating.

Keywords: Antifouling and easy decontaminating, Blend, Cotton fabric

1. Introduction

For many years, workers had done plenty of researches on fabric of water and oil proofing. fluorine-contained finishing agent has been received much attention for its excellent property of water and oil repellent, soil release (Zhen.Wan, 2005).

For overcoming the disadvantages of the single water and oil repellent or soil release finishing, the agent which contains oil repellency chain segment and hydrophilic segment was developed out. The fabric which finished by this agent can have the property of water and oil repellent on dry, and the soil release property on wet (Shungen, Zhu, 1997). At present, soil release finish agent is almost copolymer compounds which contain hydrophilic part and water and oil repellent part (Zhijun. Zhang, 2004). This finishing agent high in price and is synthesis complexly. So it is necessary to search a new method to reach the effect of antifouling and soil release property. Fluorine part of this copolymer soil release finishing agent play a role in water and oil repellent on dry, hydrophilic part plays a role in soil release in wet. So we can think that can we mix the water and oil repellent agent and hydrophilic agent to reach the same effect as the copolymer antifouling and soil release finishing agent? Use macroscopic method to solve microscopic problem, so this can reduce cost greatly.

2. Experiment

2.1 Experimental material

Cotton plain weave cloth, water and oil repellent finishing agent (FK-510), moisture adsorption and perspiration exhaust finishing agent(FK-829).

2.2 Equipment

Double roll padder (switzerland), YHW-102 dry box (changsha,china), whiteness instrument(U.S.A datacolor company), contact angle instrument(chengde, china)

2.3 Technological processes

Double-dipdouble-nip→drying (100°C×1.5min)→baking(160°C×3min)→washing→drying

Finishing prescription: FK-510: 60g/L

FK-829: Xg/L

<Table 1>

2.4 Test

Grade evaluation of water and oil repellent uses PRC professional standard ZB W 04015-89.

Use contact angle instrument to test the contact angle on every grade of water and oil repellent.

Use whiteness instrument to test the whiteness of washed cloth

3 result and discussion

3.1 Test cotton fabric property of water and oil repellent finished by mixed agent

For Studying on the influence of hydrophilic segment FK-829 on the property of water and oil repellent, we test the cotton fabric contact angle on every grade of water and oil repellent which finished by mixed agent.

<Figure 1 & Figure 2>

We can directly recognize from the Figure 1 and 2, when the oil repellent grade is 6 grades below, contact angle had no remarkable changed. So adding hydrophilic agent (FK-829) had no impact on the effect of water and oil repellent. Grade 6 can meet the daily need.

But when added the octane, contact angle increased first then decreased, the reason may be as below:

(1) In Figure 1, the property of oil repellent improved with the hydrophilic agent amount increasing, the reason may be that when adding little hydrophilic agent, this can make fiber surface rough, so the fabric obtained high water and oil repellent property.

(2) When the percentage of hydrophilic agent was 33.3%, the fabric water and oil repellent property decreased. This may be that when hydrophilic agent reached a certain percentage, arrangement and distribution of the finishing agent in fiber changed. The continuity of the membrane in fiber which the finishing agent formed decreased. So the oil repellent is lower. But the water and oil repellent grade is still 6.

3.2 Test cotton fabric easy-rinse property finished by mixed agent

<Figure 3 & Figure 4>

K/S expresses depth of fabric surface. The high value represents that much dirt residues on the fiber surface, in another words, effect of decontamination is bad. We can recognize from the Figure 3 and 4, the easy-rinse property improved with the hydrophilic agent amount increasing, namely increasing cotton fabric hydrophilicity helps to improve decontamination effect. From water and oil repellent effect whiteness test result, the proportion of water and oil repellent agent and hydrophilic agent is 2:1.

4. Conclusions

This study is a new method of antifouling and easy decontaminating finishing, namely mix water and oil repellent agent and hydrophilic agent to finish fabric to reach the same effect of fluorine-contained soil release finishing agent at present. After comparison and analysis the following results are provided:

(1) Water and oil repellent effect related to concentration of water and oil repellent finishing agent, the higher of the concentration, the better of the water and oil repellent effect. But increase to a certain concentration, water and oil repellent effect does not improve obviously with the water and oil repellent agent amount increasing.

(2) The fabric finished with the mixed agent had water and oil repellent and easy-rinse property. Feasibility of this new method was validated primitively. When water and oil repellent agent and hydrophilic agent were mixed in a best certain proportion, the fabric could obtain a good property of water and oil repellent and easy-rinse. From water and oil repellent effect and whiteness test result, the proportion of hydrophilic agent is 33.3%.

References

- Shungen, Zhu. (1997). Fluorine-containing fabric finishing. *Organo-Fluorine Industry*, (4), 21-43
- Zhen.Wan, Wei. Wang & Yun. Xie. (2005). Fluorine-containing fabric finishing. *Knitting Industry*, (3):45-47
- Zhijun.Zhang. (2004). The development and out-look of fluorine-containing fabric general finishing agents. *Polymer Materials Science & Engineering*, (5), 24-28

Table 1. The finishing agent content of every fabric sample

Serial number	water and oil repellent agent:hydrophilic agent	Proportion of hydrophilic agent
1	6:1	14.2%
2	3:1	25%
3	2:1	33.3%
4	3:2	40%
5	1:1	50%

Mangle expression : 70%

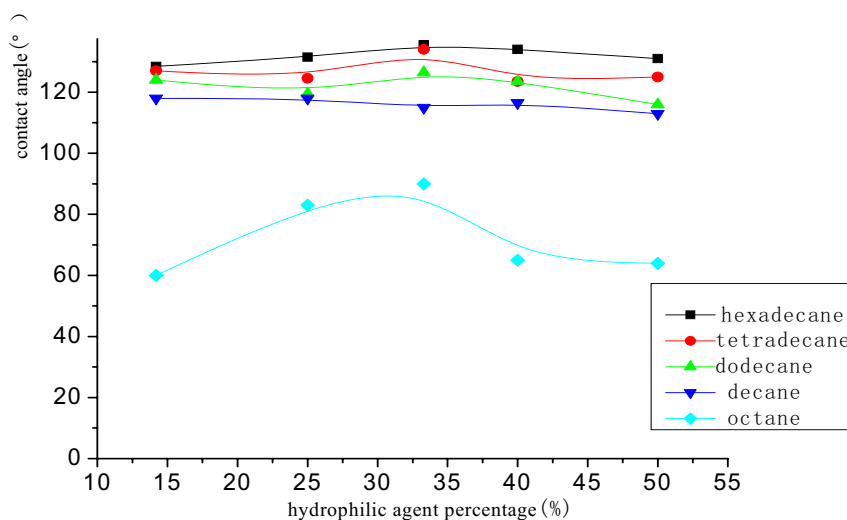


Figure 1. The relation of hydrophilic agent percentage and contact angle

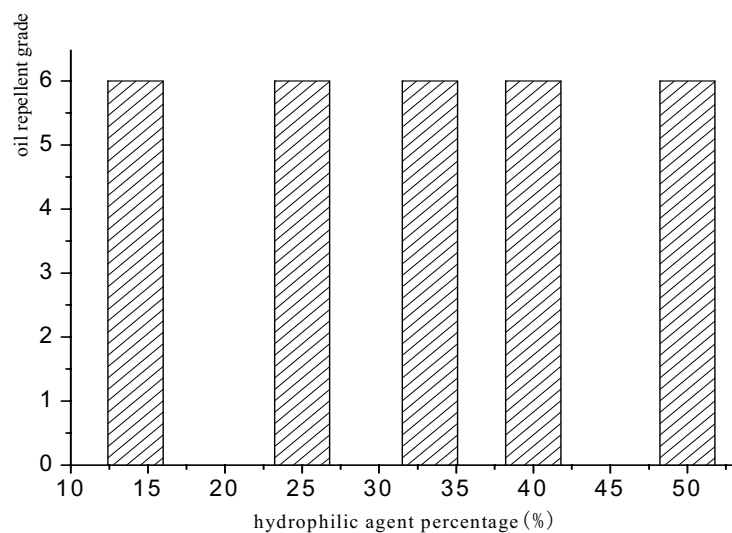


Figure 2. The relation of hydrophilic agent percentage and oil repellent grade

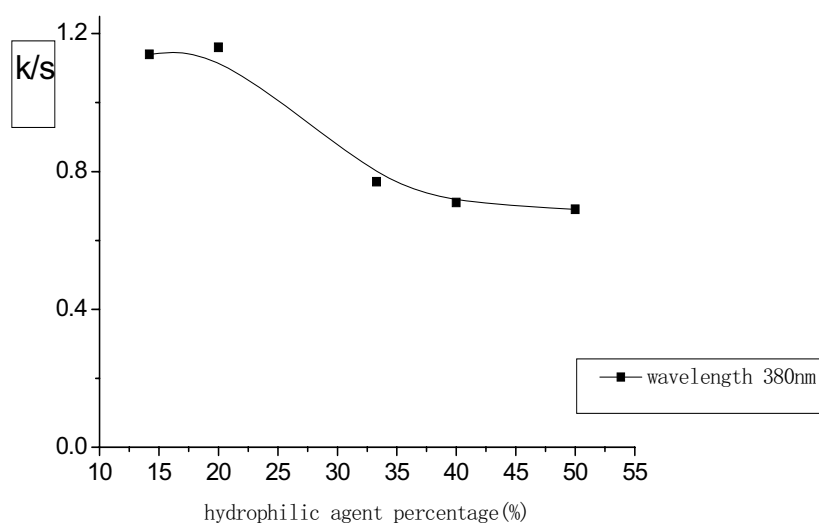


Figure 3. The relation of hydrophilic agent percentage and k/s

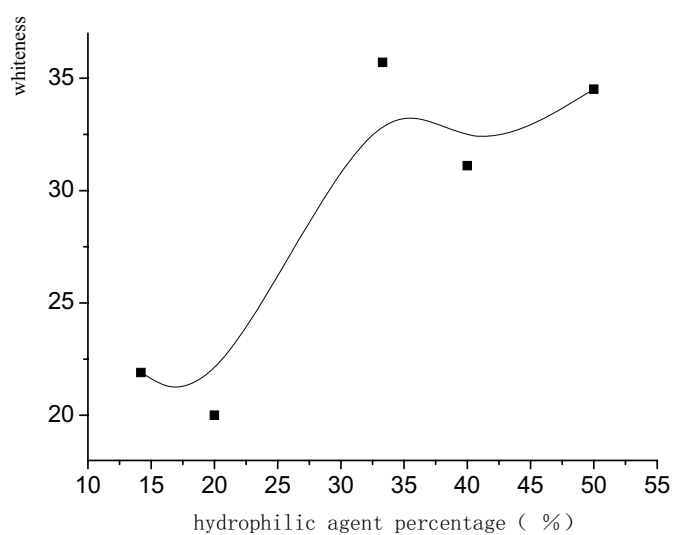


Figure 4. The relation of hydrophilic agent percentage and whiteness

A journal archived in Library and Archives Canada
A journal indexed in Canadiana
A journal indexed in AMICUS
A journal included in Ulrich's
A journal indexed in Google Scholar
A journal indexed in Genamics JournalSeek
A journal indexed in DOAJ
A journal included in PKP Open Archives Harvester

International Journal of Chemistry

Semiannual

Publisher Canadian Center of Science and Education
Address 4915 Bathurst St. Unit # 209-309, Toronto, ON. M2R 1X9
Telephone 1-416-208-4027
Fax 1-416-208-4028
E-mail ijc@ccsenet.org
Website www.ccsenet.org
Printer William Printing Inc.
Price CAD.\$ 20.00

